Order Number 9410821

A methodology to measure retrofit energy savings in commercial buildings

Kissock, John Kelly, Ph.D.

Texas A&M University, 1993

U·M·I
300 N. Zeeb Rd.
Ann Arbor, MI 48106

A METHODOLOGY TO MEASURE RETROFIT ENERGY SAVINGS IN COMMERCIAL BUILDINGS

A Dissertation

by

JOHN KELLY KISSOCK

Submitted to the Office of Graduate Studies of
Texas A&M University
in partial fulfillment of the requirements for the degree of

DOCTOR OF PHILOSOPHY

December 1993

Major Subject: Mechanical Engineering

A METHODOLOGY TO MEASURE RETROFIT ENERGY SAVINGS IN COMMERCIAL BUILDINGS

A Dissertation

by

JOHN KELLY KISSOCK

Submitted to
Texas A&M University
in partial fulfillment of the requirements for the degree of

DOCTOR OF PHILOSOPHY

Approved as to style and content by:

David E. Claridge
(Chair of Committee)

Jeff S. Haberl
(Member)

T. Agami Reddy
(Member)

N. K. Anand
(Member)

Olga Pendleton
(Member)

for G. P. Peterson
(Member)

December 1993

Major Subject: Mechanical Engineering

ABSTRACT

A Methodology to Measure Retrofit Energy Savings in Commercial Buildings.

(December, 1993)

John Kelly Kissock,

B.S., University of Colorado;

M.S., Washington University

Chair of Advisory Committee: Dr. David E. Claridge

Measured energy savings promote and sustain energy conservation retrofits by verifying the success of retrofits, determining pay-back schedules, guiding the selection of future retrofits and identifying opportunities for further savings. This dissertation develops a methodology to measure retrofit energy savings and the uncertainty of the savings in commercial buildings. The functional forms of empirical models of cooling and heating energy use in commercial buildings are derived from an engineering analysis of constant-air-volume and variable-air-volume HVAC systems. One, two, three and four parameter, temperature-dependent regression models are proposed to model baseline energy use. Retrofit savings are measured as the difference between the baseline energy use projected by the models and the measured post-retrofit energy use. A hybrid ordinary least squares / autoregressive method is developed to determine the uncertainty of the predicted energy use and savings. The annual predictive ability of models based on pre-retrofit data sets of less than a full year is investigated. The energy delivery efficiency is introduced to measure the efficiency of air-side systems at meeting the net building load. A preliminary investigation of the use of artificial neural network models to measure savings is presented. The methodology is demonstrated on case study examples using software specifically developed for the analysis of commercial building energy use.

ACKNOWLEDGMENTS

This dissertation draws upon the work of several people associated with the Texas LoanSTAR program. I have referenced their published work in the text; however, many of the most valuable contributions came in the form of suggestions, as shared ideas, or simply as the result of thinking about someone else's work. I wish to thank all of my colleagues at Texas A&M for providing a stimulating learning and research environment.

I am particularly indebted to my advisor David Claridge, who generously supported me and my family during our stay at Texas A&M. Dr. Claridge gave me broad freedom to develop solutions to the problems that presented themselves and to pursue promising areas of research. His confidence in me, and his guidance and patience while I struggled, erred and learned, greatly contributed to this dissertation and my learning experience.

Agami Reddy was instrumental in focusing this work and improved almost every aspect of it, from the conceptualization of the problems to the writing style and grammar. Dr. Reddy developed the original idea behind the energy delivery efficiency and motivated the work on the short data-sets. I greatly benefited from his guidance.

Jeff Haberl's contagious enthusiasm, encouragement and innovative ideas continuously motivated me. He kept me abreast of new developments in our field, generously shared his ideas and provided me with several opportunities for professional growth. His careful editing improved several manuscripts. EModel's bin-fit and animate functions were adapted from his ideas.

David Ruch provided the required mathematical background to quantify the uncertainty of savings. In addition, Dr. Ruch developed the original algorithm for finding the best-fit, four-parameter model and contributed several other innovative ideas.

The simulation model developed in Chapter III is similar to the simplified systems models developed by Srinivas Katipamula and David Claridge.

My mentor in the field of data exploration software is Rudolf Husar, Director of the Center for Air Pollution Information and Trend Analysis at Washington University. His unbounded interest, knowledge and enthusiasm were contagious and much of EModel is simply an extension of his ideas and the Voyager software into the building energy field.

Computer support was expertly and professionally provided by Dean Willis and Jeff Rife. In addition, Jeff Rife and Robert Sparks provided timesaving programming tips.

Many LoanSTAR personnel were involved with the tasks of calibrating metering equipment, instrumenting buildings, and collecting, cleaning and delivering the data for this analysis. In addition, the secretarial staff cheerfully helped me on numerous occasions. Although these people are too numerous to name individually, I thank each of them for their help and important contributions to this work.

Several of my fellow students provided timely help, encouragement, ideas and most importantly their humor and friendship. I would particularly like to thank my friends Yue Liu, Amitava Dhar and Jinrong Wang who cheerfully put up with my many demands while doing first-class work.

I am forever grateful to my parents and brothers, who encouraged me to dream my own dreams and gave me the love, confidence and abilities to pursue those dreams. My boys, Ethan and Kyle, contributed to this work by permitting me to work on too many days and nights when I should have been home with them. They grounded me in the here and now and have already given me more happiness than I imagined possible. Suddenly and completely, all of this is for them.

Finally, I gratefully acknowledge support for this research from the Texas LoanSTAR program of the Texas Governor's Energy Management Center and the Energy Research and Applications Program of the Texas Higher Education Coordinating Board.

To Gretchen,

who builds the dream with me.

This is as much her will, love and vision as it is mine.

TABLE OF CONTENTS

Page

LIST OF FIGURES

Figure Page

LIST OF TABLES

NOMENCLATURE

a	Mean value of periodic function of E_{nc} (W)
b	Amplitude of periodic function of E_{nc} (W)
bias	Parameter which translates the position of the sigmoid function
C	Energy storage capacitance (W h / °C)
CV-SD	Cofficient of variation of standard deviation
CV-RMSE	Coefficient of variation of root mean square error
DD	Degree days (°C)
E	Energy use during some period (W)
E*	Matrix of predicted energy use in post-retrofit period
$\hat{E}_k$	Predicted energy use (W)
$\overline{E}$	Mean energy use (W)
EDE	Energy delivery efficiency
f_{int}	Ratio of interior zone floor area to total floor area
f_o	Ratio of volume flow rate of outside air to return air
gain	Parameter which influences shape of sigmoid function used in ANN models
h	Convection coefficient (W / m^2 °C)
I	Indicator variable
L	Layer number of an ANN node
Lrate	Parameter which influences speed of convergence for ANN models
m	Number of days in the post-retrofit period
n	Number of days in the pre-retrofit period
n(L)	Number of ANN nodes in layer L
NAEU	Normalized annual energy use (W h / yr)
p	Number of model parameters

Q	Thermal load (W)
R	Resistance to heat flow (°C / W)
R^2	Coefficient of determination
RSS	Residual sum of squares
s_1	Solar load constant (W)
s_2	Solar load slope (W / °C)
t	Time (hour)
$t_{\alpha/2}$	Two sided t-statistic with $(1-\alpha)$ confidence level
T	Air dry-bulb temperature (°C)
UA_S	Building heat tranmission coefficient times the building surface area (W / °C)
v	Transfer function coefficient
V	Volume flow rate (l / s)
var( )	Variance
w( )	Weight associated with ANN connection
W	Specific humidity (kg water / kg air)
x( )	Activation level of ANN node
X	Matrix of pre-retrofit independent variables
$X*$	Matrix of post-retrofit independent variables
y( )	Output of ANN node

Subscripts

b	Balance point, baseline
c	Cooling, cold deck
cv	Convection
d	Domestic energy use other than for space heating
dp	Air dew-point

ext	Exterior
f	Fuel
h	Heating, hot deck
i	Internal, ideal multi-zone
int	Interior
L	Lighting
lat	Latent
lr	Lighting and receptacle
m	Mixed air, mass, mixed
m,inter	Inter-zone mixing
m,intra	Intra-zone mixing
nc	Net cooling
o	Outside air
p	Post-retrofit period
r	Return air
s	Savings
sen	Sensible
sol	Solar
sp	Set-point
t	Total
ua	Heat tranmission through the building envelope
v	Ventilation
w	Window of data
wb	Whole building
y	Year

Greek Letters

β	Regression coefficeints, matrix of regression coefficients
δ	Random error term
$\delta( )$	Error associated with ANN node
ε	Prediction error, first order autoregressive error term
ϕ	Phase angle of E_{nc} (radians)
ρ	Autocorrelation coefficient
ρc_p	Product of air density and specific heat at constant pressure (J / l °C)
ρh_v	Product of water density and latent heat of vaporization (J / l)
σ	Variance of model errors
$\sigma^2\Psi$	Matrix of the covariances of pre-retrofit disturbances
$\sigma^2\Psi_*$	Matrix of the covariances of post-retrofit disturbances
$\sigma^2 V$	Matrix of the covariances between pre- and post-retrofit disturbances

CHAPTER I
INTRODUCTION

This introductory chapter describes the motivation for the work presented in this dissertation, the primary objectives of the dissertation, a summary of previous related work and a brief description of the chapters that follow.

Motivation

The buildings sector consumes over a third of the total U.S. energy budget (Energy Information Administration, 1991). Moreover, experts believe that reductions in building energy use of up to 75% are now possible and cost effective using current technologies (Pacific Gas and Electric, 1990; Bevington and Rosenfeld, 1990). Some of these savings can be achieved by implementing state of the art technology and design techniques in new buildings New buildings are being designed to use as little as 20% of the energy associated with traditional buildings the same size (see for example: Norford, 1984; or Miller and Hittle, 1993).

However, the greatest potential for decreasing energy use in buildings lies in retrofitting existing buildings, which generally have lifetimes of between 50 and 100 years (Bevington and Rosenfeld, 1990). Because of these long lifetimes, the vast majority of buildings use equipment that is far less energy efficient than today's best technology and often has fallen into disrepair. In 1986 for example, over 80% of U.S. commercial building floor space was more than 13 years old (Energy Information Administration, 1986). The application of high efficiency lighting, heating, cooling, and control technology in existing buildings can therefore generate enormous savings.

Journal model is *ASME Journal of Solar Energy Engineering*.

As a case in point, consider the Zachry Engineering Center at Texas A&M University. Energy costs at Zachry during 1992 were reduced by 31% (see Table 1.1) after the constant volume air handling systems were retrofit with a variable-air-volume systems. Because of the large savings such as these, there is substantial interest in retrofitting existing buildings with energy saving technology. Retrofit programs on the national (The Energy Policy Act, 1992), state (Claridge et al., 1991), local (Bevington and Rosenfeld, 1990) and utility (Kreig and Baker, 1992) levels are now being considered and implemented.

Table 1.1 1992 Baseline and measured energy costs and savings at the Texas A&M University Zachry Engineering Center after undergoing a retrofit to the air handling system (Energy Systems Laboratory, 1993a).

	Projected Energy Costs of Unretrofitted Building ($/year)	Measured Energy Costs ($/year)	Savings ($/year)	Savings (%)
Cooling Energy	228,100	157,100	71,000	31
Heating Energy	77,500	13,200	64,300	83
Electricity	265,400	233,000	42,300	16
Total	571,000	403,400	177,600	31

Energy conservation retrofits are typically initiated based on predictions of how much energy and money a retrofit will save. Predicted energy savings are generally estimated using the performance specifications of energy-using equipment and estimates of the physical characteristics and operating conditions of the building. Frequently, several values necessary for these calculations, such as the operating hours of lights and electrical equipment, temperature set-point values, infiltration rates, solar loads, and outside-air flow rates for ventilating equipment are assumed or estimated using "engineering judgment". The calculation procedure or computer algorithm may also make simplifying assumptions in order to reduce the complexity and time required for the calculations.

Because of these factors, predicted savings often differ substantially from measured savings. In a study of over 1,700 building energy retrofits, fewer than one in six came within 20% of measured results (Greely et al., 1990). Other examples of major discrepancies between predicted and measured savings abound in the literature. For example, a Swedish study of 306 residences found that glazing retrofits achieved only 48%, insulation retrofits only 53%, and electric heating retrofits only 83% of their predicted savings (Anderlind et al., 1986). Meier and Nordman (1988) examined over 400 residential retrofits and found that predicted savings ranged from 50% to 58% of energy use while measured savings ranged from only 17% to 49% of energy use. The coefficient of determination (R^2 value) between predicted and measured savings in over 300 Minnesota residential retrofits was only 0.11 (Hirst and Goeltz, 1984). And Jamieson and Qualmann (1990) found that in a study of 16 commercial retrofits where the auditors had been supplied with hourly pre-retrofit data, the mean absolute deviation between predicted and measured savings was 165% even after four buildings with known changes in post-retrofit energy use had been eliminated from the sample. Discrepancies such as these led Jamieson and Qualmann to conclude that "utility concern regarding the reliability of model predictions for the purchase of energy savings is well-founded". And Hirst et al. (1986) report that "large discrepancies between predicted and actual energy use ... discourage efficiency investments".

Because of the large discrepancies between predicted and measured savings, there is substantial interest in measuring energy savings. Measured energy savings resulting from energy conservation retrofits in commercial buildings can be used to verify the success of the retrofits, determine the payment schedule for the retrofits, identify operational and maintenance problems and guide the selection of future retrofits. Measured savings can also benefit utilities that support energy conservation and demand side management programs where an accurate measure of savings and savings potential can be a vital

component of a utility's strategic growth plans and ability to meet its demand. Fels and Reynolds (1991) reminds us that "it is crucial not to lose sight of the need for monitoring whole building energy savings as the 'bottom line' for measuring the success of an energy conservation intervention in a building."

Objectives

In response to these needs, the primary objective of this dissertation is to develop a methodology to measure retrofit savings and the uncertainty of the savings in commercial buildings. The methodology should:

- use models which are consistent with and derived from the engineering principles which govern energy use in commercial buildings,
- require only those types of data which are readily obtainable and robust to measurement error,
- include the software necessary for implementation, and
- be demonstrated on several buildings which have received energy conservation retrofits.

To some, the word *measure* in the above objective may seem inappropriate because the measurement of retrofit savings necessarily involves modeling baseline energy use. However, we point out that measurements are of two types: *primary*, such as the measurement of mass, length, time and temperature and *derived*, such as the measurement of weight, area, velocity and energy in which primary measurements are combined to calculate a particular result (Holman, 1978, p.43). The measurement of retrofit savings is a derived measurement, and although we acknowledge the uncertainty introduced by modeling, we still choose to use the word *measure* in order to emphasize the reliance of the methodology on monitored energy use data.

This methodology is limited to those cases where post-retrofit and at least three months or so of pre-retrofit energy use data are available. It measures "actual" savings, and does not attempt to measure "normalized" savings -- the savings that would have occurred in a year of normal weather conditions. The methodology measures energy savings only and does not determine cost savings resulting from reducing the peak electrical demand. The methodology is primarily intended to be used with sub-metered daily energy use data, but in some cases it can be adapted to other data time-intervals and whole building energy use channels. The models developed here apply mainly to air-side HVAC equipment and may not be applicable for retrofits to primary HVAC equipment.

Summary of Previous Work

When an entire year of pre- and post-retrofit data are available, the simplest method to measure energy savings is to directly compare pre- and post-retrofit energy use. Because of this method's inherent simplicity, it is widely used (e.g. Greely et al., 1990; or Jamieson and Qualmann, 1990). However, varying weather conditions between the pre-retrofit and post-retrofit periods can influence energy use and obscure the change in energy use caused by the retrofit. For example, in a simulation study of commercial building energy use in five U.S. cites, Eto (1988) demonstrated that simulated gas consumption during cold years was 7.2% to 28.6% higher than gas use during average weather years; and during warm years gas use ranged from 2.5% to 26.4% less than during average weather years. Because these deviations are in many cases equal to the magnitude of the retrofit savings, the need for weather normalization techniques to determine savings in commercial buildings is clear. Unfortunately, Greely et al. (1990) report that "there is no generally accepted methodology for adjusting commercial building energy use for year-to-year changes in weather". The development and documentation of such a methodology is a principle objective of this dissertation.

The Princeton Scorekeeping Method, PRISM, is a widely used methodology for measuring weather-normalized, retrofit savings in buildings without simultaneous heating and cooling such as residences, apartments and small commercial buildings (Fels, 1986). The methodology for determining heating energy savings is based on the steady-state heat balance of the building envelope:

$$E_h = UA_S \times (T_{sp} - T_O) - Q_i \tag{1.1}$$

where E_h is the required space heating energy, UA_S is the building overall loss coefficient, T_{sp} and T_O are the inside set-point temperature, T_O is the outside air temperature, and Q_i is the sum of the heat gains from occupants, equipment and solar radiation. The balance point temperature T_b is defined as the outside air temperature for which no heating is required and can be determined by setting E_h in Equation 1.1 equal to zero and solving for T_b:

$$T_b = T_{sp} - Q_i / UA_S \,. \tag{1.2}$$

When the outside air temperature is less than the balance point temperature, heating is required. A measure of the required heating potential over a season or year is the number of degree-days referenced to T_b , $DD(T_b)$. During any period of n days, $DD(T_b)$ is defined as :

$$DD(T_b) = \sum_{i=1}^{n} (T_b - T_{sp,\,i})^{+} \tag{1.3}$$

where the + sign indicates that only positive quantities are taken into the sum. Using these definitions, the required space heating energy use can be rewritten as:

$$E_h = UA_S \times DD(T_b) \,. \tag{1.4}$$

If the same fuel used to provide space heating is also used to provide domestic hot water of for cooking, the total fuel use E_f is:

$$E_f = E_d + UA_S \times DD(T_b) \tag{1.5}$$

where E_d is the fuel used for applications other than space heating. PRISM determines the values of E_d, UA_s and T_b that give the best fit for the total fuel use E_f using a search technique and least squares regression from measured energy use and outside air temperature data. If long term daily temperature data (12 years are recommended) are available, PRISM calculates the long term degree-days referenced to T_b and estimates the building's annual energy use during a year of "normal" weather. The Normalized Annual energy Consumptions (NACs) computed by PRISM for the pre- and post-retrofit periods can then be compared to determine retrofit savings. A similar version of PRISM to model cooling energy use is also available.

PRISM's wide acceptance is due in part to its strong basis in the physical theory of energy use in buildings. While that theory adequately describes thermal energy use in buildings without simultaneous heating and cooling, it is not strictly applicable to energy use in large, multi-zone commercial buildings. Commercial buildings generally have large and continuous ventilation requirements and must supply differing amounts of cooling and heating to the various zones. To meet these requirements, a typical commercial building's space conditioning system will simultaneously cool and heat air streams and subsequently mix them in order to supply the proper amount of ventilation, cooling and heating to each zone. As a consequence of these control strategies, cooling and heating energy use in commercial buildings may not be linearly related to outside air temperature and may never encounter a no-load, balance point temperature. In addition, operational practices common in commercial buildings such as temperature set-backs or variable HVAC operating schedules cannot be accounted for by the degree-day procedure which implicitly includes temperatures from night-time and weekends. Thus, many important control and operational characteristics common to commercial buildings are not well described by the degree-day methodology, and as a result degree-day based savings methodologies have limited power to describe energy use and measure savings in commercial buildings. As

Eto (1988) says "the operation and complexity of office building heating, ventilating, and cooling (HVAC) systems tends to violate assumptions fundamental to formulation of these (degree day) techniques".

Despite the mismatch between the degree-day methodology and commercial building energy use, most attempts to provide weather normalized savings in commercial buildings still rely on some modification of the degree-day approach. For example, Eto (1988) reports that "variations of this (degree-day weather normalization) technique have appeared in more sophisticated shared-savings contracts". And in the public sector, the Washington State Energy Office normalizes for commercial building retrofit savings using a linear regression of variable-base degree days (Greely et al., 1990). The Center for Neighborhood Technology normalized for heating retrofit savings by first removing base-level (summer) energy use and subsequently applying an annual heating degree day factor to winter energy use (Greely et al., 1990). And the Minnesota ICP program multiplied annual heating energy use by the ratio of the long term average heating degree-days to the annual heating degree-days encountered during the measurement period (Greely et al., 1990).

In an attempt to assess the accuracy of degree-day based, weather normalization techniques in commercial buildings, Eto (1988) compared four methods of weather normalizing natural gas and electricity consumption for simulated buildings located in five U.S. cites. The four methods are i) no weather correction, ii) all energy use is proportional to degree-days, iii) energy use is proportional to a 18.3 °C (65 °F) based degree-days and iv) energy use is proportional to variable-base degree-days. He found that none of the methods proved clearly superior to the others for all cases and locations (which is not surprising based on the previous discussion). What is needed then, is a savings methodology which incorporates models developed explicitly for commercial building energy use.

Energy use models that can be applied to the problem of measuring commercial building retrofit savings fall into three categories: i) calibrated forward models, ii) non-linear regression models such as artificial neural network models and iii) ordinary least squares (OLS) regression models.

In the calibrated forward modeling approach, a mathematical model of building energy use is developed from engineering principles and then engineering estimates of the model parameters are input to the model in order to predict energy use. Calibrated forward models range from very complex hourly models such as DOE-2 (Lawrence Berkeley Laboratory, 1980) which simulate the dynamic behavior of a building's thermal mass, to moderately complex, steady state, bin-method models such as ASEAM 3.0 (Fireovid and Fryer, 1991), to simplified system models such as those developed by Katipamula and Claridge (1993). The values of model parameters are adjusted during the process of *calibration* to make the model's prediction of energy use match measured energy use as closely as possible. The accuracy of the final prediction of energy use is a function of the accuracy of the assumptions, parameters and algorithms used by the model.

Calibrated simulation models embody much of our understanding about how energy is used in buildings. When only a limited amount of measured energy use data are available, this knowledge is vital in order to predict energy use over the full range of operating conditions. However, when measured energy use data over the majority of operating conditions are already available, as is assumed in this methodology, the use of simulation models to estimate energy use is redundant and actually increases sources of error. Therefore, the use of simulation models to predict energy savings will not be considered here.

Artificial neural network (ANN) models attempt to simulate the learning processes of the human brain (McClelland and Rumelhart, 1989). These models are constructed from a set of connected nodes as in Figure 1.1. Information is passed from input nodes to

intermediate nodes to output nodes via connections. The output value computed by a network is then compared to the desired output and a learning algorithm is invoked to adjust the weights associated with each connection in order to minimize the deviation between the computed and desired output. Typically, an ANN may require several passes through the data in order to *learn* the relationships between the input and output data. ANNs have been applied to building control problems (Miller and Seem, 1991; Nelson, 1993) and to the area of identifying operational and maintenance problems (Kreider and Wang, 1991) with some success. At a recent ASHRAE building energy prediction competition (Building Energy Predictor Shootout, 1993), an ANN model won the competition and several other ANN models were among the most accurate models entered. Because of their demonstrated modeling ability, the use of ANN models for measuring savings will be investigated. No references describing the use of ANN models to measure savings have been found in the literature.

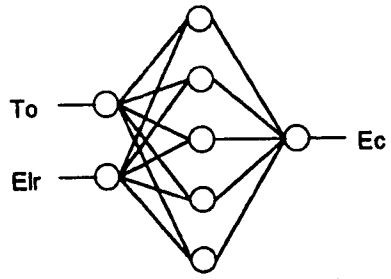

Figure 1.1 Architecture of a simple ANN to model cooling energy use E_c as a function of outside air temperature T_o and lighting and receptacle electricity use E_{lr}. The circles represent nodes and the lines represent connections.

OLS regression models are the third type of model applicable to the problem of determining retrofit savings. The OLS regression methodology can be applied to a wide variety of building energy use models including simple linear (Fels, 1986; and Kissock et al., 1992), multiple linear (Forrester and Wepfer, 1984; and Braun et al., 1987), change-

point (Schrock and Claridge, 1989; and Ruch and Claridge, 1992a), principle component (Ruch et al., 1993a; and Reddy and Claridge, 1993), singular value decomposition (Anderson et al., 1989) and Fourier series (Seem and Braun, 1991) regression models; all of which have been used to analyze building energy use. One reason for the popularity of regression models is that they are almost always easier to develop than calibrated simulation models (MacDonald and Wasserman, 1989). Another reason is that they benefit from a body of well defined theory for determining the uncertainty associated with each model (e.g. Neter et al., 1989). In addition, regression coefficients can sometimes be interpreted as parameters with physical meaning (Rabl, 1988; Reddy, 1989; Zaheer-uddin, 1990; and Cox, 1993) and thus lend insight into the behavior of building energy systems. Because of these advantages, this dissertation will mainly focus on the use of OLS regression models to determine retrofit savings.

Several building energy analysis tools such as Lodestar (Analytical Sciences Co., 1991), LoadView (Quantum Consulting Inc., 1992), Electric Eye (Lee, 1991) and PV-WAVE (Kreig and Baker, 1992) are currently available; however, none of these tools provides the integration of data manipulation, graphing, and modeling capabilities required for determining retrofit savings in commercial buildings. Therefore, a specific objective of this dissertation is to develop a tool or computerized procedure specifically suited to the analysis of commercial building energy data and the determination of savings. Previously work in the field of data exploration software that may be directly applied to this objective includes Voyager (Lantern, 1990). Voyager was one of the first data exploration applications with an interactive graphical interface in the personal computer environment. Another important development was the application of animated data graphics to the analysis of building energy use data (Haberl et al., 1993). The savings measurement tool described in this disseration draws on both of these previous works.

Description of the Following Chapters

When modeling building energy use, steady-state energy balances are appropriate when the data time-interval is much longer than the time constants of the energy storage processes in the building. In Chapter II, a transfer function method, numerical simulation, and a data analysis method are used to estimate the time-lags of radiant energy space cooling loads in commercial buildings. Using this knowledge of the typical time-lags, we determine the data-time intervals for which steady-state models of commercial building energy use are appropriate.

In Chapter III, cooling and heating coil loads from dual-duct, constant-air-volume and variable-air-volume systems are simulated. These simulation results suggest the proper forms of regression models for measuring savings in commercial buildings.

In Chapter IV an overview of the methodology and its scope are presented.

In Chapter V, we describe the software developed to implement the modeling and analysis procedures. This software reduces the time and expertise required to manipulate, comprehend and model energy use data while maintaining high levels of modeling accuracy. It integrates data processing, visualization and modeling functions in a single user-friendly environment. The use of this software to measure savings is demonstrated.

In Chapter VI, a methodology to measure the uncertainty of savings determined from regression models is developed. The methodology, which utilizes a hybrid ordinary least squares / autoregressive model, pays particular attention to the problems caused by autocorrelated residuals. The methodology is validated using measured data from four commercial buildings.

Chapter VII presents an empirical study of the ability of models based on data sets of less than one year to predict annual energy use. The chapter describes the magnitude of annual prediction error and identifies characteristics of short data-sets which influence their predictive ability.

In Chapter VIII, an index called the energy delivery efficiency (EDE) is proposed to quantify the extent of simultaneous heating and cooling in a building. Another index called the ideal multi-zone EDE is also proposed to differentiate between the intra-zone and inter-zone mixing of thermal energy. The use of EDE to evaluate the performance of constant-air-volume and variable-air-volume systems is demonstrated.

Chapter IX presents a preliminary study of the use of ANNs to determine savings. The neurobiological model for ANNs and the generalized delta, back propagation algorithm are described. The effects of different architectures and learning algorithms on the learning rate and final level of accuracy are tested. A comparison of ANNs and least squares regression models for determining savings is presented.

In Chapter X, the above methodology is applied to buildings participating in the LoanSTAR program. The use of the methodology to measure electricity, cooling energy and heating energy savings and the effectiveness of the retrofit at reducing thermal mixing is demonstrated in detail at the Zachry Engineering Center. Modeling and savings results for eight other buildings are also presented.

Chapter XI summarizes the work presented here, discusses its relevance and suggests areas for future research.

CHAPTER II

DATA TIME-INTERVALS FOR STEADY STATE MODELS

In this chapter, the time-constants associated with the storage of radiant energy in a building's internal structure and furnishings are estimated. Using these time-constants, data time-intervals which are appropriate for steady-state models of building energy use are determined.

Three methods are used to quantify the time-constants. A transfer function method quantifies the time-lag between the initiation of lighting load and the subsequent release of the lighting energy absorbed by a building's structure and furnishings into the interior air. A numerical simulation analysis estimates an upper limit to this time-lag by hypothesizing that all of the energy is absorbed by a massive concrete floor. Finally, an investigation of measured whole-building energy use data reveals that the time-constant of the whole-building cooling energy use is significantly shorter than the time-constant of the lighting load because of the influence of other drivers on cooling energy use which have little or no thermal time-lag associated with them. In each case, simplified thermal networks are solved to determine the time-constants.

The lighting load time-constant was less than five hours and the whole-building cooling energy use time-constant was less than one hour. These results indicate that over 98% of the stored radiant energy is released during a 24 hour time period. Thus we conclude that radiant energy storage effects are minimal when considering daily data, and steady-state models of daily cooling and heating energy use are appropriate.

Time-Interval of the Data

In many instances, the time-interval of the data used to measure savings may be determined simply by what type of data are available. For example, in the absence of an

energy management and control system with energy metering capabilities or dedicated energy metering equipment, only monthly billing data may be routinely available. However, the increasing use of dedicated metering equipment and energy management and control systems in commercial buildings has dramatically increased the availability of high time-resolution energy use data (Claridge et al., 1992b). In these cases, the selection of the time-interval of data used to measure savings involves a subjective trade-off between the information content of the savings, and the modeling and computational effort required to derive the savings. For example, hourly data, if properly modeled, can provide high time-resolution savings information in which the savings during any particular hour in the post retrofit period can be determined. This information is especially valuable if used to assess the effectiveness of individual retrofits and look for possible ways to improve retrofits. Long time-interval data, such as monthly data, has much coarser time-resolution, and the ability to assess hourly, daily or weekly variations in savings is lost.

There is, however, a price to pay when using high time-resolution data. This price is the increased complexity of the energy use models and the increased difficulty of acquiring, maintaining and manipulating the large data-sets associated with high time-resolution data. Energy use models based on high time-resolution, short time-interval data may have to consider the dynamic effects of energy storage in the structure and furnishings of a building to be accurate. The added complexity of dynamic models, as compared to steady-state models, makes the modeling process more difficult and the resulting models more complex.

In this chapter, we determine time-constants for radiant energy storage in the structure and furnishings of typical commercial buildings. Our intent is to determine which time-intervals are appropriate for simpler steady-state models of commercial building energy use. In the next chapter, steady-state models of commercial building energy use will be developed to guide the selection of empirical energy use models.

Time Dependency of Space Cooling Loads

Some types of heat gains to a space, such as infiltration or the heat dissipated by electric motors and people, directly increase the air temperature within the space. As the air temperature increases, the HVAC system strives to maintain the air temperature at a fixed set-point temperature. Thus, these loads provoke an almost immediate reaction from the HVAC system.

Other types of heat gains, however, such as solar and lighting radiation are first absorbed by the furnishings and structure (walls, floor and ceiling) of a space and are subsequently convected into the interior air. The delay between the initiation of the lighting or solar radiation and the time that the energy is convected into the interior air is a function of the surface area and energy storage capacity of the furnishings and structure of the room and of the heat transfer coefficients between these objects and the interior air. A measure of this delay is the time-constant, which represents the time required for 63.2% of the energy stored in the mass of the room to be convected into the air if the air temperature is kept constant.

In the following sections, a transfer function approach, numerical modeling and an investigation of measured data will be used to estimate the time-delay associated with a typical interior lighting schedule. The results apply equally to the time-delays associated with solar radiation absorbed by the interior structure and furnishings of a building.

Determining the Lighting Load Time-Lag Using ASHRAE Transfer Functions

Transfer functions were first proposed by Mitalas and Stephenson (1967). They calculated room surface temperatures and cooling loads for several typical building construction types using a detailed energy balance procedure. Based on these results, they then determined functions which represent the cooling load response to a unit input pulse

for each type of construction. These transfer functions are the basis of the Cooling Load Factors and Cooling Load Temperature Differences (American Society of Heating, Refrigerating and Air Conditioning Engineers, 1981) commonly used when calculating design cooling loads.

The transfer function equation for energy convected into the interior air Q_{cv}, at time t, due to a lighting load Q_L is (American Society of Heating, Refrigerating and Air Conditioning Engineers, 1981, p. 26.38):

$$Q_{cv}(t) = v_0 Q_L(t) + v_1 Q_L(t-1) + v_2 Q_L(t-2) - v_3 Q_{cv}(t-1) \qquad (2.1)$$

where v_0, v_1, and v_2 are transfer function coefficients for the type of room furnishings, and v_3 is a transfer function coefficient for the type of room construction and ventilation rate. Equation 2.1 is applicable when all of the lighting energy eventually becomes part of the cooling load, as it does for interior rooms. The transfer function coefficients listed in Table 2.1 (American Society of Heating, Refrigerating and Air Conditioning Engineers, 1981, pp. 26.22, 26.38-26.39) are intended to represent a typical interior space in a relatively heavy weight structure where the time step is given in hours.

Table 2.1 Transfer function coefficients for lighting loads in a typical interior room of a commercial building.

Coefficient	Value	Description
v_0	0	Lighting load with medium weight furnishings
v_1	0.55	Lights recessed, not vented
v_2	-0.49	$v_2 = 1 + w1 - v1$
v_3	-0.94	6" concrete floor with medium ventilation rate

Table 2.2 lists the ratios of the space cooling loads to the lighting input energy as calculated by Equation 2.1 for the first 10 hours after the initiation of a constant lighting

load. After the lights have been on for one hour only 12% of the lighting energy has become part of the space cooling load, the rest of this energy being stored in the building mass. As the mass warms up in the following hours, less of the lighting energy is stored and more is transmitted into the air.

Table 2.2 Ratios of lighting energy convected into the interior air to the lighting load calculated using the ASHRAE transfer function method when lights are on for 10 hours and off for 14 hours.

Time (hours)	Q_{CV}/Q_L
1	0.12
2	0.66
3	0.68
4	0.70
5	0.72
6	0.74
7	0.75
8	0.77
9	0.78
10	0.79

The delay between the time that the lights are turned on and the time that the lighting energy becomes part of the space cooling load can be quantified using a lumped capacitance, thermal network model (Sonderegger, 1978; Rabl, 1988; Taylor and Pratt, 1988; Reddy, 1989; and Claridge et al., 1992c).

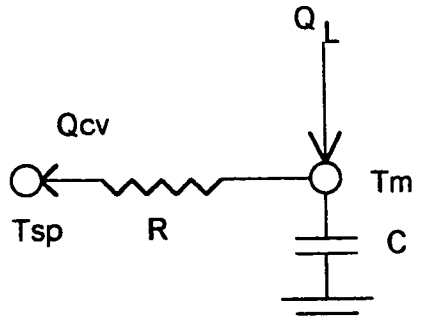

Figure 2.1 Simplified thermal network of lighting, Q_L, and lagged lighting, Q_{cv}, loads in the interior space of a building.

In Figure 2.1, the nodes T_{sp} and T_m represent the *inside* air set-point temperature and temperature of the interior *mass*, respectively. The *capacity* of the room's mass to store thermal energy is denoted by C and the *resistance* to the heat flow from the mass to the air space is denoted by R. Q_L is the *lighting* energy absorbed by the room's mass and Q_{cv} is the energy *convected* from the room's mass into the interior air.

This simplified network assumes that all of the building mass in the furniture, walls, floors, etc. is at the same temperature T_m. Similarly, the thermal capacitances of all of the objects in the space have been *lumped* into a single capacitance term C. In addition, it is assumed that the inside set-point temperature T_{sp} is constant.

An energy balance on the node T_m gives the time dependent differential equation:

$$Q_L - \frac{T_m - T_{sp}}{R} = C\frac{dT_m}{dt} \tag{2.2}$$

where t is time. Assuming that Q_L is a constant and using the initial condition: at $t = 0$, $T_m = T_i$, the solution of Equation 2.2 can be written as:

$$\frac{T_m - T_{sp}}{RQ_L} = 1 - e^{\frac{-t}{RC}} \tag{2.3}$$

The rate at which a building's mass stores and releases energy is described by the product RC, which is called the time-constant. The quotient $(T_m-T_{sp})/RQ_L$ is the ratio of

the temperature difference (T_m - T_{sp}) at time t to the temperature difference after an infinite amount of time. Because these temperature differences are directly proportional to heat flows, this quotient is also equal to the ratio of heat flow from the mass into the air space at time t to the steady-state value of the energy given off by the lights. Thus, this ratio is equal to Q_{cv}/Q_L. The time-constant RC can be found by regressing Equation 2.3 with the data from Table 2.2. Based on this regression, the time-constant for this energy storage process is found to be 4.8 hours. The R^2 of the regression is 0.88.

The time-constant is an indication of how fast the output of a system responds to changes in input. After one time-constant, t = RC, the quantity on the right side of Equation 2.3 equals 0.623 indicating that the system has reached 62.3% of its steady state value; or equivalently, the temperature of the mass has increased 63.2% of the amount it would if the lights were left on indefinitely. After four time-constants, t = 4RC, the temperature of the mass is 98.2% of its steady-state temperature. Thus, if we consider a time-interval four or more times longer than the time-constant of a system, the transient effects become less than 1.8% of the system response and the process can be safely approximated as a steady-state process.

From this analysis, it is clear that when using hourly data, heat-storage effects should be considered in order to properly model the time-dependent behavior of space cooling loads due to lighting. For example, the absence of a heat storage term in an hourly energy balance on this system would result in an error of 88% during the first hour after the lights were turned on. However, when using daily data the transient heat storage effects are only about 2%, thus justifying a steady state approximation.

Determining the Lighting Load Time-Lag Using Numerical Simulation

In this section, the time-dependent temperature response of a massive, 0.15 meter (six inch), concrete floor exposed to ten hours of lighting radiation is simulated. Assuming

that such a concrete slab is among the most massive components of a typical interior space, the time-constant determined from this simulation will be an upper limit to the lighting load time-constant.

We begin by assuming that the concrete slab is exposed to lighting radiation Q_L on the top surface and exchanges heat via convection Q_{cv} to the air at temperature T_{sp} both above and below it (Figure 2.2). This configuration corresponds to the floor and suspended ceiling arrangement common in many commercial buildings.

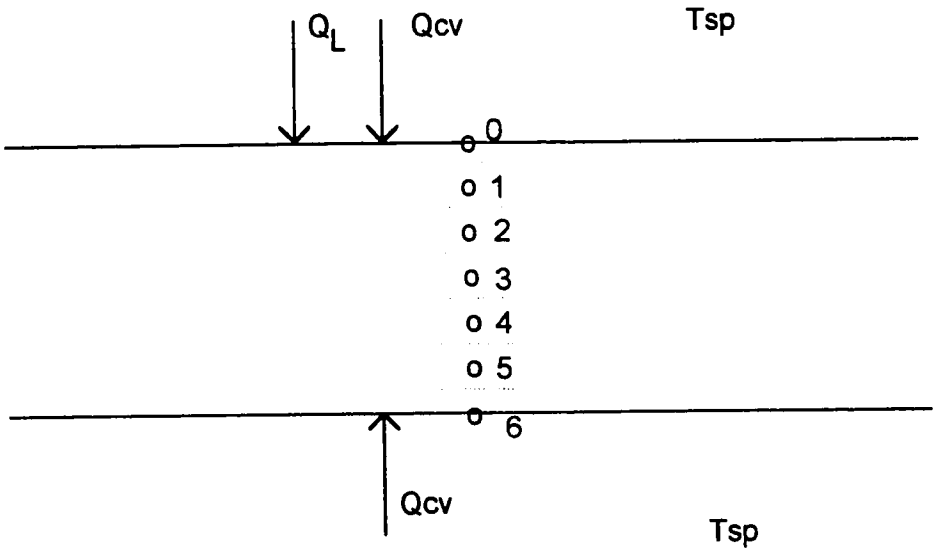

Figure 2.2 Cross section of a 0.15 meter (six inch) concrete floor with top surface exposed to lighting.

For the purpose of simulation, the slab is approximated as being of infinite area such that only one dimensional heat transfer is considered. The temperature distribution across the slab is then modeled as six discrete temperature nodes. Energy balances are performed on the regions defined by the six nodes, with the assumption that the temperature within each region is constant and is given by the node temperature. Assuming that the temperatures of the air and all of the nodes are equal to the indoor air temperature T_{sp} at

time t = 0, the node temperatures at subsequent times can be calculated by successively solving the system of energy balance equations for each time-interval using an explicit, forward-difference method (Incropera and DeWitt, 1985, pp. 212 - 217). To perform the simulation, a time-interval of one minute was chosen, which is well below the maximum time-interval required to guarantee numerical stability.

The variation of nodal temperatures in response to ten hours of lighting is shown in Figure 2.3. For this simulation, the convection coefficient is assumed to be 9.25 W / m^2 °C (1.63 Btu / hr ft^2 °F) (American Society of Heating, Refrigerating and Air Conditioning Engineers, 1981, p. 23.12). The temperature response is similar to the cooling load response calculated using ASHRAE transfer functions and found experimentally (Treado and Bean, 1990).

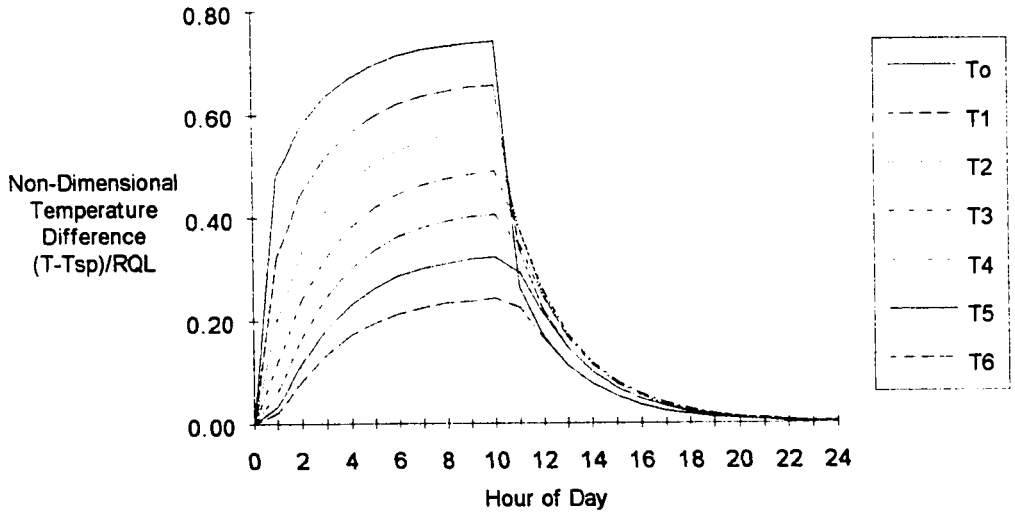

Figure 2.3 Nodal temperature variation within a six inch concrete slab exposed to ten hours of lighting radiation.

The time-constant of the heat storage process simulated here can be determined, as before, from a lumped capacitance, thermal network model (Figure 2.1). In this case Q_{CV} is calculated from the simulated temperature of the top of the floor slab T_0:

$$Q_{CV} = h \times (T_{sp} - T_0) \tag{2.4}$$

where h is the convection coefficient. The ratio of Q_{CV} to Q_L for each of the first 10 hours is calculated and listed in Table 2.2. The time-constant is determined by regression to be 9.7 hours with an R^2 of .95.

This time-constant provides an upper limit for the time-delay associated with lighting or solar loads. However, even in this limiting case, the system would achieve 91% of its steady state value after 24 hours, reinforcing our previous conclusion that the steady-state approximation is appropriate when considering daily data.

Determining the Cooling Load Time-Lag from Measured Energy Use Data

In the previous sections, the lighting load time-constant was found to be on the order of 5 hours for a typical commercial building, and was not more than 10 hours even in the limiting case. The lighting load, however, is only one of several factors that influence whole-building cooling energy use. Many of the other factors which influence whole-building cooling energy use, such as the energy required to bring outside ventilation air to the interior set-point temperature, have little or no time-lag associated with them. Because multiple factors with different time-constants influence whole-building cooling energy use, it can have a significantly different time-constant than the lighting load.

In this section, a month of hourly energy consumption data from the Zachry Engineering Center on the Texas A&M University campus is analyzed. At the time that these data were collected, the engineering center was equipped with a constant-air-volume HVAC system which mixed cool and warm air streams to maintain the set-point

temperatures in each zone. Whole-building cooling and heating energy use were monitored and recorded on an hourly basis.

The difference between whole-building cooling and heating energy use is the net cooling energy use E_{nc}. The net cooling energy use is the net amount of heat extracted from the building by the HVAC system and equals the sum of the envelope conduction load, solar load, internal load, ventilation load and energy released into interior air from the building's structure. Hourly values of the net cooling energy use are shown in Figure 2.4 plotted against outside air temperature. The strong influence of outside air temperature on the net cooling energy use is clearly evident. Net cooling energy use is also influenced by latent and internal loads and can be modeled using a multiple regression model as:

$$E_{nc} = \beta_0 + \beta_1 \times T_o + \beta_2 \times W_o + \beta_3 \times E_{lr} \qquad (2.5)$$

where T_o is the outside air temperature, W_o is the outside air specific humidity, E_{lr} is lighting and receptacle electricity use, and β_0, β_1, β_2 and β_3 are regression coefficients. This model accounts for 88% of the variation of the net cooling energy use, i.e. $R^2 = .88$, and provides a tool to predict the net cooling energy use given these inputs.

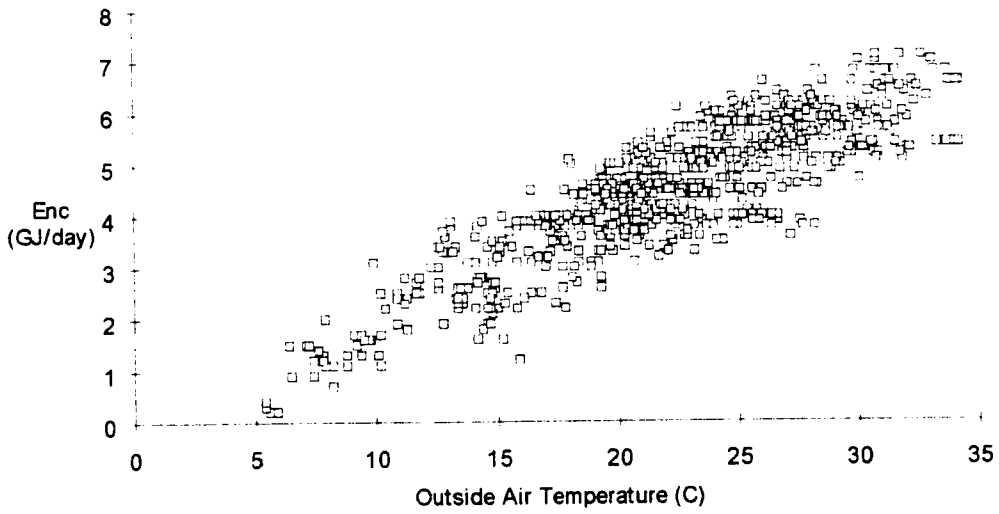

Figure 2.4 Plot of hourly values of net cooling energy use versus outside air temperature.

Figure 2.5 displays the average measured and predicted net cooling energy use for each weekday hour. The predicted net cooling energy use curve was created by predicting the net cooling energy use using Equation 2.5 for each of the 744 hours in the data set. The hourly predictions of the net cooling energy use were then separated into 24 bins corresponding to the 24 hours of the day and the mean value of each hourly bin was calculated. These mean values are the average, predicted, net cooling energy use for each hour of the day and are displayed in Figure 2.5. The average, measured, net cooling energy use was calculated by separating the measured, net cooling energy use into hourly bins and finding the mean value of each bin.

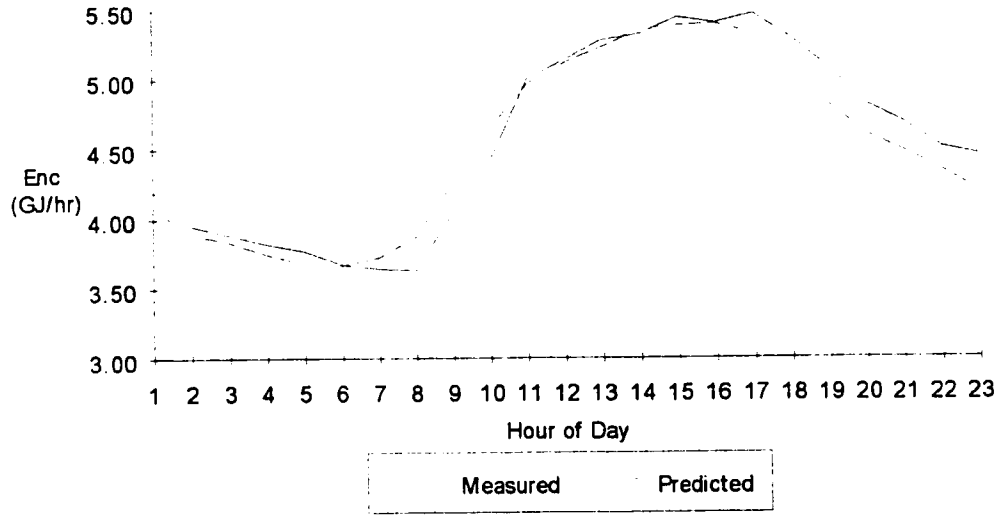

Figure 2.5 Average weekday, measured and predicted net cooling energy use for each hour of the day.

The shapes of the curves in Figure 2.5 approximate a commercial building lighting profile; the smooth edges are caused by energy storage processes. Note that the predicted net cooling load curve does not include lag effects because both the morning and evening values are included in the model, and average the time-lag effects to zero. The measured net cooling load curve, on the other hand, includes the energy storage time-lag effects. The phase lag between the two curves is the thermal time-lag caused by energy storage in the building's furnishings and structure. In the morning, the predicted cooling energy use increases rapidly in response to increasing outside air temperature, specific humidity and building electricity use. The measured cooling energy use increases more slowly because the structure of the building is cool and is absorbing part of the lighting load. In the evening, when the building occupants leave, the opposite behavior is observed. The predicted cooling energy use drops off quickly because outside air temperature, specific humidity and building electricity use are decreasing. The measured cooling energy use

declines more slowly because the building's mass is discharging the energy stored during the day into the interior air.

The magnitude of the phase lag evident in Figure 2.5 can be determined by modeling each curve as a cosine function of the form:

$$E_{nc} = a + b \times \cos(\frac{2\pi}{24} t + \phi) \tag{2.6}$$

where a is the mean value of E_{nc}, b is the amplitude of E_{nc}, ϕ is the phase angle of E_{nc} and t is the hour of the day. Using the cosine addition formula, Equation 2.6 can be rewritten as:

$$E_{nc} = \beta_0 + \beta_1 \times \cos(\frac{2\pi}{24} t) - \beta_2 \times \sin(\frac{2\pi}{24} t) \tag{2.7}$$

where β_0 is the mean value a, β_1 is b $\times$ cos(ϕ), and β_2 is b $\times$ sin(ϕ). Equation 2.7 can then be regressed against the data to determine β_0, β_1 and β_2 and subsequently a, b and ϕ. Using this procedure, the difference between the predicted and measured phase angles was determined to be 45 minutes. The R^2 values for the predicted and measured regressions were .94 and .93 respectively. The mean values, a, and amplitudes, b, of the predicted and measured net cooling energy uses were nearly identical as is evident in Figure 2.5.

The time-constant for this energy storage process can be determined from the phase-lag. To do so, we once again model the predicted $E_{nc,p}$ and measured $E_{nc,m}$ net cooling energy uses as periodic functions with identical mean values but different amplitudes and phase angles:

$$E_{nc,p} = b_p \times \cos(\frac{2\pi}{24} t) \tag{2.8}$$

$$E_{nc,m} = b_m \times \cos(\frac{2\pi}{24} t - \phi). \tag{2.9}$$

In Equation 2.9, the measured net cooling energy use is lagged by ϕ = 45 minutes behind the predicted net cooling energy use given by Equation 2.8. The input and output functions of the same thermal network shown in Figure 2.1 can then be renamed to correspond to the predicted and measured net cooling energy usages (Figure 2.6).

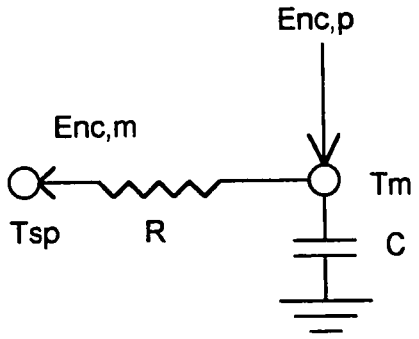

Figure 2.6 Simplified thermal network of predicted $E_{nc.p}$ and measured $E_{nc,m}$ net cooling energy use.

An energy balance on T_m in Figure 2.6 gives:

$$E_{nc,p} + \frac{T_{sp} - T_m}{R} = C\frac{d\,T_m}{dt}. \tag{2.10}$$

and the measured net cooling energy use is:

$$E_{nc,m} = \frac{T_m - T_{sp}}{R}. \tag{2.11}$$

Combining Equations 2.8, 2.9, 2.10 and 2.11 to give the difference ($E_{nc,p}$ - $E_{nc,m}$), gives the following equation for the time-constant RC:

$$RC = \frac{(b_p/b_m) \times \cos(\frac{2\pi}{24}t) - \cos(\frac{2\pi}{24}t - \phi)}{-\left(\frac{2\pi}{24}\right) \times \sin(\frac{2\pi}{24}t - \phi)} \tag{2.12}$$

Since RC is a constant, the value of RC can be determined by finding the ratio (b_p/b_m) which gives a near constant value of RC. For a phase lag of 45 minutes, the net cooling energy use time-constant is found to also equal 45 minutes.

The net cooling energy use time-constant of 45 minutes is significantly shorter than the lighting load time-constant of 4.8 hours, however, the two results are not inconsistent. The reason for this behavior is that the lighting load is only one of the influences on the net cooling energy use. When multiple input functions with different amplitudes and phase angles are summed to produce a single output function, the phase angle of the output function will be different than the phase angles of the input functions.

This behavior can be demonstrated by developing a thermal network which includes the effects of both outside air temperature and lighting loads on the net cooling energy use (Figure 2.7). In this model, we make the following simplifying assumptions: i) infiltration, solar, latent and instantaneous internal loads are small compared to lighting and outside air temperature loads and are neglected, ii) lighting and outside air temperature loads are nearly in phase, and iii) the outside air temperature load can be modeled without an energy storage term. Although the third assumption is not strictly true because of time-lagged conduction loads through the building's envelope, we note that in commercial buildings much of the net cooling energy use's temperature dependence is due to the energy required to bring ventilation air to the interior set-point temperature; a load that is nearly instantaneous. It is for this reason that we use an *unlagged* outside air temperature load to demonstrate the effect of multiple loads with different time-lags on the net cooling load.

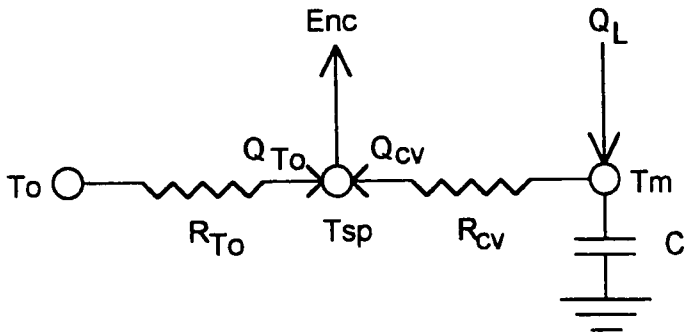

Figure 2.7 Simplified thermal network of net cooling energy use E_{nc} as a function of the outside air temperature load Q_{To} and the lighting convection load Q_{cv}.

To find the phase shift of the net cooling energy use E_{nc} in terms of the amplitudes and phase angles of the outside air temperature load Q_{To} and the lighting convection load Q_{cv}, we sum Q_{To} and Q_{cv} to get E_{nc}:

$$E_{nc} = Q_{To} + Q_{cv} \tag{2.13}$$

and once again model each load as a cosine function:

$$Q_{To} = a \times \cos(\frac{2\pi}{24}t) \tag{2.14}$$

$$Q_{cv} = b \times \cos(\frac{2\pi}{24}t - \frac{2\pi}{24}\phi) \tag{2.15}$$

$$E_{nc} = c \times \cos(\frac{2\pi}{24}t - \frac{2\pi}{24}\theta) \tag{2.16}$$

In Equations 2.14 and 2.15 we assume that the lighting Q_L and temperature Q_{To} loads are initially in phase, however, the lighting convection load Q_{cv} is lagged by ϕ hours due to the thermal storage effect. Equations 2.13, 2.14, 2.15 and 2.16 can be manipulated to give:

$$\theta = \left(\frac{2\pi}{24}\right)^{-1} \tan^{-1} \frac{(b/a) \times \sin(\frac{2\pi}{24}\phi)}{1 + (b/a) \times \cos(\frac{2p}{24}\phi)} \tag{2.17}$$

Using a method similar to that described by Equations 2.8 to 2.12, the phase-lag associated with the lighting load time-constant of 4.8 hours is found to be 3.4 hours. Substituting 3.4 hours for ϕ in Equation 2.17 and solving for the ratio of amplitudes (b/a)

that gives a net cooling load phase lag θ of 45 minutes gives (b/a) equal to 0.30. This result, that the lighting load is roughly 30% of the outside air temperature load seems plausible. In addition, this exercise demonstrates that a net cooling energy use time-constant of 45 minutes is not inconsistent with a lighting load time-constant of 4.8 hours.

A net cooling energy use time-constant of 45 minutes indicates that the system achieves 99.99% of its steady state value after 24 hours, thus clearly demonstrating the appropriateness of a steady-state approximation when modeling cooling and heating energy use with daily data.

Chapter Summary

The results derived in this chapter indicate that for a data time-interval of one hour or less, lighting energy thermal storage effects are significant and models of heating and cooling energy use should account for energy storage processes. On the other hand, the results also indicate that for models which use data with a time-interval of 24 hours or more, energy storage effects are negligible and the use of steady state models of heating and cooling energy use is appropriate.

Based on the above findings, steady state models of heating and cooling coil energy use are developed in the next chapter. These models are appropriate for daily or longer time-interval data. In general, we find that for the purpose of determining savings, daily data (the summation of hourly values of energy use over a 24 hour period) provide the best compromise between the high resolution provided by short time-interval data and the modeling and computational convenience of longer time-interval data. For this reason, we will use primarily daily data for the remainder of this analysis.

CHAPTER III

ENGINEERING DERIVATION OF EMPIRICAL MODELS FOR MEASURING SAVINGS

In this chapter, the functional forms of regression models used to measure retrofit savings are derived. Weather independent energy use, such as constant-air-volume electricity use, is modeled using one parameter, mean models. Cooling and heating energy use are modeled using regression models which depend only on outside air temperature. The proper functional forms of cooling and heating energy use models for constant-air-volume (CAV) and variable-air-volume (VAV) systems are suggested from simulation results. The effects on heating and cooling energy use of hot-deck reset schedules, economizer cycles, latent and internal loads are also simulated. The results suggest that one, two, three and four parameter regression models are appropriate for most of the energy use patterns generated by the HVAC systems and control options investigated. These regression models are used in subsequent chapters to model pre-retrofit energy use and determine savings.

Modeling Weather Independent Energy Use

Certain types of energy use in commercial buildings, such as lighting and receptacle electricity use and constant-air-volume air handler electricity use, are insensitive to variations in weather and are primarily determined by a building's occupancy or operating schedule. In many cases, these weather independent types of energy use are relatively constant during each occupancy or operational period and may therefore be accurately modeled as the mean energy use during each period. A common example occurs when air handlers are partially shut down on weekends. In this case, air handler electricity use is modeled with separate mean models for weekdays and weekends. Mean models of energy

use are called one-parameter models because only one parameter, the mean, is determined statistically.

Occasionally, it is not clear whether the energy use in one period is different enough from energy use in another period to justify separate models for each period. In these cases, a t-test (Appendix D) can be administered to determine whether the use of separate models for each operational period is statistically justified.

The use of separate models for different operating or occupancy schedules enhances the resolution of the savings but does not affect the determination of how much energy is saved. Consider for example, a hypothetical lighting retrofit in a building with much higher lighting loads on weekdays than on weekends. Separate weekend and weekday models of pre-retrofit lighting use enable the analyst to determine the savings on both weekdays and weekends and hence gain more insight into the performance of the retrofit. If the differences between weekday and weekend electricity use are ignored and a single "all-days" model for all seven days of the week is used as the baseline model, then neither weekday nor weekend savings can be properly identified. The savings determined using the all-days and the separate weekday and weekend models will, however, be the same for any post-retrofit period which is a multiple of seven days. Therefore, the use of separate models for the different operating or occupancy schedules enhances the information content of the savings but does not affect the determination of how much energy is saved.

Choice of Independent Variables for Weather Dependent Models

The goal of modeling energy use to measure savings is to characterize building energy use using a few readily available and highly reliable input (independent) variables. In addition, each independent variable must be unaffected by the retrofit so that the model can accurately predict the energy use that would have occurred if the retrofit had not taken place. Environmental variables which meet the above criteria for modeling heating

and cooling energy use include outside air dry-bulb temperature, solar radiation and specific humidity. In commercial buildings, internally generated loads, such as the heat given off by people and electrical equipment, are also strong determinants of heating and cooling energy use. We have found that lighting and receptacle electricity use, which is calculated as the difference between whole-building electricity use and motor-control center electricity use, is a good surrogate variable for internal loads because it varies with the occupancy level of the building. HVAC system variables, such as the zone set-point temperatures or the outside air damper position in economizer cycles may also be important.

Although all of these variables influence heating and cooling energy use, there are strong practical incentives for identifying the simplest model that results in acceptable accuracy. Multivariable models require more metering and are more sensitive to metering errors and failures; thus models which depend on multiple independent variables become useless if even one of the independent variables is unavailable. In addition, some independent variables in multiple linear regression models may be linearly related. This condition, called multicollinearity, decreases the precision with which regression coefficients can be estimated and hence decreases the predictive ability of a model when used on a new data set (Neter et al., 1989). Although principal component (Ruch et al., 1993a; Reddy and Claridge, 1993; and Cox, 1993) and singular value decomposition (Anderson, 1990) techniques have been developed to deal with multicollinearity, these techniques significantly increase the complexity of the modeling process and in many cases do not substantially increase the accuracy of the prediction (Ruch et al., 1993a; Reddy and Claridge, 1993).

For these reasons, this analysis will focus on identifying empirical models for heating and cooling energy use which use only outside air dry-bulb temperature. Like the choice of data time interval, this is a subject tradeoff. Some accuracy will be lost when

temperature is used as a surrogate variable for solar gains and latent loads. In addition, changing internal loads and other operational changes which affect building cooling and heating energy use must be accounted for by developing separate models for each occupancy or operational period. On the other hand, the simplicity and relatively good accuracy (see Chapter IX) of temperature based models makes them highly desirable. In addition, outside air temperature is easily measured and the data are widely available. For those cases where the accuracy of temperature based models is not sufficient, multiple linear regression or artificial neural network models (Chapter VIII) may be appropriate.

Dual-Duct Air Distribution Systems

A dual-duct HVAC system is shown in Figure 3.1. A single fan blows air through a cooling coil c and a heating coil, h. The latent and sensible heat removed from the air stream in the cold deck is E_c and the heat added in the hot deck is E_h. From the cold and hot decks, the air travels through supply ducts and mixing boxes mb to an interior zone and an exterior zone. The building's exterior zone is defined to be the top floor of the building and the first 5 meters or so inward from the exterior walls. In many cases the width of the exterior zone can be defined by a ring of exterior offices or rooms. The exterior zone is subject to conduction loads through the building's shell, solar loads through fenestration and internally generated loads. The total load to the exterior zone is Q_{ext}. The interior zone, which comprises the rest of the building, is effectively insulated from conduction and solar loads by the exterior zones and is subject only to internally generated loads, Q_{int}. The return air streams leaving the interior and exterior zones are denoted as r,int and r,ext respectively and the total return air stream is denoted as r. Part of the return air is exhausted to the outdoors and an equal amount of outside air, o, is added to the return air stream. The mixed air entering the fan is denoted as m.

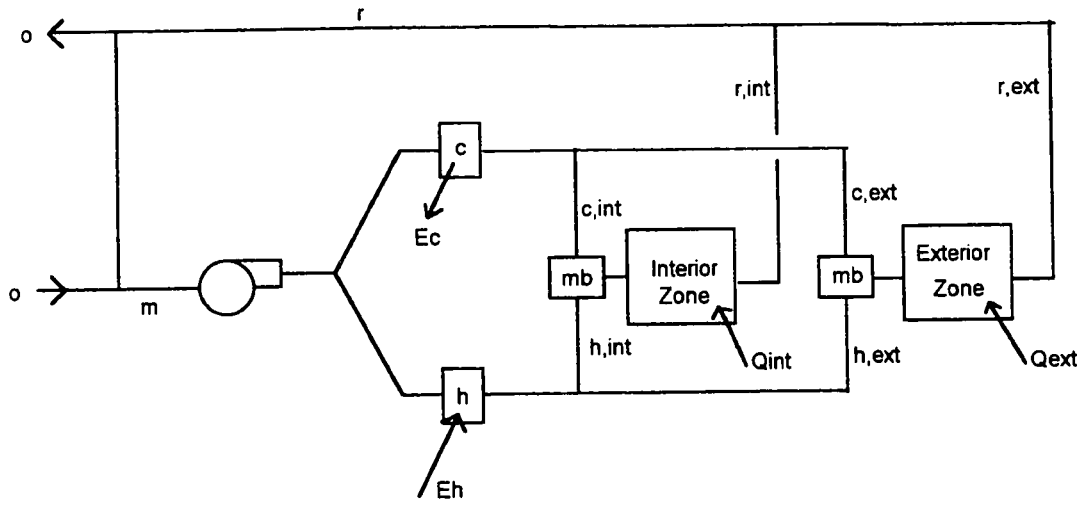

Figure 3.1 Schematic of dual-duct air handling system.

In order to simplify the modeling of this system, we make the following assumptions. The building is assumed to be maintained at a slight positive pressure and so no air infiltrates the building through the shell. The temperature of the return air is assumed to be constant at the room set-point temperature and the air leaving the cooling and heating coils is assumed to be at constant set-point temperatures. Internally generated heat is distributed evenly over the entire floor area. In addition it is assumed that the energy added to the air stream by the fan is negligible, no heat enters or leaves the air ducts, and the density of the air throughout the system remains constant.

Constant-Air-Volume Systems

Dual-duct, constant-air-volume HVAC systems are common in commercial buildings. They provide excellent control of the space temperature and humidity level. In this section, we examine the relationships between cooling and heating coil energy use and outside air temperature in dual duct, CAV systems. These relationships will be used to determine the proper form of empirical models of cooling and heating coil energy use.

The process of deriving empirical, temperature-based models of cooling and heating coil energy use begins with an energy balance on each coil. The sensible portion of the cooling coil energy, $E_{c,sen}$, is:

$$E_{c,sen} = V_c \times \rho c_p \times (T_m - T_c) \tag{3.1}$$

where V_c is the volume of air flowing through the cooling coil, ρc_p is the product of the density and specific heat of the air, T_m and T_c are the temperatures of the mixed air entering and cool air leaving the cold deck respectively. Since ρc_p and T_c are assumed to be constant, the relationship of $E_{c,sen}$ with outside air temperature depends on the relationships of V_c and T_m with outside air temperature.

An energy balance on the outside air mixing boxes gives the mixed air temperature, T_m:

$$T_m = f_o \times T_o + (1 - f_o) \times T_r \tag{3.2}$$

where f_o is the fraction of outside air, T_o is the temperature of the outside air and T_r is the temperature of the return air stream. For a simple CAV system, f_o and T_r are constant making T_m linear with outside air temperature.

The volume of air passing through the cooling coil, V_c, is the sum of the volume of cooling air supplied to the interior zone, $V_{c,int}$, and the volume of cooling air supplied to the exterior zone, $V_{c,ext}$. An energy balance on the interior zone yields:

$$V_{c,int} = \frac{V_{r,int} \times \rho c_p \times (T_r - T_h) - Q_{int}}{\rho c_p \times (T_c - T_h)} \tag{3.3}$$

where $V_{r,int}$ is the volume of return air exiting the interior zone and T_h is the temperature of the air leaving the heating coil. In a CAV system, the total flow rate to the interior and exterior zones, $V_{r,int}$ and $V_{r,ext}$, are fixed quantities that are defined in the design process. Thus, $V_{c,int}$ is entirely independent of outside air temperature.

$V_{c,ext}$ can be found from an energy balance on the exterior zone:

$$V_{c,ext} = \frac{V_{r,ext} \times \rho c_p \times (T_r - T_h) - Q_{ext}}{\rho c_p \times (T_c - T_h)} \quad (3.4)$$

The total load in the exterior zone, Q_{ext}, is the sum of conduction, solar and internal loads:

$$Q_{ext} = UA_s \times (T_o - T_r) + (s_1 + s_2 \times T_o) + Q_{i,ext} \quad (3.5)$$

where UA_s is the overall building load coefficient, s_1 and s_2 are constants used to approximate the solar load to the building and $Q_{i,ext}$ is the sum of all the internally generated loads in the exterior space. We assume here that the solar load can be approximated as a linear function of daily outside temperature (Vadon et al., 1991). From Equations 3.3, 3.4 and 3.5 it is apparent that $V_{c,ext}$, like T_m, is linear with outside air temperature. However, $E_{c,sen}$ (Equation 3.1), includes the product of V_c and T_m and has both linear and quadratic outside air temperature terms.

The dependence of V_c on outside air temperature can be summarized as:

$$V_c = k_1 + (UA_s + s_2) \times T_o \quad (3.6)$$

where k_1 is a constant independent of outside air temperature. Substituting Equations 3.2 and 3.6 in Equation 3.1 gives a quadratic dependence of the sensible cooling coil load on outside air temperature of the form:

$$E_{c,sen} = \beta_0 + \beta_1 \times T_o + \beta_2 \times T_o^2 \quad (3.7)$$

where β_0, β_1 and β_2 are constants. This quadratic relationship results from the fact that both the mixed air temperature T_m and the volume of air passing through the cooling coil V_c in Equation 3.1 are functions of outside air temperature. Outside air temperature affects the mixed air temperature because outside air and return air are mixed before entering the cooling coil. The flow rate of air passing through the cooling coil is dependent on outside air temperature because outside air temperature influences the

conduction and solar loads in the exterior zones, hence influencing the quantity of cool air required by these zones. When T_m and V_c are multiplied to give the sensible energy removed in the cold deck (Equation 3.1), a quadratic temperature term is created. The energy added in the hot deck, E_h, also has a quadratic term for the same reasons.

Although the previous mathematical derivation yields considerable insight into relationships between thermal energy use and outside air temperature, the complexity of the resulting equations can diminish their instructive value. To better understand these relationships, then, a simplified systems simulation model of energy use in commercial buildings was developed. The simulation model uses the equations developed above to simulate heating and cooling coil energy use. Table 3.1 lists the values of the parameters used in the simulation. The equations and methodology employed by the simulation program are listed in Appendix A.

Table 3.1 Values of parameters used in simulation model.

T_r (temperature of return air)	22.2 (°C)
T_c (temperature of air leaving the cooling coil)	12.8 (°C)
T_h (temperature of air leaving the heating coil)	48.9 (°C)
f_i (ratio of interior to total floor area)	0.65
f_o (ratio of outside air flow rate to return air flow rate)	0.10
UA_s (building load coefficient)	10,550 (W/°C)
s_1 (solar load constant)	2,930 (W)
s_2 (solar load slope)	211 (W/°C)
V_r (volume flow rate of return air in CAV systems)	235,800 (l/s)
ρc_p (product of air density and specific heat at constant pressure)	1.21 (J/l °C)
ρh_v (product of water density and latent heat of vaporization)	2,980 (J/l)
E_{lr} (lighting and receptacle electricity use)	750,000 (W)

The sensible cooling and heating coil loads from the simulation model are shown plotted against outside air temperature in Figure 3.2. The quadratic behavior predicted by

Equation 3.7 is not evident to the eye, indicating that the value of the coefficient of the quadratic term in Equation 3.7 must be relatively small. The quadratic coefficient, β_2, is:

$$\beta_2 = \frac{(UA_S + s_2) \times f_O}{\rho c_p} \quad . \tag{3.8}$$

Even if β_2 is increased by a factor of 10, the quadratic aspects of the sensible cooling and heating coil loads are barely visible (Figure 3.3). Thus it appears that simple linear models may adequately describe sensible cooling and heating coil loads in many buildings with simple CAV systems. However, we expect the relationship between cooling and heating coil energy use and outside air temperature to become increasingly non-linear in buildings with large overall load coefficients, in buildings which require large quantities of outside air and in buildings with large solar apertures (Equation 3.8).

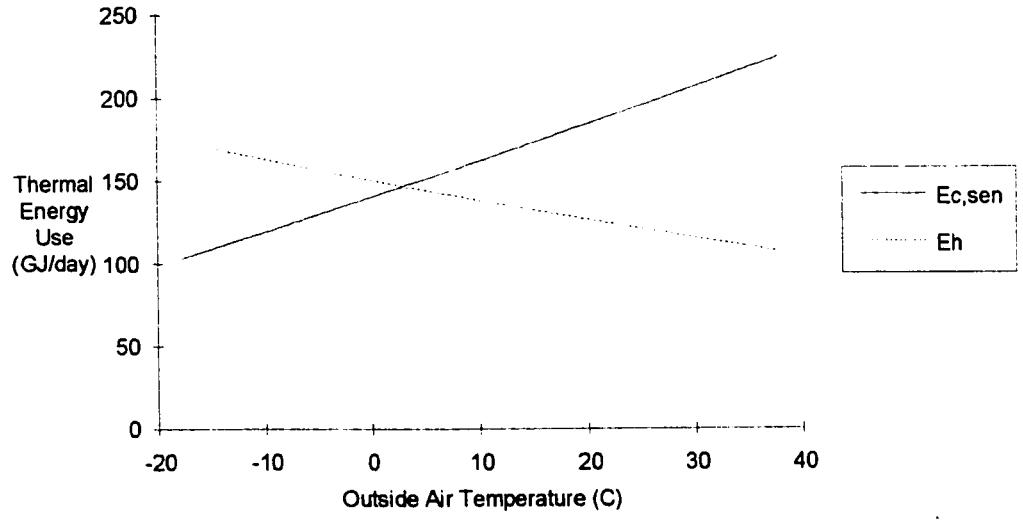

Figure 3.2 Simulated cooling loads for a CAV system. The loads appear to be linearly related to outside air temperature.

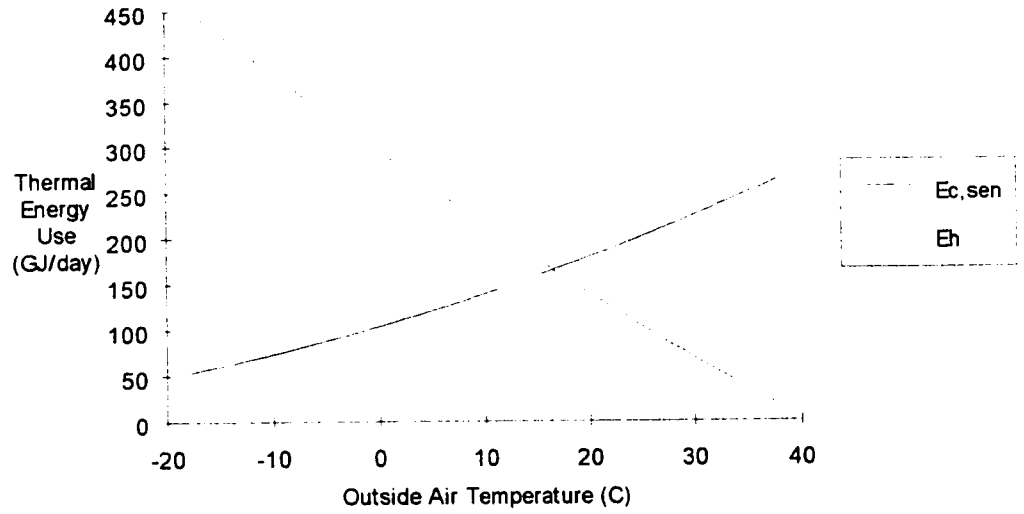

Figure 3.3 Simulated coil loads for a CAV system with β_2 multiplied by 10. The slight quadratic effect is barely visible.

Hot-Deck Reset Schedules in CAV Systems. Many commercial building CAV systems are equipped with additional control options such as hot-deck reset schedules or economizer cycles in order to reduce energy use and improve the level of comfort in the conditioned space. These control options can significantly change the relationship between coil loads and outside air temperature and are examined here.

A hot-deck reset schedule controls the flow of steam or hot water through the heating coils in order to vary the temperature of the air leaving the coils. One type of hot-deck reset schedule is controlled based on outside air temperature as shown in Figure 3.4. The temperature of air leaving the coils is maintained at 48.9 °C when the outside air temperature is less than 10.0 °C and declines linearly to a minimum of 26.7 °C when the outside air temperature reaches 26.7 °C. At outside air temperatures above 26.7 °C, the temperature of the air leaving the heating coils is maintained at 26.7 °C, barely above the temperature of the return air. This type of control can significantly reduce heating and

cooling energy use by limiting the amount of heating added to the building during warm weather.

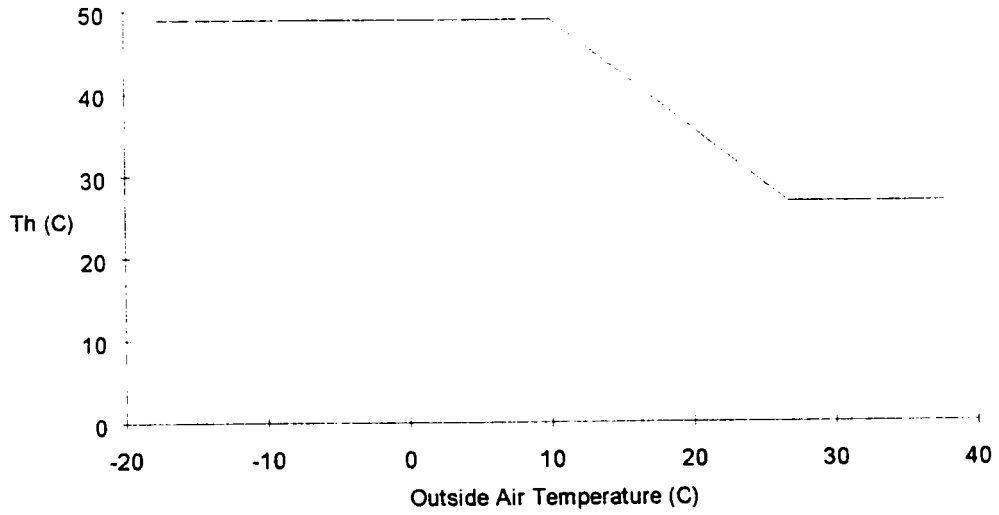

Figure 3.4 A typical outside air, hot-deck reset schedule.

The effect of a hot deck reset schedule on cooling and heating coil energy use can be demonstrated by adding this control option to the simulation model of the engineering center. The previously linear relationships between outside air temperature and coil energy use are now highly non-linear in the temperature interval where the heating coil temperature is being reduced (Figure 3.5). The significant reduction in heating coil energy use as the outside temperature increases is because the heating coil air discharge temperature is being reduced. Less cooling energy use is required to balance the warm air during mixing conditions now that the warm air stream is at a lower temperature.

In practice, the magnitudes of the reductions in energy use caused by a hot-deck reset schedule will differ depending on the set-points and design characteristics of the actual system. However, these simulation results clearly indicate the dramatic effects that hot-

deck reset controls can have on heating and cooling coil energy use. These results also suggest the need for non-linear models of cooling and heating coil loads when hot-deck reset controls are operational.

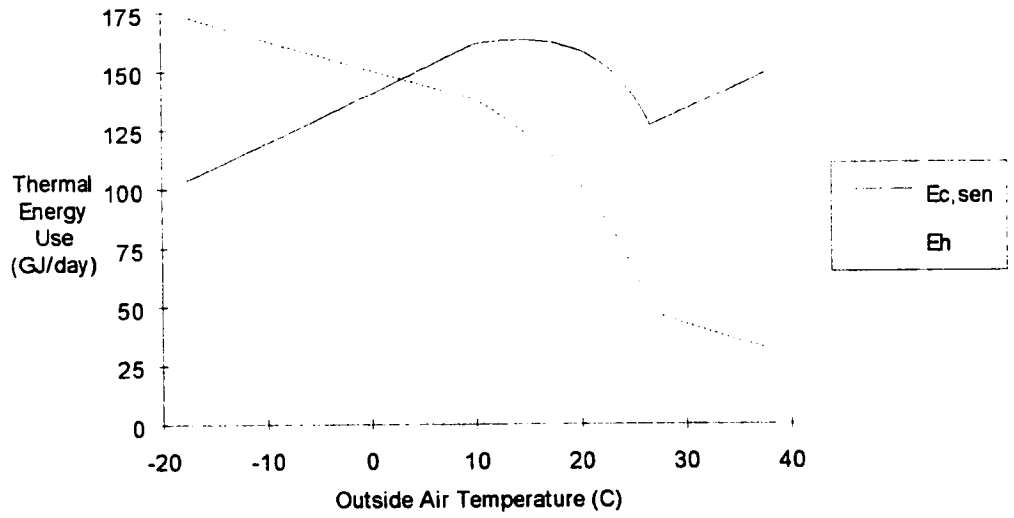

Figure 3.5 Simulated coil loads for a CAV system with an outside air, hot-deck reset schedule.

Economizer Cycles in CAV Systems. An economizer cycle is another control feature commonly used with CAV systems. Economizer cycles vary the amount of outside air mixed with the return air stream in order to minimize the load on the cooling coil. Although there are many different control algorithms, a typical control algorithm based on outside air temperature is shown in Figure 3.6 (Mitchell, 1983). At temperatures below the cooling coil temperature (taken here as 12.8 °C), the fraction of outside air to return air is varied so that the mixed air temperature exactly equals the cooling coil temperature, thus eliminating all load on the cooling coil. When the outside air temperature is between the cooling coil temperature and the return air temperature (taken here as 22.2 °C), all of

the return air is exhausted to the out of doors and replaced by outside air, thereby minimizing the cooling coil load. At outside air temperatures above the return air temperature, the fraction of outside air is set to the minimum required for ventilation (here taken as 10% outside air).

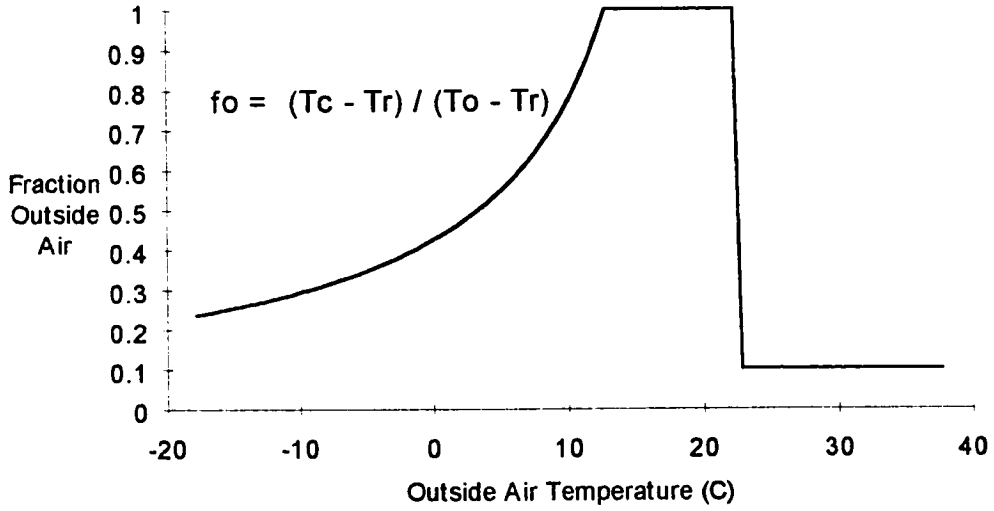

Figure 3.6 Typical economizer control based on outside air temperature.

Sensible cooling and heating coil loads for a CAV system with this type of economizer control have been simulated for the engineering center (Figure 3.7). As expected, the economizer eliminated the sensible portion of the cooling coil load for ambient temperatures below the cooling coil temperature (12.8 °C). As the outside air temperature climbs higher than the cooling coil temperature, the cooling coil load exhibits a segmented linear behavior. The heating coil load also appears to have three linear sections. As in the case of the hot-deck reset schedule, the exact change-points and slopes of the coil loads will depend on the set-points and design characteristics of the system. Once again, we conclude that highly flexible, segmented linear or polynomial models

appear necessary to model cooling and heating energy use when an economizer cycle is in use.

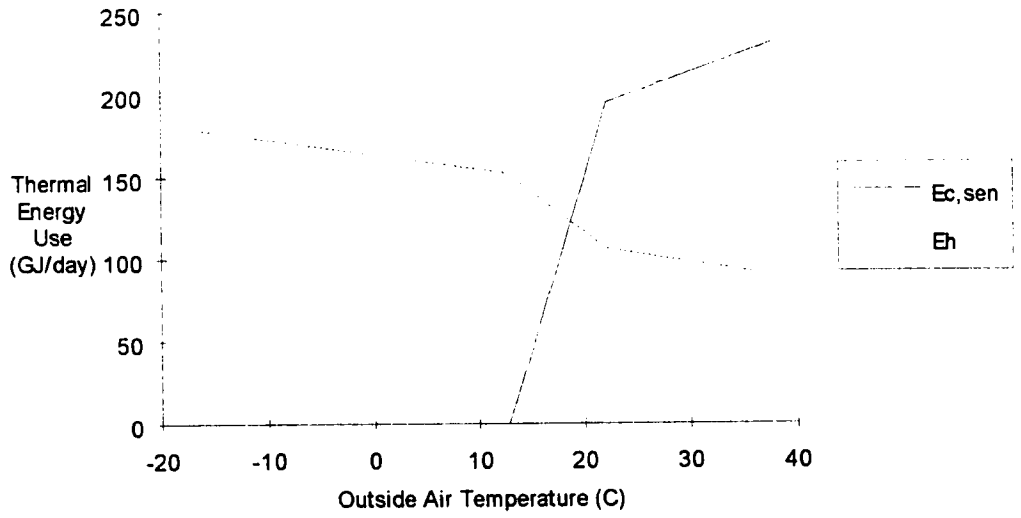

Figure 3.7 Simulated coil loads for a CAV system with an economizer cycle.

Variable-Air-Volume Systems

Dual-duct, VAV systems differ from dual-duct CAV systems in two important ways. First, many VAV systems utilize variable-frequency-drive technology to modulate the speed of the supply air fan(s) and hence modulate the supply of air to the zones. Second, VAV systems use a control algorithm which minimizes the mixing of hot and cool air streams in the zone mixing boxes. Because of these differences, VAV systems typically use far less fan and coil energy than CAV systems and in many cases are specified as retrofits to replace CAV systems.

Figure 3.8 shows the different mixing box control algorithms used by CAV and VAV systems (Knebel, 1983). In a CAV system, the total flow rate (represented by the dotted line) is constant. This flow rate is determined during the design process so that the zone

set-point temperature can be maintained when the maximum cooling or heating load anticipated is applied to the zone. Because of this, the volume of air flowing through the space far exceeds the minimum required to provide adequate ventilation. In addition, warm and cool air streams are mixed to meet the zone load, thereby consuming much more energy than is actually required to heat or cool the space.

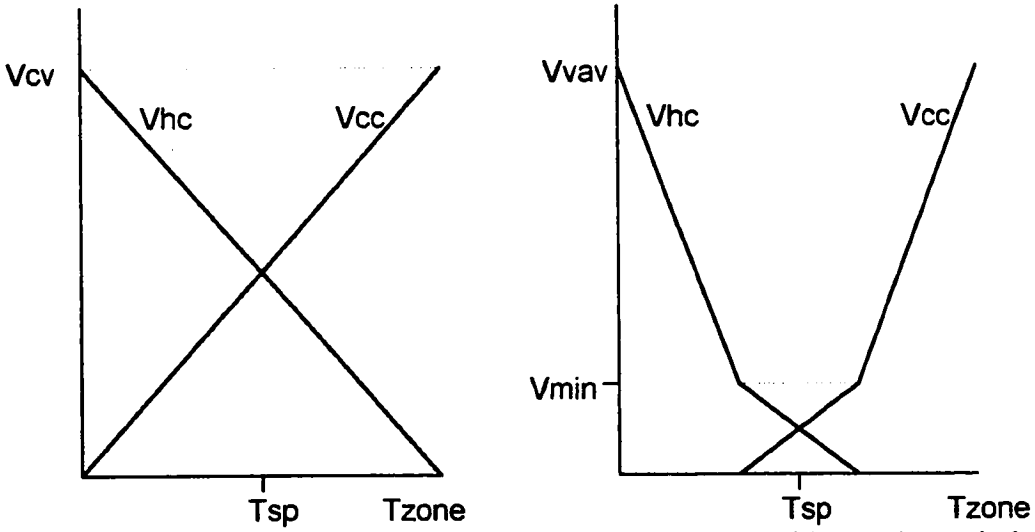

Figure 3.8 Schematic of CAV and VAV mixing box control algorithms. The vertical axis is the volume flow rate of air through the mixing box and the horizontal axis is the zone temperature.

In a VAV system, when a large cooling load is applied to a zone the flow rate of the cool air stream is modulated to exactly match the cooling load while no warm air is allowed to flow into the zone. Similarly, when a large heating load is applied to a zone, the flow rate of the warm air stream is modulated to meet the heating load while the flow of cool air to the zone is shut off. This type of control eliminates the mixing of cool and warm air streams during high load conditions. During low load conditions, heating and cooling air streams are mixed to satisfy the minimum ventilation requirement.

VAV system sensible cooling and heating coil loads at the engineering center were simulated and the results are shown in Figure 3.9. Two differences between VAV and CAV coil loads are immediately apparent. First, energy use in the VAV system is significantly less than the energy use in the CAV system at all temperatures (see Figure 3.2 for comparison). Second, VAV coil energy use exhibits a strong change-point behavior in contrast to the nearly linear relationship between CAV coil energy use and outside air temperature. Thus, it appears that VAV sensible coil energy use can be modeled using a segmented linear model. Note that in both CAV and VAV systems, the presence of internal loads precludes cooling energy use from going to zero even at low outside air temperatures.

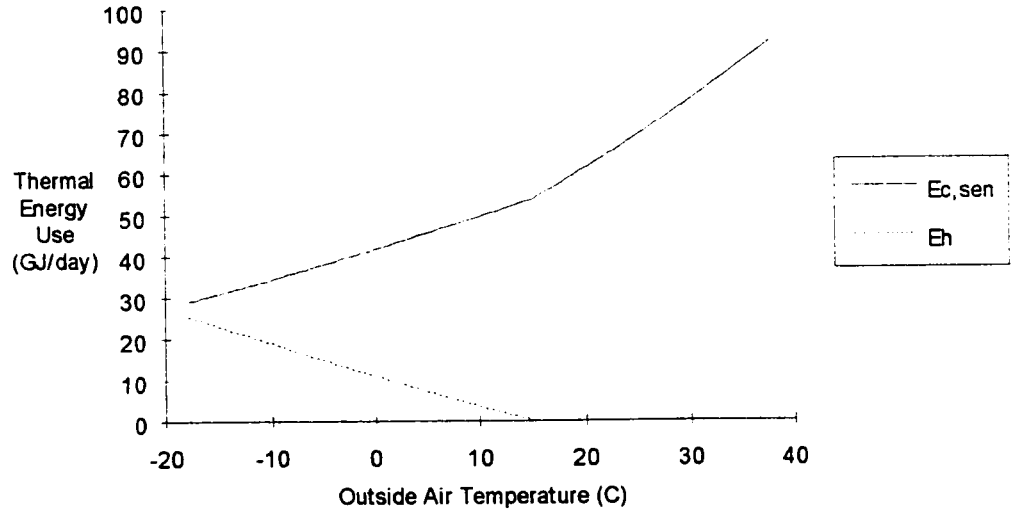

Figure 3.9 Simulated coil loads for a VAV system.

It is apparent in Figure 3.9 that for the building simulated here no heating energy is required when the outside air temperature is above 15 °C. It is also apparent that in this building the flow of cool air is never entirely shut off. These results are, however,

somewhat specific to the building being simulated. To understand what the form of the coil loads may look like in a different building with lower internal loads and a higher building load coefficient, the UA value of the building was increased by a factor of five and the simulation repeated.

The coil loads shown in Figure 3.10 show the three modes of VAV operation apparent in Figure 3.8: cooling off and heating on, both cooling and heating on, and heating off and cooling on. At outside temperatures above 21 °C, the cooling and heating coil energy use correspond to the condition in Figure 3.8 where no heating is required and cooling energy use increases rapidly with increasing zone temperatures. At moderate outside air temperatures between 8 °C and 22 °C, some mixing of cool and warm air streams is required in order to meet minimum air flow requirements, thus the building is simultaneously using both cooling and heating energy. During cold weather below 8 °C, heating energy use increases sharply to meet zone heating requirements (Figure 3.8). Although no cooling is required in the exterior zones, the interior zones still require some cooling to offset internal gains from people and equipment resulting in cooling loads of between 25 and 30 GJ/day. Outside air temperature has less influence on cooling energy use at low temperatures because only the interior zones, which have no conduction losses to the environment, are requiring cooling.

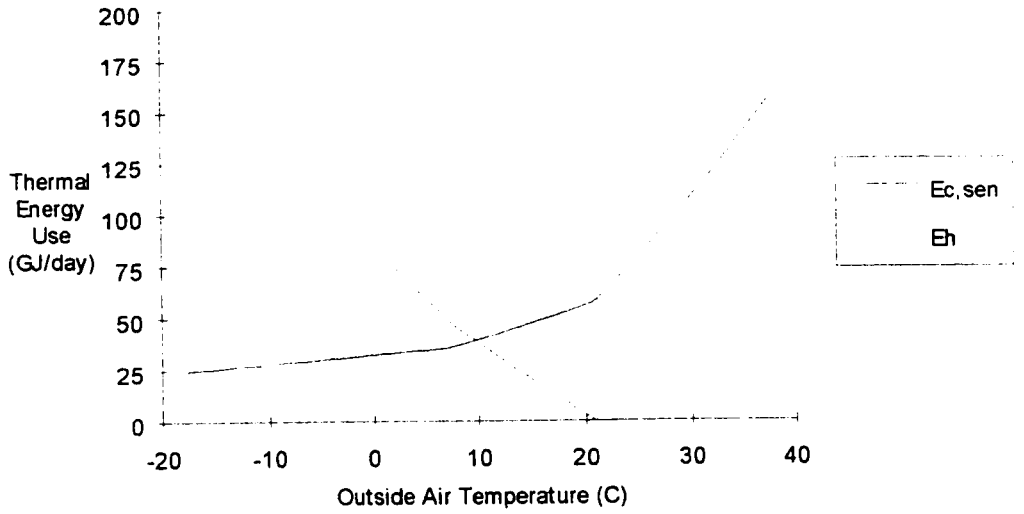

Figure 3.10 Simulated coil loads for a VAV system in a building with a high building load coefficient (UA value).

Economizer Cycles in VAV Systems. While hot-deck schedules are redundant in VAV systems, economizer cycles reduce the cooling coil load by using free cooling provided by the outside air whenever possible. The economizer cycle described in the previous section was used in conjunction with a VAV system to simulate the coil loads shown in Figure 3.11. By comparing sensible cooling coil loads in Figures 3.9 and 3.11, it is apparent that economizer cycles significantly reduce cooling coil energy use during cool weather even when used with a VAV system. The economizer cycle limits simultaneous heating and cooling to outside air temperatures between 13 °C and 15 °C and is by far the most efficient system considered thus far. As before, segmented linear models appear adequate to describe coil loads in a VAV system with an economizer cycle.

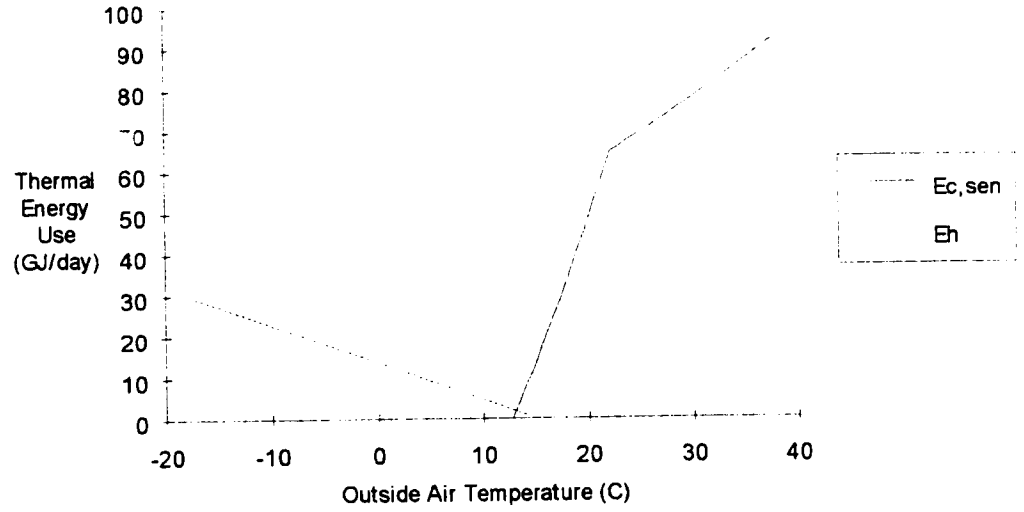

Figure 3.11 Simulated coil loads for a VAV system with an economizer cycle.

Latent Loads

Latent loads can be a significant part of the overall cooling coil load in commercial buildings, especially in humid climates. Internal sources of moisture in commercial buildings include human respiration and perspiration, plant respiration and moisture evaporated into the air during cooking and cleaning. These sources are essentially independent of the outside air temperature and depend on the occupancy and functionality of the building.

Moisture is also carried into the building with ventilation air. When the dew-point temperature of the ventilation air is greater than the dew-point temperature of the cooling coils, water vapor is condensed on the cooling coils and removed from the air stream. The energy required to condense the water vapor in the ventilation air is the latent ventilation load, $E_{c,lat}$:

$$E_{c,lat} = V_r \times f_o \times \rho h_v \times (W_o - W_{dp,c})^+ \qquad (3.9)$$

where ρh_v is the product of the air density and the latent heat of vaporization of water, W_O is the specific humidity of the outside air and $W_{dp,c}$ is the specific humidity that corresponds to the dew-point temperature of the air leaving the cold deck.

An examination of six months of outside air specific humidity and dry-bulb temperature data in central Texas reveals a general trend of increasing specific humidity with increasing temperature (Figure 3.12). However, there is also significant scatter in the data reflecting periods of high and low humidity at nearly every temperature. The smooth boundary to the upper left of the data points is the 100% relative humidity line. Specific humidity peaks in the pre-dawn hours when temperatures are usually less than 28 °C and decreases after sunrise as the outside temperature climbs.

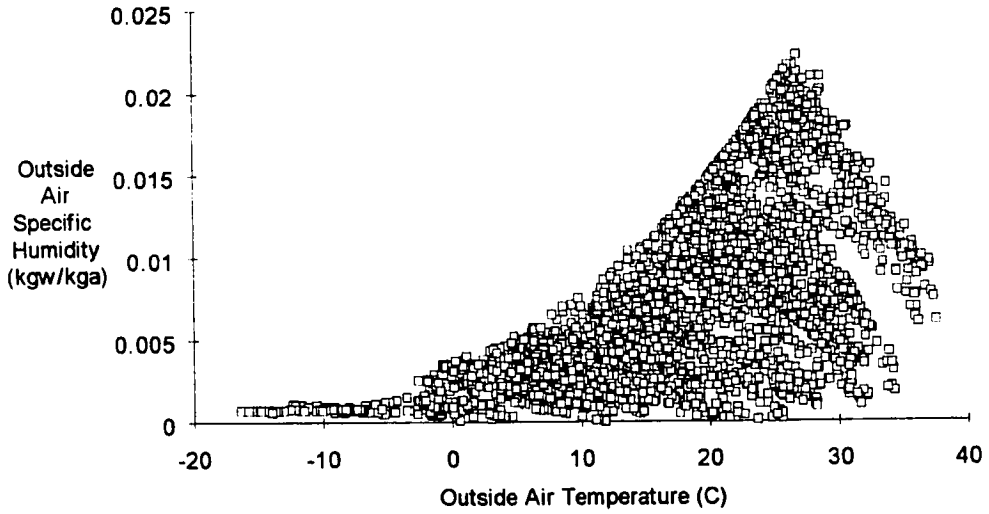

Figure 3.12 Six months of hourly, outside air specific humidity data plotted versus dry-bulb temperature data from central Texas.

To determine the effects of outside air humidity on the cooling load, the data set shown in Figure 3.12 was used as input to the simulation model. Other parameter's which influence the cooling coil load such as internal loads were held constant. Figure 3.13

shows the total hourly cooling coil load, E_C, for CAV and VAV systems plotted against outside air temperature. The lines of points forming the bottom of the data represent the sensible cooling loads at different outside air temperatures. The fan shapes are caused by the latent ventilation loads. Regression models of cooling energy use would show a clear change-point at about 13 °C where latent loads begin to appear and the shape of the cooling energy use data increases. The significant reduction in cooling energy required by the VAV system is also clearly evident.

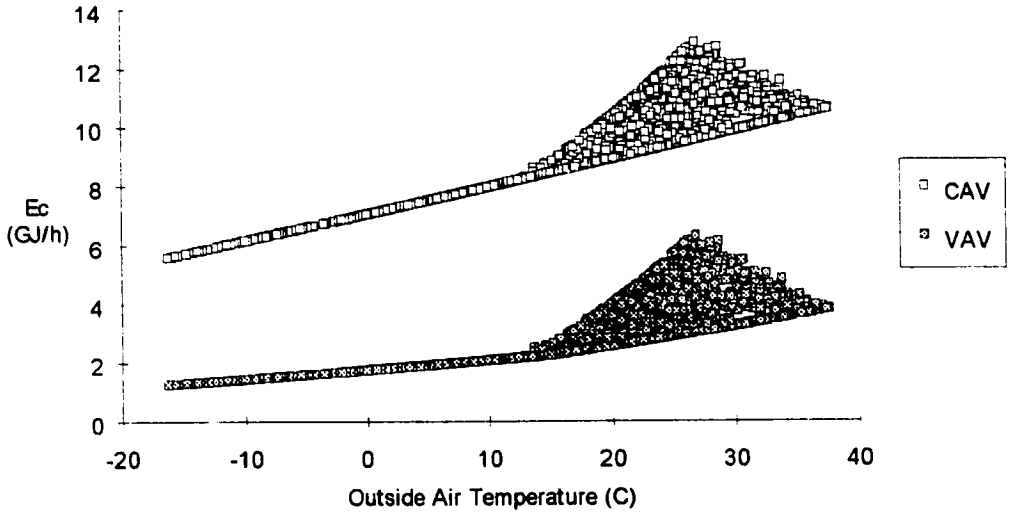

Figure 3.13 Simulated hourly cooling coil loads for CAV and VAV systems. The fan shapes are caused by the latent ventilation loads.

In Figure 3.14, the hourly cooling coil loads have been summed to daily values and the temperatures averaged to give daily average temperatures. The relationship between daily cooling coil loads and outside air temperature is similar to the hourly relationship where the slope of the cooling energy data increases when the outside air temperature is above 13 °C.

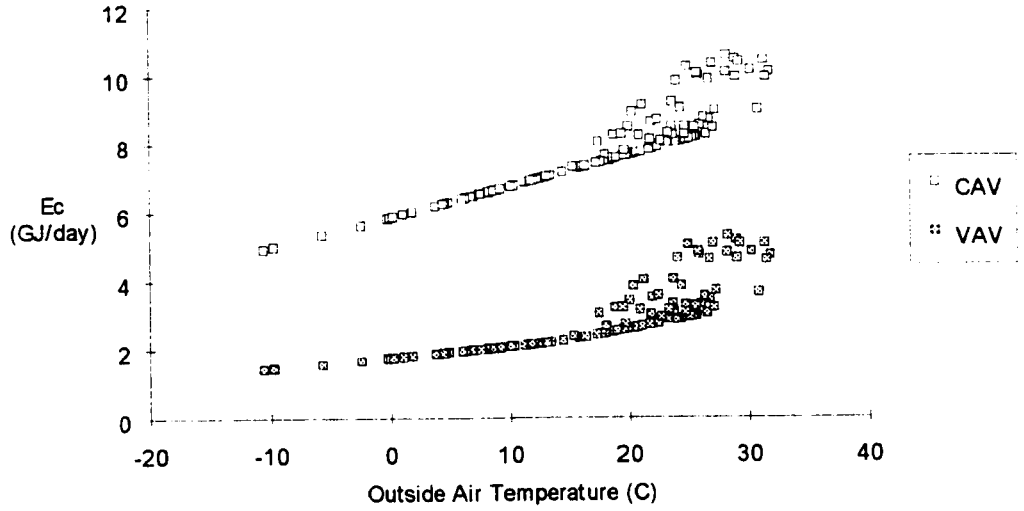

Figure 3.14 Simulated daily cooling coil loads for CAV and VAV systems. The scattered data at high temperatures represent the latent ventilation loads.

Figures 3.13 and 3.14 suggest that temperature dependent regression models of the total cooling coil load should be of change-point or quadratic form to account for the increased latent load at high temperatures. If a change point model is selected, the humidity induced change-point temperature will be approximately equal to the cooling coil dew-point temperature (12.8 °C in this simulation) assuming that the relative humidity of the air leaving the cooling coil is 100%. In VAV systems, both the sensible and latent cooling loads appear to have a temperature change-point near the cooling coil dew-point temperature. Thus, cooling coil energy use in VAV systems may be even more non-linear with temperature than in CAV systems.

Internal Loads

Internally generated loads, such as the heat given off by people and electrical equipment, can be a significant fraction of total cooling load in commercial buildings. The effect of variations in internal loads on cooling and heating coil energy use can be

investigated by varying the electrically generated internal loads from a typical weekday value of 750 kWh/day to a typical weekend value of 375 kWh/day. Figure 3.15 shows that heating energy use increased and cooling energy use decreased when the internal loads were reduced by one half. The magnitude of the differences between weekday and weekend thermal energy use suggests that separate weekday and weekend models may be appropriate for buildings with large differences in internal loads. Separate models will decrease the model error and increase the resolution of the savings. Separate models may also be appropriate for holidays and/or periods when the HVAC system is operated differently.

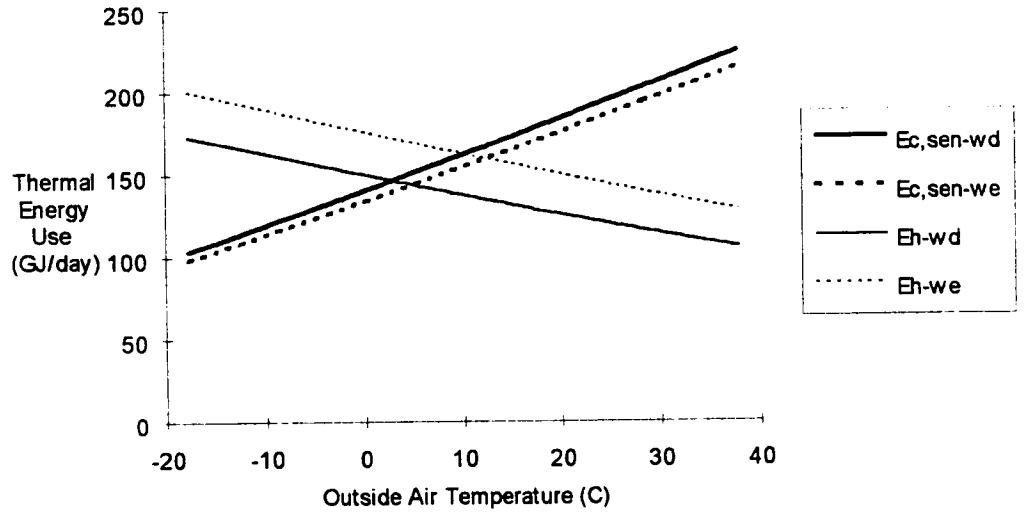

Figure 3.15 Simulated CAV daily cooling and heating coil energy use for hypothetical weekday (750 kWh/day) and weekend (375 kWh/day) internal loads.

As in the case of CAV systems, the effect of differing internal loads on weekdays and weekends on VAV heating and cooling energy use can be significant (Figure 3.16). In these cases, separate models of weekday and weekend thermal energy use are appropriate.

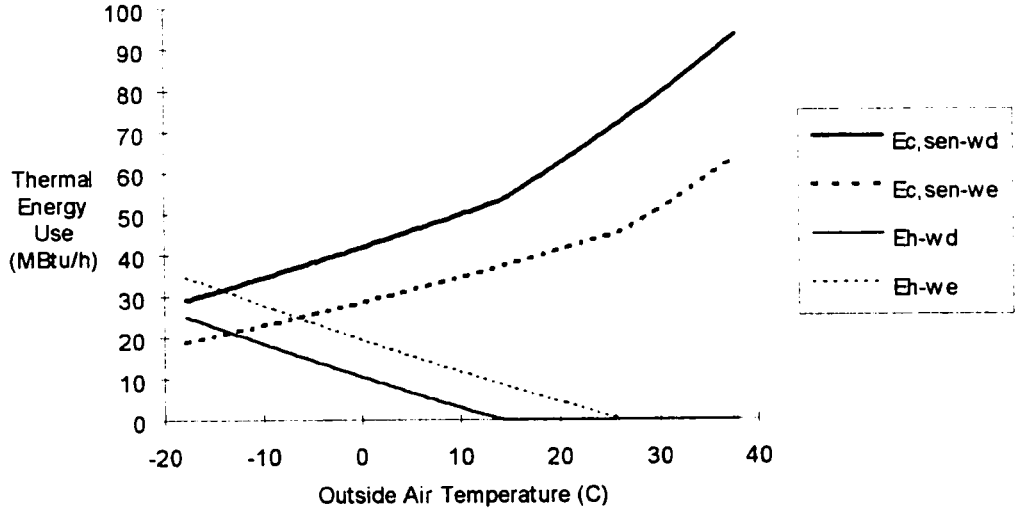

Figure 3.16 Simulated VAV daily cooling and heating coil energy use for hypothetical weekday (750 kWh/day) and weekend (375 kWh/day) internal loads.

Empirical Models of Commercial Building Energy Use

Analysis of mathematical models and simulation results of cooling and heating coil loads from CAV and VAV systems strongly suggests that no single empirical model is appropriate for all energy types and coil loads. This is in contrast to buildings without simultaneous heating and cooling where a three-parameter, degree-day model such as that used by PRISM is widely applicable.

In commercial buildings, we find that some types of energy use are weather independent and are appropriately modeled as the mean energy use in each operating or occupancy period. Weather dependent energy use is strongly influenced by system type, control options, environmental conditions such as ambient humidity, and the physical and operational characteristics of the building such as the building load coefficient and quantity of internal loads. Although a mathematical model of CAV coil loads suggests a quadratic relationship between coil load and outside air temperature, the actual non-linearity appears to be minimal. Much more prevalent are linear and segmented linear relationships between

coil loads and outside air temperature. In general a two, or in some cases three, change-point segmented linear model will describe most of load shapes examined here. Hence, we propose the following empirical models to describe commercial building energy use.

The simplest model is the one-parameter, mean model appropriate for weather independent types of energy use such as constant-air-volume air handler and lighting and receptacle electricity use (Figure 3.17a):

$$\hat{E} = \beta_0 \tag{3.10}$$

where $\hat{E}$ is the predicted energy use and β_0 is the mean energy use.

The simplest empirical model appropriate for weather dependent energy use is the linear relation (Figure 3.17b)

$$\hat{E} = \beta_0 + \beta_1 \times T_o \tag{3.11}$$

where β_0 and β_1 are regression coefficients. This relation is called a two-parameter model because two parameters, β_0 and β_1, are determined by regression. Simple linear models may be appropriate for constant-air-volume systems without added control features such as hot deck reset or an economizer cycle (Figures 3.2 and 3.3).

Three-parameter models are appropriate when the energy use is flat or zero at some ambient temperatures and essentially linear at other temperatures. Three parameter heating and cooling models are (Figures 3.17c and 3.17d):

$$\hat{E}_h = \beta_0 + \beta_1 \times (T_o - \beta_2)^- \tag{3.12}$$

$$\hat{E}_c = \beta_0 + \beta_1 \times (T_o - \beta_2)^+ \tag{3.13}$$

respectively, where β_0 is a constant, β_1 is the model slope and β_2 is the change-point temperature. The minus sign on the set of parentheses in Equation 3.12 indicates that the value of the quantity is zero when $(T_o - \beta_2)$ is positive. Similarly, the plus sign on the parentheses in Equation 3.13 indicates that the value of the quantity is zero when $(T_o - \beta_2)$ is negative. Three-parameter models are suggested for cooling energy use for systems with economizer cycles (Figures 3.7 and 3.11) and for VAV heating energy use (Figures

3.9, 3.10 and 3.11). Three parameter models are also appropriate for buildings without simultaneous heating and cooling where the degree-day approach (Equation 1.5) is justified.

Four-parameter, change-point models (Ruch and Claridge, 1992a) of the form (Figures 3.17e and 3.17f:

$$\hat{E} = \beta_0 + \beta_1 \times (T_o - \beta_3)^- + \beta_2 \times (T_o - \beta_3)^+ \qquad (3.14)$$

describe the segmented linear relationships found in many of the systems described above. These models are particularly appropriate for describing VAV energy use (Figure 3.9) and non-linearities caused by hot deck reset schedules (Figure 3.5), economizer cycles (Figures 3.7 and 3.11) and latent loads (Figures 3.13 and 3.14).

Chapter Summary

In this chapter, the appropriate forms of regression models were derived for heating and cooling energy use in constant-air-volume (CAV) and variable-air-volume (VAV) air distribution systems. These particular systems were chosen for analysis because of their wide use and because the replacement of CAV with VAV air distribution systems is a common retrofit to commercial buildings. In addition, the effects on heating and cooling energy use of commonly used control options and latent and internal loads were also investigated. The simulation results suggested that the relationship between heating energy use and outside air temperature is strongly influenced by the type of HVAC system, control options, and latent and internal loads. Thus, no single functional form of regression equation is appropriate for all cases. We therefore propose a "tool kit" of one, two, three and four parameter models which between them embody the flexibility to model a wide variety of energy use patterns typically found in commercial buildings.

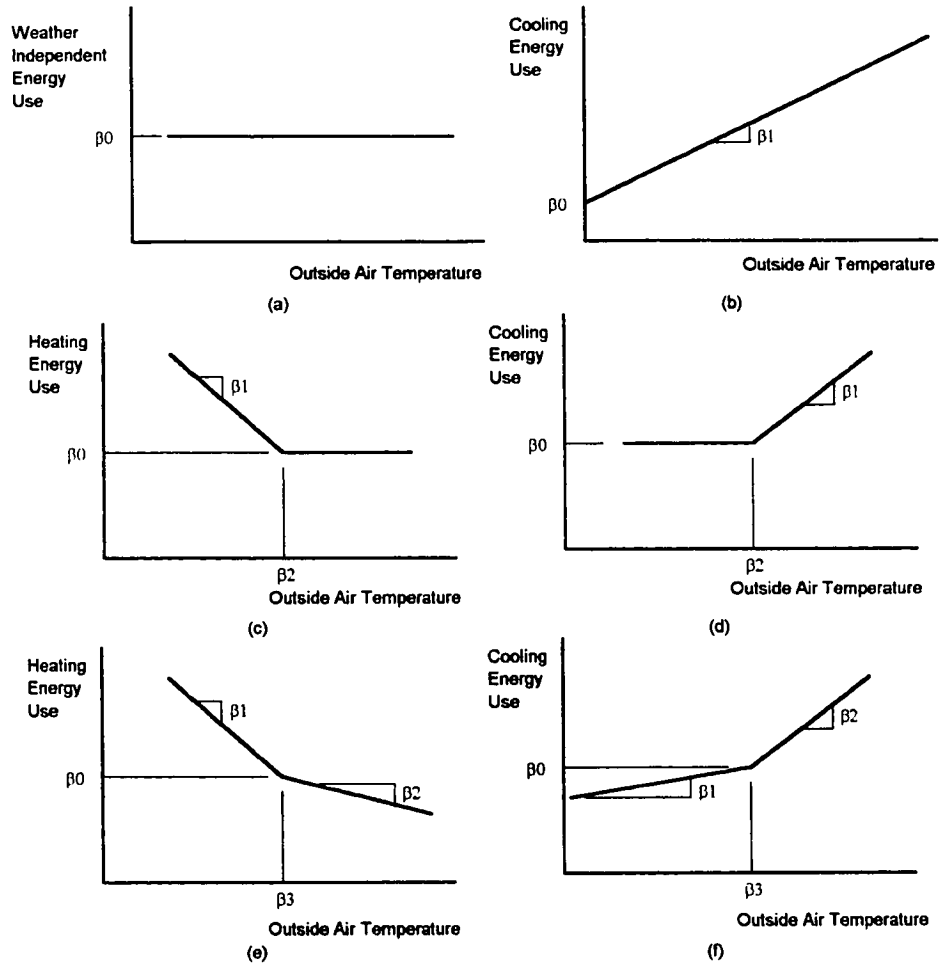

Figure 3.17 Empirical energy use models appropriate for commercial building energy use: a) one-parameter model, b) two-parameter model shown for cooling energy use, c) three-parameter heating energy use model, d) three-parameter cooling energy use model, e) four-parameter heating energy use model and f) four-parameter cooling energy use model.

CHAPTER IV

OVERVIEW OF METHODOLOGY TO MEASURE ENERGY SAVINGS

This chapter provides an overview of the methodology developed in this dissertation to measure energy savings in commercial buildings. In the preceding and subsequent chapters, individual aspects of the methodology are developed in detail. In Chapter X, the entire methodology is demonstrated with a detailed example of measuring savings at a single building, followed by modeling and savings results for eight other buildings which underwent energy conservation retrofits as part of the Texas LoanSTAR program.

Scope of Savings Methodology

This methodology is limited to those cases where post-retrofit and approximately three months or more of pre-retrofit energy use data are available. Although there are no absolute rules for determining the minimum acceptable length of the pre-retrofit period, Chapter VII discusses the likely annual prediction error when the pre-retrofit period is less than one year. When very little or no pre-retrofit energy use data is available to establish baseline conditions, it may still be possible to estimate energy savings using simulation models (Katipamula and Claridge, 1993).

This methodology measures "actual" energy savings, and does not attempt to measure "normalized" savings -- the savings that would have occurred in a year of normal weather conditions (Fels, 1986; and Ruch and Claridge, 1992b). This methodology can be adapted to measure normalized savings by using long-term, average weather data as input to the pre- and post-retrofit models; however, the methodology to determine the uncertainty of savings presented in Chapter VI was not developed for this application and so the uncertainty of normalized savings cannot be determined using the methodology presented in this dissertation.

The methodology measures energy savings only and does not determine cost savings resulting from reducing the peak electrical demand.

The weather-dependent, empirical models used in this methodology are most appropriately used with data time-intervals long enough that transient energy storage effects are negligible. In Chapter II it was shown that data time intervals of 24 hours or longer generally satisfy this requirement. The use of this methodology with monthly billing data has not been tested.

The methodology was developed to use whole-building heating, cooling and electricity use data. No models were explicitly developed for the case in which a single fuel supplies both heating and cooling. EModel, which is described in Chapter V, is sufficiently flexible, however, that it can identify quadratic and multiple regression models which may describe this behavior.

The empirical models used in this methodology were developed to describe energy use in commercial building, air-side HVAC systems. In some cases, however, they have been shown to adequately model energy use by primary HVAC equipment (Ruch and Claridge, 1992a; and Kissock et al., 1993a). The ability of these models to describe energy use in residences and buildings without simultaneous heating and cooling has not been tested; however, it is expected that the three parameter model will be applicable to this class of buildings because of it's intrinsic similarity to the degree-day methodology used by PRISM.

Savings Measurement Methodology

This methodology developed in this dissertation involves the following six tasks.

Collecting and Pre-Processing the Data. The savings measured by this methodology are only as good as the energy use data from which they are derived. The first tasks

therefore, are to collect the relevant energy use and temperature data, inspect and clean the data to assure its quality, and pre-process the data into daily time-intervals. A brief description of how these tasks are performed in the LoanSTAR program is included in Chapter X with several references cited for more detailed information.

Identifying the Pre- and Post-Retrofit Periods. The next step in the process of measuring savings is identifying the pre-retrofit, construction and post-retrofit periods. The pre-retrofit period extends until retrofit construction influences the energy consumption of the building. If a detailed schedule of construction activities is available, then the end of the pre-retrofit period may be determined from the schedule. In many cases, however, exact retrofit construction dates are difficult to obtain. In these cases, the end of the pre-retrofit period and the beginning of the construction period can often be determined by inspecting energy consumption data for irregularities. Identification of the pre-retrofit period by inspection of time-series plots is demonstrated in Chapters V and X.

Pre-Retrofit Model Selection. The next step is to identify a pre-retrofit model for each type of energy-use affected by the retrofit. In this methodology, weather-independent energy use is described by one or more one-parameter, mean models. Weather-dependent energy use, such as the energy used to supply heating and cooling to a building, is modeled using one or more two, three or four-parameter models. Multiple models are required when the energy use during different operating periods is significantly different, as may be the case for weekdays and weekends.

The criteria used to select the most appropriate model is to maximize the goodness-of-fit using the simplest model or combination of models. Although several measures of a model's goodness-of-fit are available, we prefer to use the coefficient of variation of the standard deviation (CV-SD) for one-parameter models and the coefficient of variation of

the root mean square error (CV-RMSE) for two, three and four-parameter models (SAS, 1989).

$$\text{CV-SD} = 100 * \frac{\left[\sum_{d=1}^{n}(Ed - \bar{E})^2 / (n-1)\right]^{\frac{1}{2}}}{\bar{E}} \tag{4.1}$$

$$\text{CV-RMSE} = 100 * \frac{\left[\sum_{d=1}^{n}(Ed - \hat{E}_d)^2 / (n-p)\right]^{\frac{1}{2}}}{\bar{E}} \tag{4.2}$$

In Equations 4.1 and 4.2, E_d is energy use on any day d, $\bar{E}$ is the mean daily energy use, $\hat{E}_d$ is the daily energy use predicted by the pre-retrofit model, n is the number of days in the pre-retrofit period, and p is the number of regression parameters in the model. The CV-SD and CV-RMSE are non-dimensional measures of the deviation of the data from the model. As defined in Equations 4.1 and 4.2, CV-SD and CV-RMSE are expressed as percentages. The squared term in each numerator has the effect of giving more weight to the larger residuals.

The R^2 value, another popular measure of goodness of fit, compares the fit of a regression model to the fit of a mean model. This is apparent in Equation 4.3 where the sum of the squared deviations of the data from the model are normalized by the sum of the squared deviations from the mean.

$$R^2 = 1 - \frac{\sum_{d=1}^{n}(E_d - \hat{E}_d)^2}{\sum_{d=1}^{n}(E_d - \bar{E})^2} \tag{4.3}$$

A low R^2 value indicates that a mean model will fit the data nearly as well as a regression model; a high R^2 value indicates that the addition of a predictor variable(s) in the regression model has substantially improved the fit of the regression model over the mean

model. R^2 gives little indication, however, of the overall fit of the model because the deviation (scatter) of data from the regression model is divided by the deviation (scatter) of data from the mean model. Hence, two data sets with very different amounts of scatter can have similar R^2s if the importance of the relative predictor variables in each model are similar. For these reasons, we prefer to use CV-RMSE as the primary measure of two, three and four-parameter models' goodness of fit.

If the sole criteria for model selection was simply to maximize goodness of fit, then separate four-parameter models for weekdays and weekends would always be chosen because this combination of models has a high number of "degrees of freedom" with which to fit the data. However, in many cases the differences between the CV-RMSEs of two-, three- and four-parameter models are very modest. In these cases, we select the simplest model, i.e. the model with the smallest number of parameters. The same procedure is used to determine when weekday and weekend models are appropriate. If subjectivity in model selection is to be minimized, an f-test or t-test will measure the likelihood that for a given confidence level two models are identical (this test procedure is outlined in Appendix D). Note, however, that this test does not entirely eliminate the subjective nature of the choice of the proper combination of models because a somewhat arbitrarily chosen confidence level must still be specified. The model selection procedure is demonstrated in Chapters V and X.

Calculating Savings. Once the pre-retrofit model(s) has been selected, retrofit savings are determined by subtracting measured energy use in the post-retrofit period E_p from the baseline energy use predicted by the pre-retrofit model $\hat{E}_b$. The total savings E_s during any period of m days in the post-retrofit period is the sum of the individual daily savings:

$$E_S = \sum_{i=1}^{m} (\hat{E}_{b,i} - E_{p,i}) \tag{4.4}$$

Savings can be automatically calculated according to Equation 4.4 by EModel.

Determining the Uncertainty of Savings. The determination of the uncertainty of savings must take into account both systematic and random errors. A major potential source of systematic error (sometimes called bias) can arise when the pre-retrofit period is less than a full year in length. Chapter VI develops guidelines to assess the likely magnitude of this type of error.

A methodology to determine the uncertainty of savings due to random (or modeling) error is developed in Chapter VI. This methodology can be implemented through the program PredErr. The determination of the uncertainty of savings is demonstrated in Chapters VI, VII and X.

Measuring the Efficiency of Air-Side HVAC Systems. Chapter VIII develops a methodology to measure the efficiency with which air-side HVAC systems provide the required heating and cooling to a building. This efficiency is called the Energy Delivery Efficiency. If a retrofit to the air-side HVAC systems is performed, then determining the Energy Delivery Efficiency of the pre and post-retrofit HVAC systems can help to evaluate the effectiveness of the retrofit and the potential for further energy efficiency improvements. The Energy Delivery Efficiency is calculated and interpreted for the case study buildings in Chapter X.

Chapter Summary

This chapter discussed the scope of the savings methodology and then outlines the major sub-tasks. The entire methodology except for the determination of the uncertainty

of savings can be implemented in the EModel program described in the next chapter. Each of these tasks is developed in detail in subsequent chapters and applied to nine buildings in Chapter X.

CHAPTER V

EMODEL: AN INTEGRATED ENERGY ANALYSIS AND MODELING TOOL

While computer technology has vastly increased the quantity and quality of measured building energy use data, our ability to analyze the data has not kept step. As a result, building energy use data that could be used to identify operational and maintenance problems, point to new and innovative ways to reduce energy costs or determine retrofit savings are routinely discarded. In this chapter, we draw upon information system and data analysis theory to introduce EModel, a tool for the analysis of building energy use data and the determination of retrofit savings.

EModel simplifies the previously laborious tasks of data analysis and modeling through a user-friendly interface. The non-linear and multiple regression models of commercial building energy use derived in Chapter III are easily implemented in EModel. The use of EModel's data handling, graphics and modeling features to determine savings are demonstrated. This chapter was adapted from Kissock et al. (1993b).

Introduction

> Data have typically been easier to gather than to analyze. J. W. Tukey (Tukey, 1988)

The much heralded reduction in the cost and the coincident increase in the power of microprocessors and computer memory has fundamentally changed the way building environmental systems are controlled. Traditional pneumatic analog controls are being replaced by direct digital controls that are often coordinated by a single desk-top microcomputer. At first, the analog control algorithms were simply translated into the

digital environment. In recent years, however, new control theories and algorithms have been developed to more fully exploit the enormous computational power of the digital environment.

Central to the new control algorithms is the availability of measured pressure, temperature, flow and environmental data. It is now common for a building's energy management and control system (EMCS) to regularly process and record hundreds of channels of measured data at time intervals as short as a second. As a consequence of this, enormous quantities of data are now available for analysis. Shoshona Zuboff discussed this phenomena in her seminal work, *In The Age of the Smart Machine* (Zuboff, 1988). She proposed that today's smart machines have a double capacity for information; not only do they require information (in the form of coded instructions and input data) to perform their designated task, but they also produce information in the process. The production of information by intelligent machines, which Zuboff calls their capacity to "informate as well as automate" (Zuboff, 1988, p. 10), was often unanticipated by the machine designers. In many cases, however, the information *produced* by the machine is as valuable as the task that the machine was designed to accomplish. For example, bar-code readers were originally designed to speed the retail check-out process, however, their ability to log which items were purchased revolutionized the inventory process and allowed sales to be linked to sales clerks and to customers via credit cards.

Today's EMCSs focus on the primary task of controlling a building's environmental systems. Their ability to make further use of their data collecting ability, however, is under-developed. If they were programmed to collect energy use data, for example, this data could perform several important functions such as identifying operational and maintenance problems (Haberl and Vajda, 1988), identifying new ways to reduce energy costs and improve the productive environment within a building (Reddy et al., 1993), and measuring retrofit savings. In order to perform these tasks, however, the information

content of the data must be enhanced, and this information made accessible to those who can effect the desired changes.

While computer technology has vastly increased the quantity and quality of measured data, our ability to analyze (upgrade) the data has not kept step. Many of the traditional techniques of data analysis, the process of extracting useful information and knowledge from data, are simply too slow, cumbersome and technical to deliver meaningful and timely results to the building energy community. For example, statistical programs powerful enough to consider the complex interactions inherent in the building environment often require a sophisticated knowledge of statistics and the program's unique operating language. Spread sheets, which once revolutionized the graphing process, are still too slow and cumbersome to provide useful *data browsing* tools since each graph must be individually and painstakingly defined. Because of this, the energy use data collected by EMCSs are in many cases simply discarded and any information contained in the data is lost. Thus, a whole new generation of data analysis tools are desperately needed to unlock the information hidden in the vast amount of energy use data now available.

In this chapter, we describe EModel -- a tool developed explicitly for the analysis of energy use in buildings and the determination of retrofit savings. EModel was created using theories and techniques from the fields of data analysis and information systems. We describe EModel within these frameworks, frequently referencing the work of Princeton mathematician John Tukey. Tukey has been called the father of modern data analysis. He pioneered many of the organizing principles of data analysis and overcame the traditional bias in statistics against graphical analysis. We listened closely to his advice when designing EModel.

The EModel Environment

> In particular, we must have flexibility, not only of the choice of a model for summarization, but also in the selection of the data to be employed... as well as in choosing the fitting procedure. J. W. Tukey (Tukey, 1988)

EModel is designed to speed and simplify the data analysis process for the building energy community. It operates in the Windows™ (Microsoft®, 1992) operating system for IBM® compatible personal computers. The Windows operating system was chosen because of its widespread use within this community and it's user-friendly, point and click interface.

The EModel work screen is displayed in Figure 5.1. An ASCII (standard text format) file of columnar data can be loaded into EModel by selecting *File, Open* from the menu. Once a data file has been loaded, the user can accept default names for each channel of data, specify new names, or load a file containing names for each data channel into the program. With these two simple steps, the data are now loaded, named and ready for analysis.

The upper window in Figure 5.1, which is displaying information about the data file just loaded "DAILY.DAT ....", is called the value window. EModel displays all numeric information such as model parameters and the name, size and date/times of the data file in this window. Just below it is the graph window inside which all graphs are displayed. The *Y Variable* and *X Variable* text-boxes to the upper right list the variable names specified by the user. To select a variable for analysis, click on it in these text-boxes. Time series, XY, animated and histogram graphs are displayed by simply clicking on the preferred graph button at the right of the screen. The six types of statistical models provided by EModel are displayed along the bottom of the screen. Clicking on a model button commands EModel to draw the model line in the graph window and display the model parameters and measures of goodness-of-fit in the value window.

The menu bar at the top of the screen is where most of the data processing and manipulation features can be accessed. Numeric and graphic output can be sent to the printer by selecting *File*, *Print* or copied into the clipboard for easy transfer into other Windows applications by selecting options from the *Edit* menu item. Options for modifying the data and creating new variables are included in the *Data* menu item. Options to alter graphics, such as the capability to *Zoom In* on a part of a graph or adjust the scales of the axes are included under the *Graphics* menu item. Retrofit savings calculation procedures are available under the *Savings* menu item. General information about EModel is available from the *Help* menu item.

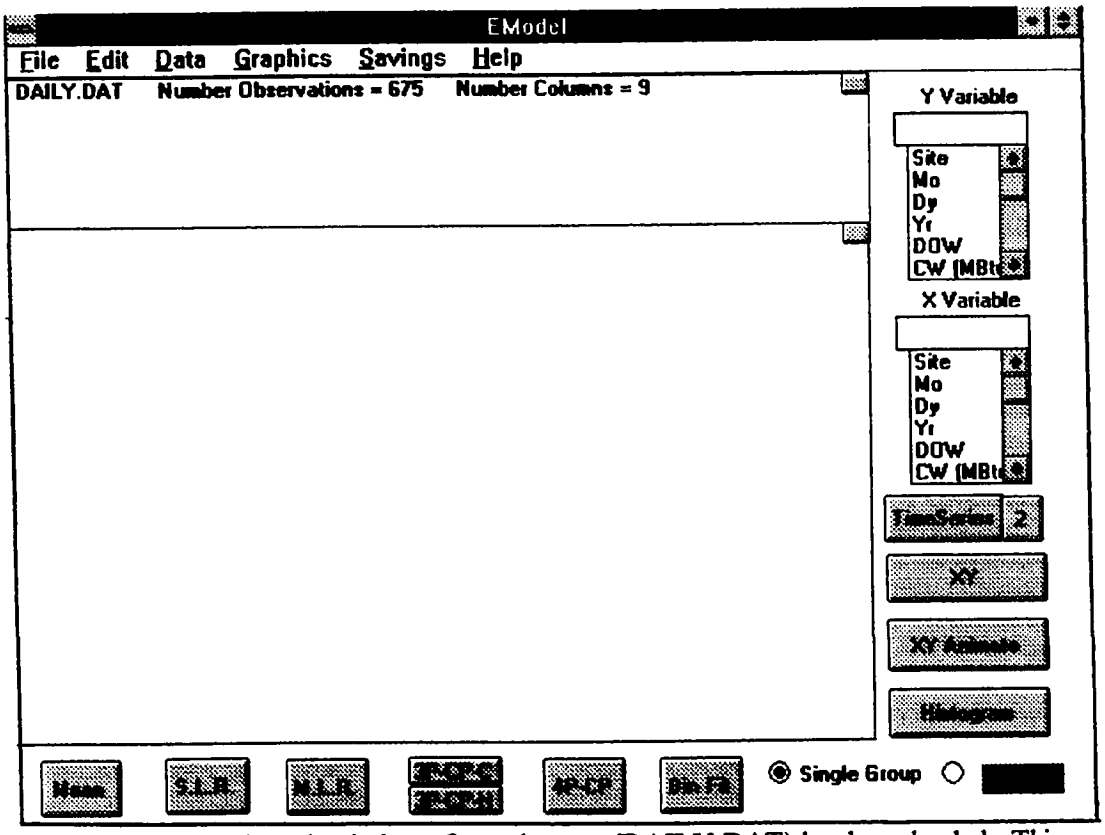

Figure 5.1 EModel work window after a data set (DAILY.DAT) has been loaded. This screen remains visible during the entire work session.

These features provide a high degree of flexibility, ease of use, and modeling power to the analyst. Their use is demonstrated in the following sections.

Graphical Analysis of Energy Use Data

> Exposure, the effective laying open of data to display the unanticipated is to us a major portion of data analysis. Formal statistics has given almost no guidance to exposure; indeed, it is not clear how the informality and flexibility appropriate to the exploratory character of exposure can be fitted into any of the structures of formal statistics so far proposed. J. W. Tukey (Tukey, 1988)

Data analysis begins, Tukey thought, with "flexibility in viewpoint and facilities" and graphical analysis "which dominates any use of numbers" (Tukey, 1988, ps. 8 and xxxvii). Flexible graphical analysis is essential in the early stages of data analysis where new tendencies and relationships among data are explored. This exploratory process, called data browsing, is facilitated in EModel by point and click access to all of the variables in the data base, flexible grouping of the data and automated display of time series, relational (XY), animated and histogram graphs. Graphic displays are produced by simply clicking on the variables to be displayed and then clicking on the appropriate graph button.

Figure 5.2 demonstrates a time-series graph of daily whole-building electricity use at the Winship Building on the University of Texas at Austin campus. The CAV air-handling system at this building was replaced with a VAV system causing the large reduction in electricity use evident in Figure 5.2. The date and time when the VAV retrofit came on line can be determined by simply clicking on the last data point before the precipitous drop in electricity consumption. The selected data point is highlighted with a cursor and the date/time (July 1, 1991) and value of the data point is displayed in the value window. One

can also step through the data by pushing the forward or backward arrow key on the keyboard.

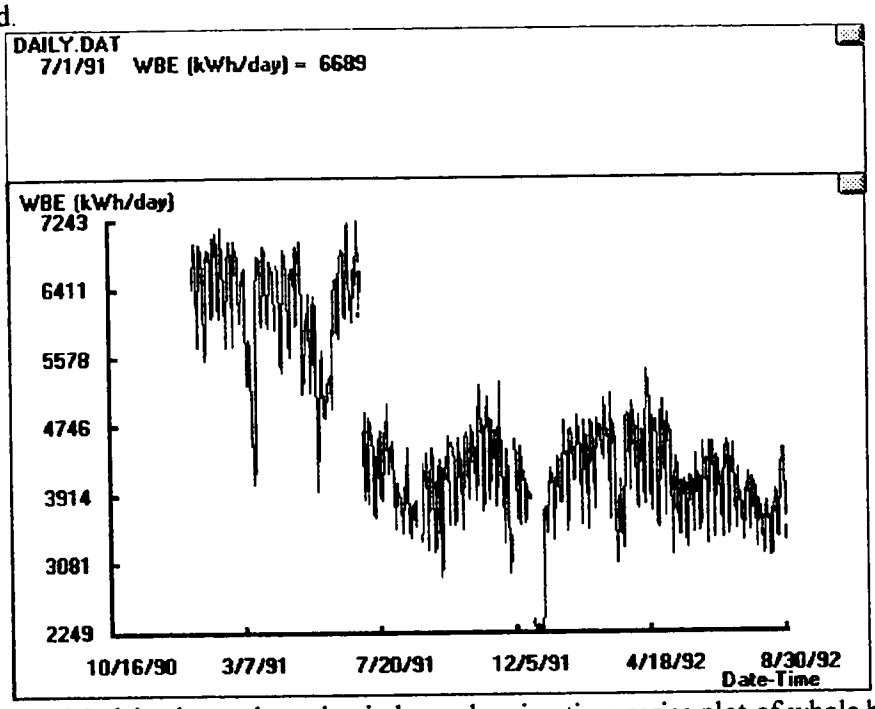

Figure 5.2 EModel value and graph windows showing time-series plot of whole building electricity use. The marked reduction in electricity use caused by the VAV retrofit occurred on July 1, 1991 and is indicated by a cursor on the data point.

Enhanced resolution on the time-series plot is easily obtained by selecting *Graphics, Zoom In* from the menu. Figure 5.3 shows a zoomed-in view of four weeks of whole building electricity use. The distinction between weekday, Saturday and Sunday electricity use is now readily apparent.

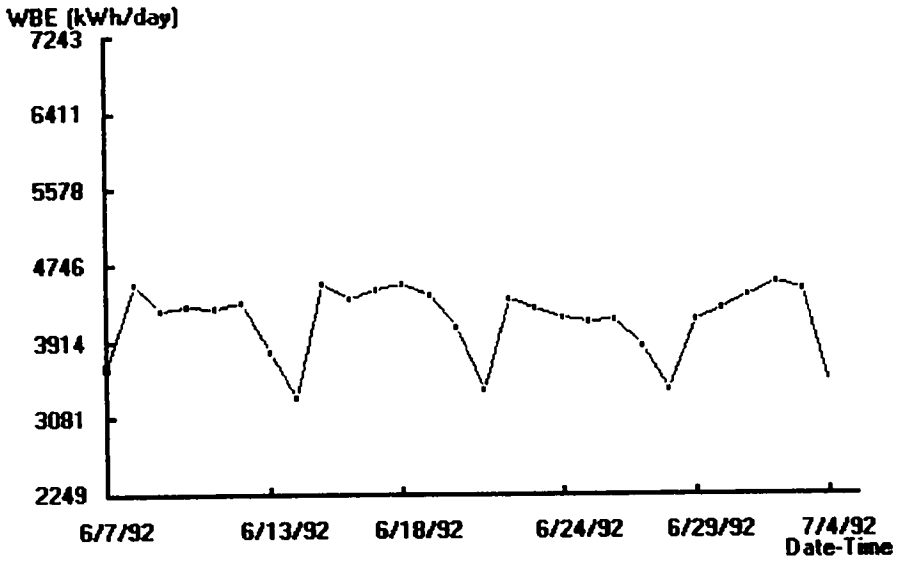

Figure 5.3 Zoomed-in time-series plot of four weeks of whole building electricity use data.

A powerful addition to standard graphing and modeling is the ability to divide the data into groups; each group is then graphed with separate colors and symbols and is modeled separately. Groups can be defined in two ways. If the data is to be grouped in a time series fashion, such as when dividing the data into pre and post-retrofit periods, the date/time of the division can be defined by selecting *Data, Add Grouping Variable*. Other groups can be defined by adding a coded variable named *Group* to the data set such that the value of the variable is 1 or 7 for *Group One* and any other number for *Group Two*. This grouping procedure enables the user to define groups according to any criteria. It also makes dividing the data into weekday and weekend groups very easy. Once the grouping variable is defined, grouping can be turned on and off by simply toggling the *Single Group* or *G1G2* button at the lower right of the EModel work screen.

EModel's grouping capabilities are demonstrated by dividing the data set into pre- and post-retrofit groups by selecting *Data, Add Grouping Variable* and entering 7/1/91 as the end of the pre-retrofit period. Clicking on the Temp variable in the *Y Variable* box, the

G1G2 button to enable grouping, and the *Histogram* graph button creates histograms of pre- and post-retrofit average daily outside air temperatures. In Figure 5.4, these histograms reveal strikingly different temperature distributions in the two periods. In the pre-retrofit period, the most frequently occurring outside air temperature was near 15 °C, while in the post-retrofit period the most frequently occurring temperatures were greater than 30 °C. This example demonstrates the significant differences possible between pre- and post-retrofit weather and reinforces the necessity of removing the effect of changing weather on energy use when determining savings.

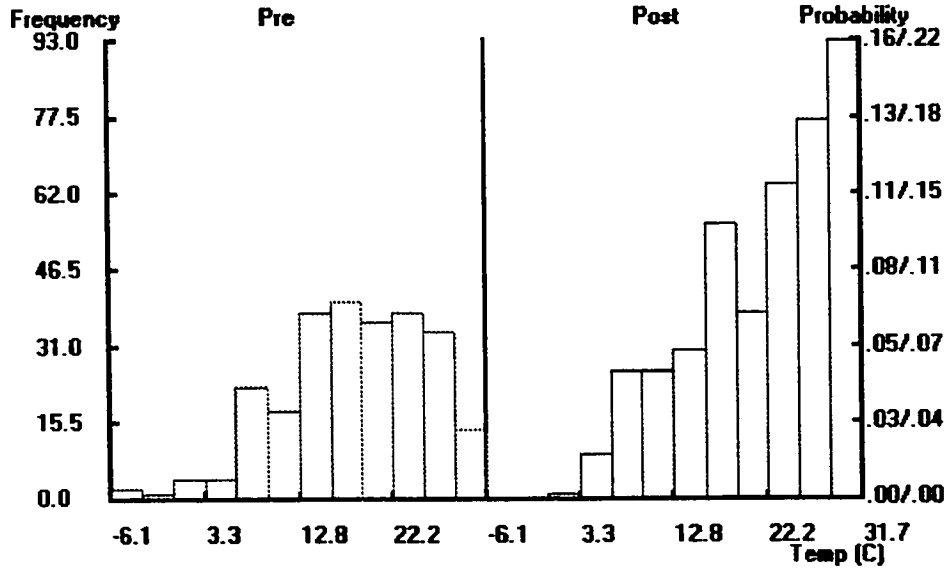

Figure 5.4 Temperature histograms from the pre- and post-retrofit periods.

Relational aspects of the data are just as easily explored. To examine the relationship between cooling energy use and outside air temperature and to also determine what influence the retrofit had on cooling energy use, we click on the variables C (GJ/day) and Temp (C), click the *G1G2* button to enable grouping, and then click the *XY* graph button. The two clouds of data evident in Figure 5.5 correspond to pre-retrofit (the upper cloud)

and post-retrofit (the lower cloud) cooling energy use. The significant reduction in cooling energy use subsequent to the VAV retrofit is readily apparent.

The date/times and values of outlying data points such as those near the top, center of Figure 5.5, can be identified by pointing and clicking on them with the mouse. Outlying data points such as these often reveal metering or operational and maintenance problems. In this case, the three outlying data points occurred while the metering equipment was being serviced and are due to a metering error. The erroneous data is easily removed before modeling using the data processing functions in the *Data* menu item.

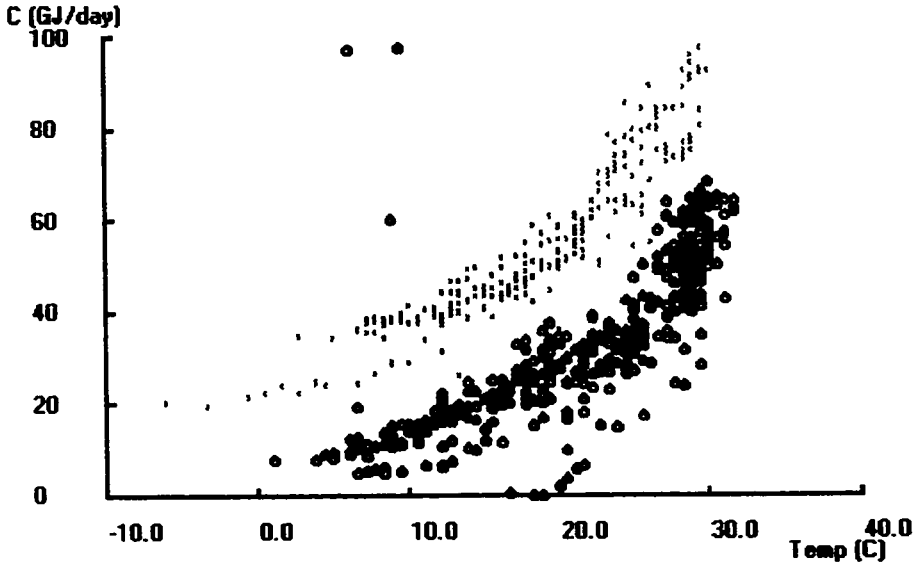

Figure 5.5 Relational plot of whole building cooling energy use and outside air temperature. The light dots are from pre-retrofit period and the heavy circles are from the post-retrofit period. The significant reduction in cooling energy use subsequent to the VAV retrofit is readily apparent.

As we have just seen, graphical analysis is an extremely effective method for quickly discerning problems, trends and relationships in large quantities of data. EModel has been specifically designed to provide incisive data views in a user friendly manner in order to make this important method of analysis more accessible.

Modeling Energy Use Data and Determining Savings

> The iterative and interactive interplay of summarizing by fit and exposing by residuals is vital to effective data analysis. J. W. Tukey (Tukey, 1988)

While graphical analysis is extremely effective at transmitting a qualitative, phenomenological understanding of the relationships among data, those relationships can often be described more concisely by a mathematical model. Further, mathematical models can be applied to a wide range of problems such as system control, the automatic identification of operating problems, and the measurement of retrofit savings. Traditionally, modeling building energy use data involved the use of dedicated statistical software such as SAS (SAS, 1992) or special function models such as PRISM. The time and effort involved in learning how to use, pre-process the data into a suitable form, and interpret these programs often precluded their widespread use. EModel simplifies the modeling process by providing a tool kit of the most commonly used types of building energy use models. These models were derived in Chapter III. The modeling procedure is reduced to simply clicking on the button of the desired model. EModel will then display the model parameters, important measures of goodness of fit *and overlay a graph of the model on top of the data*. This combined statistical and graphical approach greatly speeds the analysis and documentation process.

To continue the present example, the positive relationship between cooling energy use and outside air temperature can be modeled using simple linear regression by simply clicking on the *S.L.R.* button. In Figure 5.6, the model parameters are shown in the value window and model lines are drawn with the data.

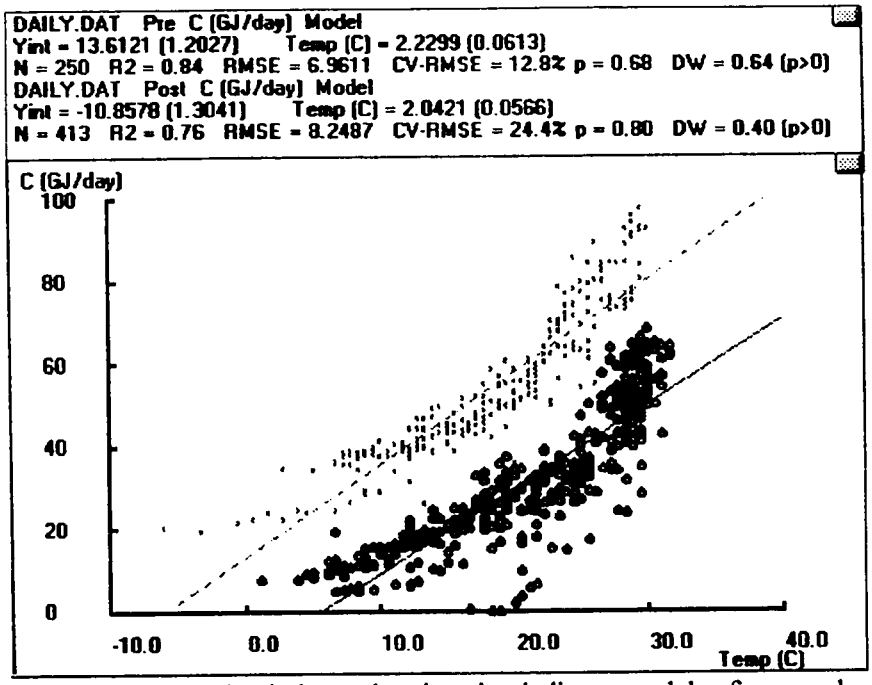

Figure 5.6 Value and graph windows showing simple linear models of pre- and post-retrofit cooling energy use vs. outside air temperature.

The R^2 values of 0.84 in the pre-retrofit period and 0.76 in the post retrofit period are displayed in the value window of Figure 5.6 and indicate reasonable fits to the data. In addition, the standard errors of the regression coefficients, shown in parenthesis next to the regression coefficients, and the CV-RMSEs of each model are also reasonable. The only inferential statistics which may indicate a problem are the autocorrelation coefficients of 0.68 and 0.80 for the pre- and post-retrofit periods respectively. The resulting values of the Durbin-Watson test for each model, 0.64 and 0.49, and interpretations of the Durbin-Watson tests, (p>0) and (p>0), indicate that at the 95% confidence level, neither autocorrelation coefficient is zero. Inspection of the pre-retrofit period residuals, which are automatically calculated by EModel, shows the residuals migrating from positive to negative to positive (Figure 5.7). This non-random pattern is duplicated in the post-retrofit period and indicates that the SLR models were misspecified (Figure 5.7).

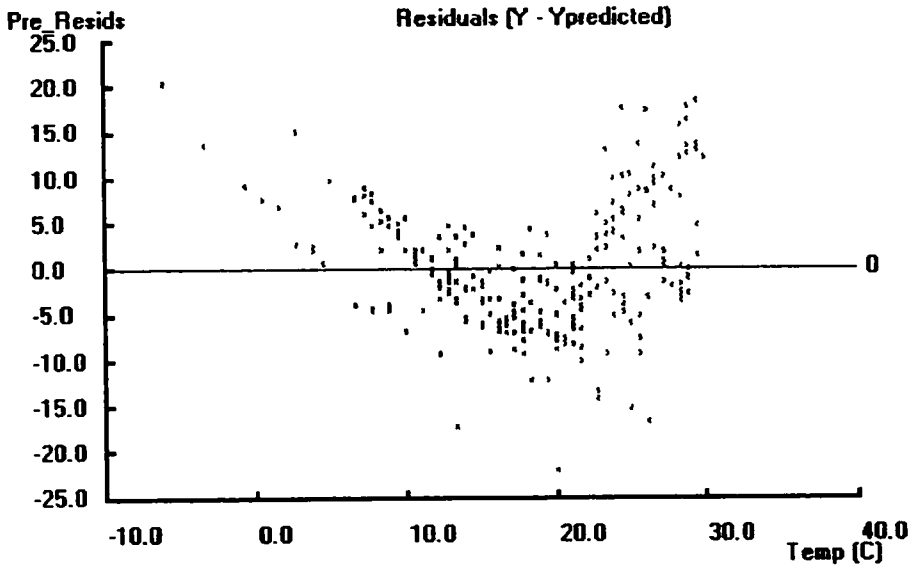

Figure 5.7 Plot of pre-retrofit S.L.R. residuals versus temperature. The residuals will have a more random pattern when the model is correctly specified.

The results of a second modeling attempt, this time choosing four-parameter, change-point models by pressing the *4P-CP* button , are displayed in Figure 5.8. Note that the new measures of goodness of fit: $R^2 = .90$ and $R^2 = .83$, CV-RMSE = 10.3% and CV-RMSE = 20.7%, and $\rho = .61$ and $\rho = .69$ all indicate a better fit. The residuals from this model (not shown) are much more randomly distributed. We conclude that the four-parameter model is the appropriate model for this data set.

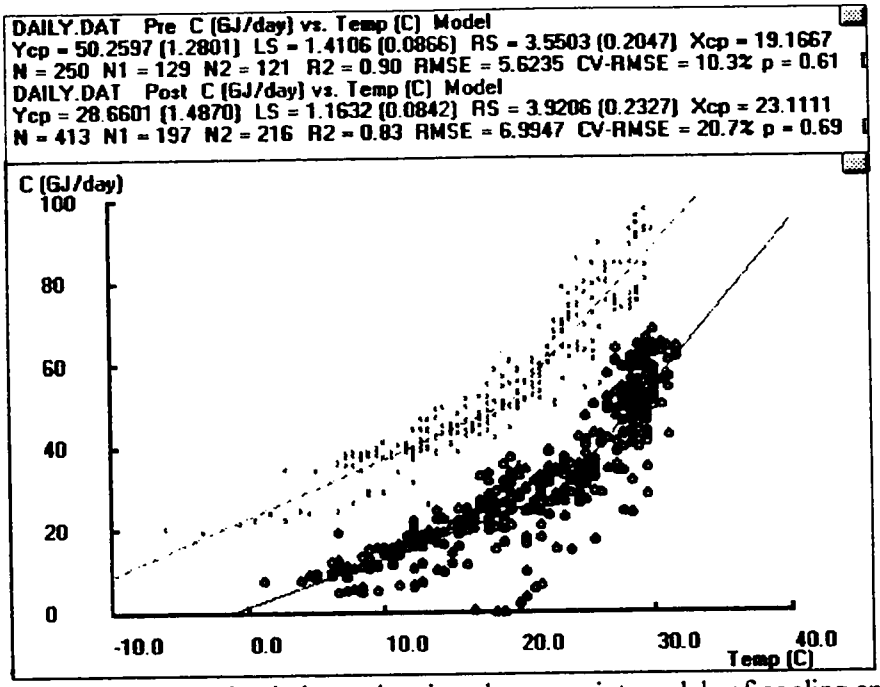

Figure 5.8 Value and graph windows showing change-point models of cooling energy use. The pre-retrofit data are shown as light dots with a dashed model line and the post-retrofit data are shown as heavy circles with a solid model line. These model provide better fits than the simple linear models of Figure 5.6.

Cooling energy savings can now be determined by simply selecting *Savings, Calculate Savings* from the menu. This procedure subtracts measured post-retrofit cooling energy use from the baseline energy use predicted by the pre-retrofit model for each day in the post-retrofit period. The sum of these daily savings values is the total savings and is displayed in an updated value window (Figure 5.9). Figure 5.9 shows that during the 413 days since the VAV retrofit was completed, 12,541 GJ of cooling energy has been saved for an average savings of 30.4 GJ/day.

DAILY.DAT
C (GJ/day) Post-retrofit observations = 413
Baseline = 26529 Measured = 13988 Saved = 12541

Figure 5.9 Value window showing quantities of predicted baseline cooling energy use, measured post-retrofit cooling energy use and their difference, the cooling energy savings.

This procedure removes the effect on savings of changing weather between the pre and post-retrofit periods. However, the weather in the post-retrofit period may have been abnormally warm or cool and the measured savings may be different than savings that would have occurred during "normal" weather conditions. EModel facilitates determination of "weather normalized" savings by identifying both the pre- and post-retrofit models (see Figure 5.8). Weather normalized savings can then be determined by predicting *both* pre and post-retrofit energy use from the models identified by EModel and "normal" weather data. The PRISM method suggests using 10 or more years of average daily temperature data to estimate normal weather (Fels, 1986). Weather normalized savings are preferable if savings are to be compared to predicted savings. In this case, the same normalized weather should be used for both predicting savings and normalizing the measured savings.

Occupancy and equipment operating schedules can significantly influence energy use in commercial buildings (See Chapter III). In many cases, scheduling changes can be effectively incorporated into energy use models by making separate models for each occupancy or operating period. EModel facilitates this through its grouping capabilities. For example, weekday and weekend groups are easily defined using EModel's built-in calendar function which adds a day of the week variable to the data set. Naming the variable *Group* and clicking the *G1G2* button instructs EModel to display and model weekday and weekend data separately. Figure 5.10 shows a time-series plot of pre-retrofit, weekday/weekend, whole building electricity use. The weekday and weekend mean models were calculated and displayed by simply clicking the *Mean* model button. Electricity savings resulting from the VAV retrofit can be determined simply by selecting *Savings, Calculate Savings* from the menu (Figure 5.11). In this case, nearly 900,000 kWh of electricity have been saved in the 416 days of the post-retrofit period.

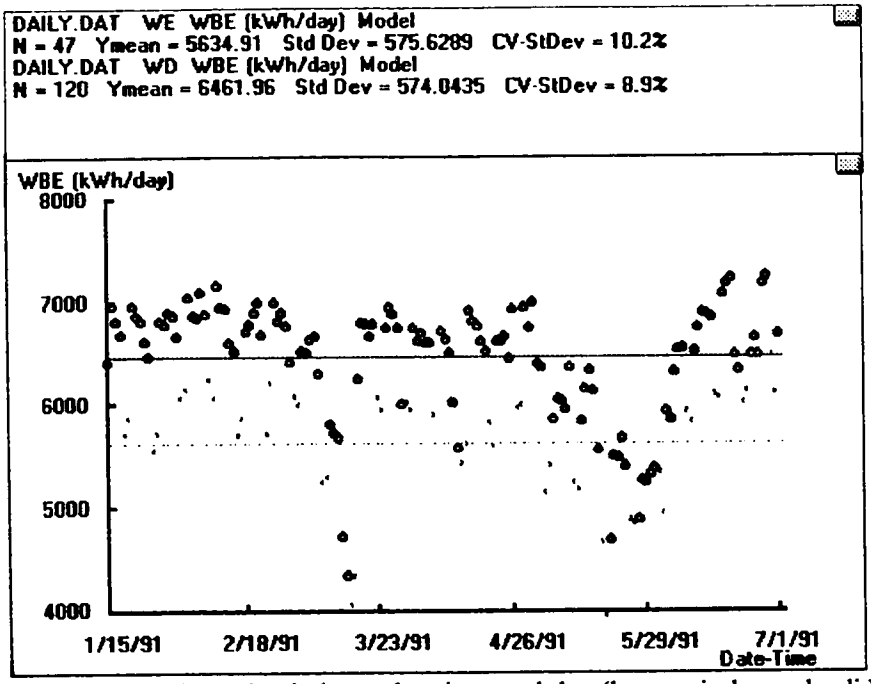

Figure 5.10 Value and graph windows showing weekday (heavy circles and solid line) and weekend (light dots and dashed line) values and models of pre-retrofit electricity use.

```
DAILY.DAT
WBE (kWh/day)     Post-retrofit observations = 416
Baseline = 2591346   Measured = 1704361   Saved = 886985
```

Figure 5.11 Value window showing quantities of predicted baseline electricity use, measured post-retrofit electricity use and their difference, the electricity savings.

Other models supported by EModel include multiple linear regression, three-parameter change-point and bin-fit models. Although their use will not be demonstrated here, these models are well suited to certain types of energy use patterns. The multiple linear regression model enables the user to create polynomial, Fourier series and indicator models, as well as multiple linear regression models that include the effects of multiple drivers of energy use such as humidity or lighting and receptacle electricity use. Three-parameter change-point models of heating and cooling use versus temperature are

appropriate for buildings without simultaneous heating and cooling. Finally, the bin-fit model provides superior flexibility for highly non-linear energy use patterns.

This extensive tool box of models is necessary because of the wide variety of energy use patterns found in commercial buildings (see Chapter III). No single model is appropriate for all commercial building energy use patterns. However, judicious use of these models gives the user great flexibility and power to model commercial building energy use for the purpose of determining savings.

The model parameters and inferential statistics computed by EModel were compared to other benchmark statistical software packages in order to test the accuracy of EModel's statistical algorithms. The results of these comparisons are presented in Appendix B. In comparisons with SAS (SAS, 1992), a widely used statistical software application, regression coefficients and inferential statistics determined by EModel and SAS were identical to four or more significant figures or to the number of significant figures reported.

Chapter Summary

EModel integrates data processing, graphing and modeling capabilities in a single user-friendly environment. It also embodies much of the theory developed in this dissertation and is currently the primary vehicle for putting this theory into practice, where it can be tested and improved upon. As such EModel not only facilitates the use of this methodology, it also facilitates its improvement; the most effective guidance for which will come from the engineers, building operators and energy managers who put the theory to work. Such a "user-driven approach" (Taylor 1986, p. 2) will ensure the utility and maximize the effectiveness of both EModel and this savings methodology.

A more detailed explanation of EModel can be found in the EModel User's Guide (Kissock, 1993).

CHAPTER VI

DETERMINING THE UNCERTAINTY OF SAVINGS

A model of energy use should include a statistically sound measure of uncertainty to be considered complete. This chapter develops a methodology to determine the uncertainty of temperature-dependent energy use models when used to predict baseline energy use in the post-retrofit period. The methodology devotes special attention to the problem of autocorrelated residuals in energy use models. The procedure for combining modeling and post-retrofit measurement errors is presented to estimate the total uncertainty of the savings. This chapter is adapted from Ruch et al. (1993b).

Autocorrelation in Energy Use Models

When data are fit using a regression model, the error term may not be independent across time; in such a situation the errors are said to be non-random or *autocorrelated.* The presence of autocorrelation is important because it will cause statistical problems. Most importantly for our purposes, estimated prediction error bounds will be too small, leading to undue confidence being placed on the accuracy of predicted energy use. In addition, the mean square error of the regression fit may underestimate model variance, and the standard errors of the ordinary least squares (OLS) regression coefficients will be too small (Neter et al., 1989).

Autocorrelation in energy use models may be caused by time dependent operational changes in the building, by the omission of variables that may influence energy use, such as humidity, occupancy loads and solar radiation or by the use of an improper functional form.

Changes in the way that an HVAC system is operated can significantly impact energy consumption. Common operational changes in commercial buildings include changes in

the zone set-point temperature and switching air-handlers, chillers and pumps on or off. These changes may cause residuals from an energy use model to be grouped according to the operational changes. Some operational changes may cause obvious changes in the energy use pattern and can be accounted for by developing separate models for each operating period. However, less significant operational changes may also occur on a regular basis. These unknown or unmeasured changes are difficult to model and, when not accounted for, become sources of autocorrelation in energy use models.

Another major cause of autocorrelation is the omission of important influencing variables from the energy use model (Neter et al., 1989). This analysis focuses on the use of temperature-dependent energy use models because of the wide availability and robust nature of temperature data and the acceptable level of accuracy achieved by temperature-dependent models. However, as was shown in Chapter III, many other variables such as outside humidity, solar radiation, and internally generated loads also affect building energy use. Because of the non-random nature of these variables, their omission from an energy use model can cause autocorrelation. It should also be noted that many of the variables which influence energy use in buildings are virtually unmeasurable, and because of this some autocorrelation is a natural consequence of an imperfect model.

Another cause of autocorrelation in energy use models is due to misspecifying the proper mathematical form of a model. For example, if the data are quadratically related to outside air temperature and a linear model is specified, the model will systematically mispredict energy use at various temperatures, thus causing autocorrelation. For this reason, it is extremely important to specify the proper mathematical model for the data or to transform the data so that they fit one of the available mathematical models.

There are a number of ways to detect autocorrelation in OLS residuals. The Durbin-Watson test for first order autocorrelation is quite popular and can be computed by many software packages when fitting a regression. Another standard method for detecting

autocorrelation is to examine plots of residuals against time. If autocorrelation exists, then the residuals will be patterned (Draper and Smith, 1981).

If possible, autocorrelation should be addressed by redesigning the model to include time dependent changes, all significant predictor variables and the proper mathematical form. As noted above, however, practical measurement constraints often limit the effectiveness of model redesign. If the autocorrelation cannot be completely removed by model redesign, another modeling approach is to use an autoregressive (AR) model to eliminate the autocorrelation of errors.

AR models of daily energy use perform best when the energy use from the previous day(s) is available for use in a corrective error term. However, an AR model with a corrective error term is not appropriate for measuring savings because the building's pre-retrofit measured energy use, which is an essential component of the corrective error term, is not known in the post-retrofit period. In some cases, an AR model without a correcting error term may adequately predict energy use; however, when using data from the Texas LoanSTAR program, standard OLS models have predicted better than AR models without corrective error terms. We conclude that standard AR models have limited use in the measurement of savings.

In this chapter, a "hybrid" approach to predicting baseline energy consumption in the post-retrofit period is proposed. The hybrid model predicts energy consumption using the OLS regression coefficients, but estimates the model variance and prediction error in the framework of an AR model. The hybrid model benefits from the prediction accuracy of OLS regression coefficients but does not use the standard OLS error diagnostics that are inaccurate when autocorrelation is present. The hybrid model's estimate of uncertainty is generally larger and more realistic than the OLS estimate since it reflects the autocorrelation in the data.

The two methods for dealing with autocorrelation - model redesign and hybrid models - will be discussed in the following subsections.

Model Redesign For Time Dependent Changes

Models with autocorrelated residuals may be redesigned in several ways in order to remove some or all of the autocorrelation. As noted above, the problem may be due to missing variables, in which case including additional predictor variables may decrease autocorrelation. Several variable selection routines are available (SAS, 1989) to find the optimal group of predictor variables based on different criteria.

If autocorrelation is still present after the selection of all important predictor variables, time dependent changes in the building energy use can sometimes be identified by data and residual analysis. In these cases, it is appropriate to develop a single *indicator model* (Neter et al., 1989) that accounts for the time dependent changes.

Indicator models can be constructed by creating an independent *indicator* variable, I, that is assigned a value of 1 or 0 so that all observations from each time-dependent group have the same value. For example, if a building's HVAC system is operated differently during the summer than during the rest of the year, then the indicator variable I could be added to a model of building energy use and assigned the value of zero for each summer day and one for all other days. An indicator model of daily energy use, $\hat{E}_k$, as a function of the daily average outside air temperature T_o is:

$$\hat{E}_k = \beta_0 + \beta_1 T_o + \beta_2 I + \beta_3 I T_o \qquad (6.1)$$

where β_0, β_1, β_2 and β_3 are coefficients to be determined from the regression fit. The daily summer energy use, when $I = 0$, is given by:

$$\hat{E}_k = \beta_0 + \beta_1 T_o \qquad (6.2)$$

and daily energy use during the remainder of the year is:

$$\hat{E}_k = (\beta_0 + \beta_2) + (\beta_1 + \beta_3)T_o . \quad (6.3)$$

These same regression coefficients could be found by grouping summer and non-summer days into separate bins and performing separate regressions on each bin. However, the use of a single indicator model allows for an accurate estimate of the remaining autocorrelation, which can then be used, if necessary, for the development of an autoregressive or hybrid model that incorporates time-dependent changes.

Model Redesign Using Autoregressive Models

Another method to redesign models is to use autoregressive models to eliminate or reduce autocorrelation. For this study, we assume *first order* autocorrelation of errors for statistical simplicity and because the addition of higher order AR terms only marginally improved the fits over first order AR models.

A simple linear OLS model of predicted energy use, $\hat{E}_k$, of day k is:

$$\hat{E}_k = b_0 + b_1 T_k \quad (6.4)$$

where T_k denotes the temperature on day k.

If autocorrelation is present, an autoregressive model (assuming first order autocorrelation) of the energy use has two components: a structural term and a conditional error term. The predicted energy, $\hat{E}_k$, of day k is:

$$\hat{E}_k = \beta_0 + \beta_1 T_k + \rho \varepsilon_{k-1} \quad (6.5)$$

ρ is the autocorrelation coefficient, and $\varepsilon_{k-1} = E_{k-1} - \hat{E}_{k-1}$ is the prediction error from the k-1 day. The *structural component* of the model is:

$$\beta_0 + \beta_1 T_k$$

and the *conditional error component* is:

$$\rho\varepsilon_{k-1}.$$

Usually the regression coefficients of the OLS model (b_0 and b_1) will be different than those of the autoregressive model (β_0 and β_1). In some applications, however, there is little difference between the models' coefficients and an autoregressive model will predict much like an OLS model but with more reliable error bounds (Neter et al., 1989). In such cases, the conditional error component is only a minor contributor to the data fit.

On the other hand, there are also cases where the conditional error component is the major contributor to the data fit, and the structural component alone is a poor predictor (SAS, 1984, p. 208). Unfortunately, the prediction of pre-retrofit energy consumption under post-retrofit weather conditions cannot use updated errors since measured pre-retrofit energy data from post-retrofit weather conditions are unavailable. Consequently the conditional error component cannot be used in the predictor model and the prediction must essentially be done by the structural component of the AR model. Hence the AR model will not be appropriate if the structural component alone gives a poor fit to the data.

Application of Model Redesign Techniques

As an illustration of the problems of using an AR predictor with the structural component alone, a data set was generated using 91 days (September - November 1989) of real daily temperature data from central Texas and synthetic energy data according to the model:

$$E_k = 2000 + 100T_k + 1500I + \varepsilon_k \qquad (6.6)$$

where:

$$I = \begin{cases} 1 & \text{for days } k = 1, 2, \ldots, 61 \quad \text{(September – October)} \\ 0 & \text{for days } k = 62, 63, \ldots, 91 \quad \text{(November)} \end{cases}$$

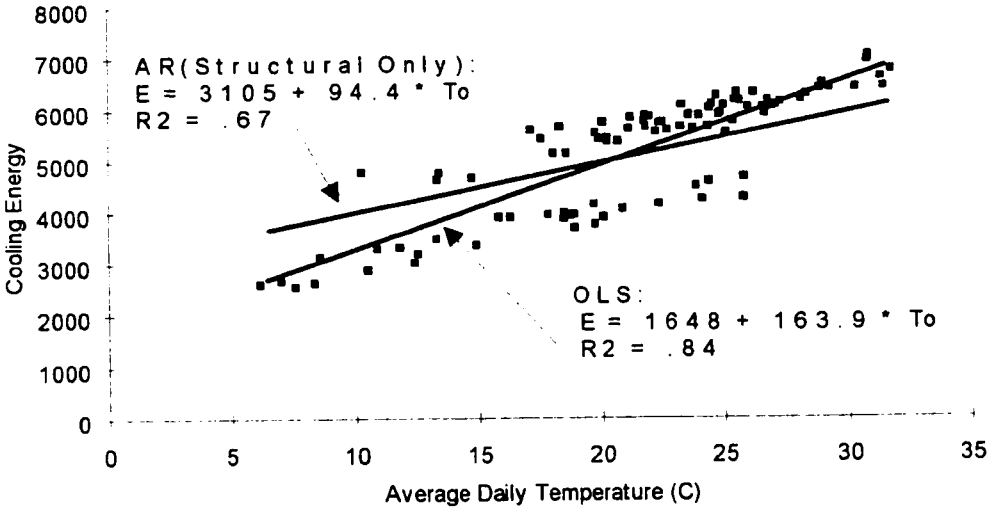

(a)

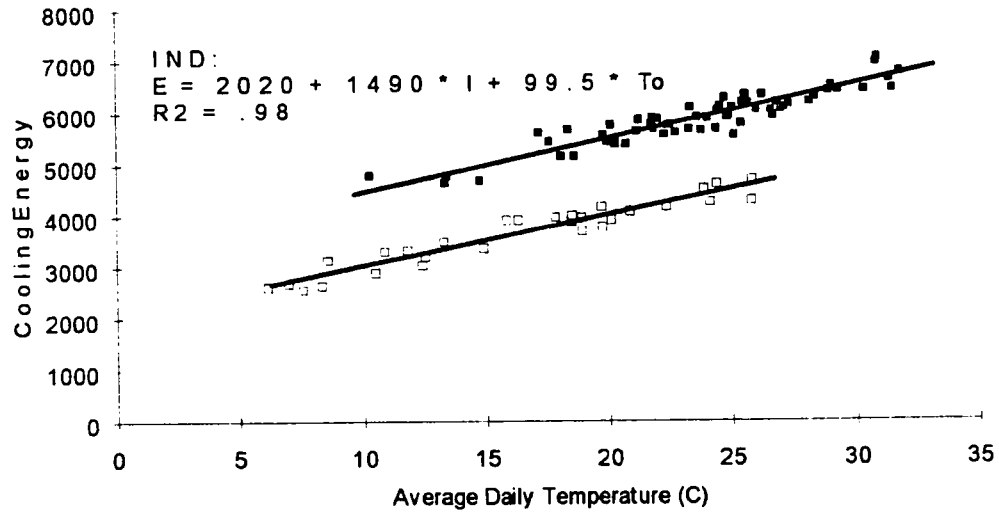

(b)

Figure 6.1 Synthetic data with a time dependent operational change: a) data with OLS and AR models; and b) the same data with different symbols for the different modes of operation and corresponding indicator models.

and where the error terms ε_k are independently and normally distributed.

This hypothetical building undergoes a regular operational change at the end of October each year, the result being a 1500 unit shift in energy use. The slope is kept equal

over the entire year for simplicity of presentation. Synthetic data are used in order to isolate the cause of the autocorrelation: not always an easy task with real data.

A superficial glance at a scatter plot of the data (Figure 6.1a) suggests a single linear model, while the true model requires an indicator variable to account for the shift in energy use after October. For illustrative purposes, a simple OLS, a full autoregressive model, and an autoregressive model without a conditional error component were fit to the data. The OLS fit was reasonable, with an R^2 of 0.84, but it had an estimated autocorrelation coefficient of 0.80, indicating significant autocorrelation. The full autoregressive model fit was considerably better than OLS, with an R^2 of 0.94, but if only the structural component was used, the autoregressive fit was considerably worse (R^2 = 0.67). It is clear from Figure 6.1a that the autoregressive model without an error correcting term will be a poor predictor of energy use, especially when daily temperatures are above 25 °C or below 10 °C. The OLS model will predict respectably during those times, but it is not satisfactory in the sense that its error diagnostics will be unreliable because of the autocorrelation.

For this example, of course, the clear solution is to redesign the model as an indicator model to account for the change-point in time (see Figure 6.1b). This fit gives an R^2 value of 0.98 and the autocorrelation is now negligible. The difficulty with real data is to find the change-point in time. One way to accomplish this is by plotting the OLS residuals against time. A clear time change-point will be marked by a sharp change in sign of the residuals.

However, time dependent changes are often complex, short-lived and not readily detectable in many buildings. These sorts of irregular changes cannot be built into the actual prediction of energy in the post-period, but must be reflected in a model's uncertainty estimate. The hybrid model is designed precisely with these two facts in mind. For cases like these, the hybrid approach is developed and applied below.

A Hybrid OLS-AR Model With Reliable Uncertainty Estimates

For many buildings it may not be possible to completely eliminate autocorrelation through model redesign, and autoregressive models are inappropriate for retrofit savings due to the reason discussed above. Fortunately, even if autocorrelation is present the regression coefficient estimates given by OLS are reasonable in the sense of being statistically unbiased (Theil, 1971, p. 254), and thus give the best estimates of the coefficients under the circumstances. In this situation, the problem with an OLS model is that the usual error diagnostics are biased and may severely underestimate the prediction uncertainty. We therefore propose a "hybrid" model that uses the OLS regression coefficients for the actual prediction of energy consumption, but accounts for the autocorrelation in its uncertainty estimate. This new approach to estimating the uncertainty of prediction requires a statistical derivation, which is given below.

To develop the hybrid model, we first note that because of the autocorrelation, which we assume to be first order, the errors from the OLS fit on consecutive days k and k-1 are related as:

$$\varepsilon_k = \rho\varepsilon_{k-1} + \delta_k \tag{6.7}$$

where δ_k is a random error term, and ρ is the autocorrelation coefficient of the residuals.

Thus, to predict the energy use E_1 on the first day of the "post" period we use Equation 6.7 to obtain:

$$E_1 = \beta_0 + \beta_1 T_1 + \varepsilon_1 = \beta_0 + \beta_1 T_1 + \rho\varepsilon_0 + \delta_1. \tag{6.8}$$

where ε_0 is the actual error on the final day of the "pre" period. Because E_1 and δ_1 are unknown, the best predictor of E_1 is:

$$\hat{E}_1 = \beta_0 + \beta_1 T_1 + \rho\varepsilon_0. \tag{6.9}$$

Similarly, the best predictor of E_2 is:

$$\hat{E}_2 = \beta_0 + \beta_1 T_2 + \rho\varepsilon_1 \approx \beta_0 + \beta_1 T_2 + \rho^2\varepsilon_0. \tag{6.10}$$

By induction, it follows that the best predictor of day k of the "post" period is:

$$\hat{E}_k = \beta_0 + \beta_1 T_k + \rho^k\varepsilon_0. \tag{6.11}$$

The term $\rho^k\varepsilon_0$ estimates the autocorrelation effect and rapidly diminishes with time since $|\rho| < 1$. It is negligible within the first 30 days of the "post" period (even when $|\rho|$ is close to 1) and we have not found it significant in our energy predictions. Consequently, we drop this term to obtain the energy predictor for the hybrid model, which is:

$$\hat{E}_k = \beta_0 + \beta_1 T_k \tag{6.12}$$

Note that this predictor will give energy estimates identical to those of the OLS model because the regression coefficients are the same. What sets this hybrid model apart from OLS is its superior error diagnostics, which are discussed next.

The derivation of proper error estimates begins with equation 6.11, before the simplification to equation 6.12 is made. We now switch to matrix notation to outline the derivation, which is given in detail in Ruch (1992). The model above can be written as $E = X\beta + \varepsilon$, where E is a (n x 1) vector of pre-retrofit energy observations and X is a (n x k) matrix whose first column is a column of ones and remaining columns are the pre-retrofit observations of the independent variables (such as temperature, humidity or indicator variables).

To describe m observations of predicted energy use in the post-retrofit period, E_*, we have $E_*=X_*\beta+\varepsilon_*$ where X_* is the matrix of post-retrofit independent variables. Let $\sigma^2\Psi$ and $\sigma^2\Psi_*$ be the covariances of pre-retrofit and post-retrofit disturbances

respectively, and let $\sigma^2 V$ be the covariances between pre and post-retrofit disturbances where σ^2 is the variance of the model error terms and first order autocorrelation is assumed. Then the hybrid model (Equation 6.11) can be written in matrix notation as:

$$\hat{E}* = X*\hat{\beta} + V'\Psi^{-1}\left(E - X\hat{\beta}\right) \tag{6.13}$$

where $\hat{\beta} = (X'X)^{-1}X'E$ is the usual OLS estimator of the regression coefficients. The prediction error is:

$$\begin{aligned} \hat{E}* - E* &= X*\left(\hat{\beta} - \beta\right) + V'\Psi^{-1}\left(E - X\hat{\beta}\right) - \varepsilon* \\ &= X*(X'X)^{-1}X'\varepsilon + V'\Psi^{-1}M\varepsilon - \varepsilon* \\ &= P\varepsilon - \varepsilon* \end{aligned} \tag{6.14}$$

where $M = I - X(X'X)^{-1}X'$ and $P = X*(X'X)^{-1}X' + V'Y^{-1}M$. The variance-covariance matrix of the prediction error is thus:

$$\text{var}\left(\hat{E}* - E*\right) = \sigma^2\left(PYP' - PV - V'P' + Y*\right) \tag{6.15}$$

The variance of the prediction error for day i is the diagonal element i-i of this m x m matrix, and the off-diagonal elements are the covariances of the daily prediction errors. The variance of the sum of the daily prediction errors is:

$$\text{var}\left(\sum_{i=1}^{m}\left(\hat{E}* - E*\right)_i\right) = \sigma^2\,\bar{1}'\cdot\left(PYP' - 2PV + Y*\right)\cdot\bar{1} \tag{6.16}$$

where $\bar{1}$ is a column of ones. Note that matrix $PYP^{-1} - 2PV + Y_*$ in Equation 6.16 is m x m, the length of the "post" period. Pre and post-multiplying of this matrix by $\bar{1}$ is just a compact notation for summing all of the terms in the matrix.

The actual computation of this estimate of the variance of the total prediction error involves a straightforward matrix calculation, which can be done easily using matrix

oriented software (SAS/IML is excellent for this task). The method is also implemented in the program PredErr, which will be used to calculate the uncertainty of savings in Chapter X. The variance can then be used to obtain *prediction error bounds* as follows. At a confidence level 1- α, the prediction error bound is:

$$t_{\alpha/2}\,\sigma\sqrt{\bar{1}'\cdot(PYP' - 2PV + Y*)\cdot\bar{1}} \qquad (6.17)$$

where $t_{\alpha/2}$ is the t-statistic with (n-k) degrees of freedom, n is the number of pre-retrofit observations and k is the number of regression parameters in the model (see Ruch, 1992 for more details). Thus, the total prediction error $\sum_{i=1}^{m}\left(\hat{E}* - E*\right)_i$ for the "post" period energy use is expected to be less than its prediction error bound at the specified confidence level.

There are two major sources of variance when the "post" data set is fairly long (two or more months). In this situation, the correlation between pre-retrofit and post-retrofit disturbances becomes small when compared to the other sources of error. We can thus approximate this condition by setting σ^2V, the matrix of covariances between pre-retrofit and post-retrofit disturbances, equal to zero in the definition of matrix P and in Equation 6.16. The major sources of variance in the sum of daily prediction errors are therefore: (a) the matrix σ^2PYP', which is due to sampling error in the estimation of the regression coefficients; and (b) the matrix $\sigma^2\Psi*$, which is due to variance in the post-retrofit disturbances.

A problem related to finding prediction error bounds is estimating the model error terms' variance σ^2. Unfortunately, the standard OLS estimate of σ^2 by the mean square error (MSE) of the regression is biased (Theil 1971, p. 256). This requires that an

alternate estimate of σ^2 be made. An unbiased estimate of the variance σ^2 under the assumption of first order autocorrelation is (Theil 1971, p.256):

$$\hat{\sigma}^2 = \frac{RSS}{\sum_{k=1}^{n} (M\Psi)_{kk}} \tag{6.18}$$

where RSS is the residual sum of squares from the OLS regression. This will generally be larger than the MSE, which partly explains why the OLS error bounds are too small. The variance estimate described in Equation 6.18 is used for estimating the hybrid model's variance.

If there is no autocorrelation present in the original OLS fit, these results still hold and become much simpler since the matrix V is now zero, and the matrices Ψ and Ψ^{-1} become the identity matrix. In this case the estimate of the variance of the prediction error is (Theil 1971, p. 123):

$$\mathrm{var}\left(\sum_{i=1}^{m} \left(\hat{E}* - E* \right)_i \right) = \sigma^2 \vec{1}' \cdot (X*(X'X)^{-1}X*' + I) \cdot \vec{1} \tag{6.19}$$

which is used for computing prediction error bounds for OLS models.

A common but incorrect practice for computing prediction error bounds of the sum of daily predictions is to sum in quadrature the prediction error bounds of the daily predictions. This amounts to assuming that the daily prediction errors are independent:

$$\mathrm{var}\left(\sum_{i=1}^{m} \left(\hat{E}* - E* \right)_i \right) = \sum_{i=1}^{m} \mathrm{var}\left(\hat{E}* - E* \right)_i \tag{6.20}$$

or, equivalently, that the off-diagonal entries in variance-covariance matrix (Equation 6.15) are all zero. However, this is not generally the case because all of the daily predictions of energy use are based on the same estimated regression coefficients and are

therefore correlated. Consequently, summing in quadrature will underestimate the correct prediction error bound. This is true even when there is no autocorrelation of errors in the OLS regression fit (Theil 1971, p. 122).

Procedure for Linear Model Fitting When Autocorrelation is Present

A variety of techniques for explaining and dealing with autocorrelation in modeling energy use have been discussed above. In this section we develop a procedure for putting these ideas together. We assume that the given building data suggest that energy is a linear function of temperature, i.e. no temperature change-point is apparent that requires PRISM (Fels, 1986) or a four-parameter fit (Ruch and Claridge, 1992a).

The first step is to perform an OLS fit to the data (see the flow chart in Figure 6.2). An analysis of the residuals should be undertaken to check for autocorrelation. For example, plots of the OLS residuals versus time and computing the Durbin-Watson statistic are recommended (Draper and Smith, 1981). If there is no indication of autocorrelation or other statistical problems, use the OLS model for predicting energy use and Equation 6.19 for estimating the prediction error bounds. If autocorrelation exists, redesign the model if possible, looking for time-dependent operational changes or omitted variables. Plots of residuals against time are essential for this task. If, after this is done, autocorrelation is still present, or if redesign is not possible, try fitting an autoregressive model. If the structural component is the major contributor - i.e. its R^2 is nearly as high as the OLS fit and its fit to the data reasonable - then this autoregressive model can be used as a predictor. Note that this has not been the case for any LoanSTAR buildings studied thus far, so this step is omitted from the flow chart in Figure 6.2. Finally, after all possible model redesign efforts have been exhausted, and if the autoregressive model is inappropriate, use the hybrid model to predict energy use (Equation 6.12) and estimate uncertainty (Equations 6.16 and 6.17).

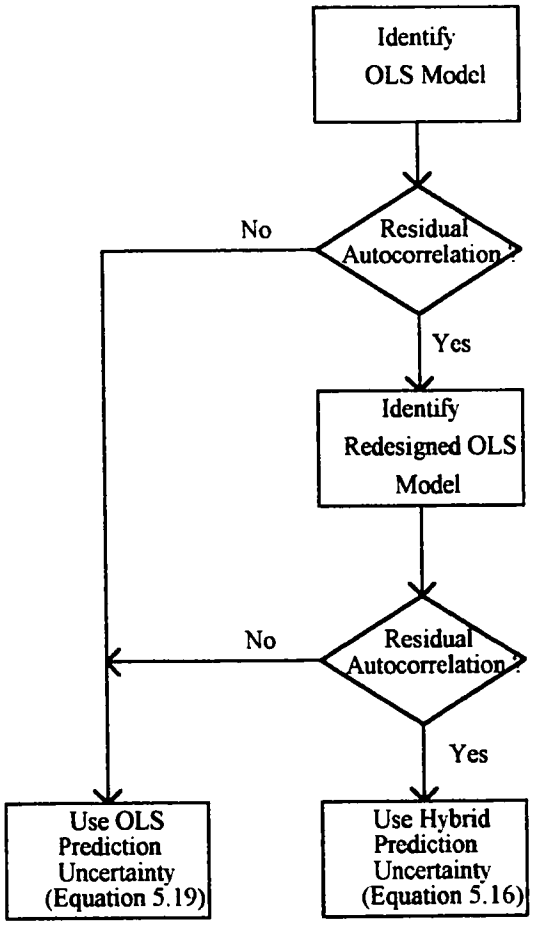

Figure 6.2 Flow chart summarizing model fitting procedure.

Model Comparison and Validation

In this section the performance of the hybrid and OLS models is tested on real energy use data from three buildings participating in the LoanSTAR program. Data sets of cooling and heating energy use at the Zachry Engineering Center on the Texas A&M University Campus, cooling energy use at the Perry Castenada Library on the University of Texas at Austin campus, and heating energy use at the Education classroom building on the University of Texas at Austin campus were selected. In each case, energy use appeared to be a linear function of outside air temperature, and no additional independent

variables were available. For each building, the data were split into two parts: hypothetical "pre" and "post" periods with energy use modeling done on the "pre" data and the models tested on the "post" data. The "pre" set was selected so that the range of daily temperatures was as representative as possible of the annual temperature variation for the region. Given this constraint, the data were split in half where possible. The data periods are given in Table 6.1.

Table 6.1 Descriptions of buildings used in case studies. E_c is cooling energy and E_h is heating energy. Classroom building data from 5/1/91 through 10/1/91 were not available due to metering difficulties.

Building	Principle Use	Type of Data	Dates of "Pre" Data	Dates of "Post" Data
Engineering Center	classrooms, offices, labs	E_c (GJ/day) E_h (GJ/day)	1/15/90 - 6/30/90 6/1/90 - 10/31/90	7/1/90 - 11/27/90 11/1/90 - 11/27/90
Campus Library	library, offices, computer facility	E_c (GJ/day)	8/7/91 - 1/31/92	2/1/92 - 4/30/92
Classroom Building	classrooms, offices	E_h (GJ/day)	12/5/90 - 4/30/91	11/1/91 - 3/16/92

For each building, residuals from an OLS fit to the "pre" data were examined and autocorrelation found. However, no clear or long-term operational change could be identified, so model redesign using indictor variables was not possible. Autoregressive models without an error correcting term fit the data poorly and so were dropped from consideration. Hence the modeling procedure discussed above led to a hybrid model for predicting energy use (Equation 6.12) and estimating uncertainty (Equations 6.16 and 6.17). For comparative purposes, both OLS and hybrid models were fit to each building's "pre" period data set. The models were then used to predict the cumulative energy use for the "post" period, and prediction error bounds were calculated at the 95% and 99% confidence levels. To illustrate the problem with summing the prediction error bounds in

quadrature, prediction error bounds were also computed in this way. The results are listed in Table 6.2.

Note that in every case the hybrid model's prediction error bound was greater than that of the OLS model. In all four cases the OLS error is greater than the predicted OLS error bound at the 99% confidence level, while the hybrid error is less than its predicted error bound at the 95% level. This supports the theoretical argument that OLS prediction error bounds are generally too small and hybrid error bounds are more realistic. The quadrature method produced prediction error bounds even smaller than the OLS error bounds for every case, again supporting the theoretical argument that summing errors in quadrature underestimates the true error.

Table 6.2. Uncertainty estimates of OLS and hybrid models compared to actual data. The percentages are relative to the actual energy use. For a correct estimate of uncertainty, the actual prediction error should be less than the prediction error bound at the given confidence level. ρ is the autocorrelation coefficient.

Building & Energy Type	Model Type	ρ	Predicted Energy Use (GJ)	Actual Energy Use (GJ)	Actual Prediction Error (%)	95% Prediction Error Bound (%)	99% Prediction Error Bound (%)
Library Cooling	OLS	.78	8419	7779	8	3	4
	Hybrid					8	11
Eng. Ctr. Heating	OLS	.96	1268	1569	19	7	9
	Hybrid					33	44
Eng. Ctr. Cooling	OLS	.73	3244	3435	6	4	5
	Hybrid					9	12
ClassRm. Heating	OLS	.94	2194	2609	16	3	4
	Hybrid					17	22

Measurement Error and the Uncertainty of Savings

This method quantifies the uncertainty of models used to measure energy savings. However, in addition to modeling uncertainty, measurements of energy use and

temperature are also subject to error. Measurement errors in the dependent variable, energy use, are simply absorbed by the model uncertainty. The model uncertainty accounts for the composite effects of all factors not related to the independent variable, including measurement error (Neter et al., 1989, pp. 170-172). Measurement errors in the independent variable temperature, on the other hand, cannot be accounted for in OLS regression. Thus, we implicitly assume no temperature measurement error. In our case, this is not a bad assumption because the uncertainty of LoanSTAR temperature sensors is specified as +- 0.28 °C (Katipamula and Claridge, 1993).

To determine retrofit savings, measured post-retrofit energy use is subtracted from energy use predicted by the baseline model. The savings uncertainty should generally include both the model uncertainty and the uncertainty of the measured post-retrofit energy use. If we assume that the covariance between the model and measurement uncertainties is negligible, the overall uncertainty of the savings is (Holman, 1978, p. 45):

$$\varepsilon_{savings} = \left[(\varepsilon_{model})^2 + (\varepsilon_{post-measurement})^2 \right]^{1/2} \qquad (6.21)$$

where ε is the uncertainty associated with the savings, model and post-retrofit measurement of energy. In cases where the uncertainty of the post-retrofit measurements is small compared to the modeling uncertainty, the measurement uncertainty can be neglected.

Chapter Summary

Autocorrelated residuals from regression models of building energy use present problems when measuring the uncertainty of retrofit savings. This chapter discussed the causes of autocorrelation in energy use models and proposed and demonstrated two methods to deal with autocorrelation: model redesign for time dependent changes and a

hybrid OLS-AR model. The hybrid OLS-AR model accurately determines baseline energy use and gives realistic uncertainty estimates. The methodology was tested on data from three commercial buildings participating in the LoanSTAR program. In every case examined, the hybrid OLS-AR model provided an uncertainty estimate for energy use far more accurate than the OLS estimate. When determining the overall uncertainty of savings, we assume that the measurement error in the independent variable, temperature, and the measurement error in the post-retrofit energy use are both very small compared to the model error and can be neglected.

CHAPTER VII

THE ANNUAL PREDICTION ACCURACY OF REGRESSION MODELS FROM SHORT DATA SETS

Whenever possible, a full year or more of energy use and weather data should be used to construct empirical models of building energy use. However, in many cases a full year of data are not available and one is constrained to develop models using shorter data sets. This chapter examines how temperature-dependent regression models of energy use based on short data sets fare in terms of annual predictive ability compared to models based on a full year of data. This chapter is adapted from Kissock et al. (1993a).

Introduction

Ideally, a full year or more of energy use and weather data should be used to construct a baseline model of building energy use because in most cases a year of data will include a complete weather and operational cycle. In many cases, however, a full year of data is unavailable either because of instrumentation failure or due to the time constraints inherent in many energy retrofit projects. This chapter uses a case-study approach to investigate the prediction accuracy of regression models of energy use based on periods of less than one year, which we call short data periods, by comparing them to models based on a full year of data (which we shall assume to yield the correct baseline model). The results of this analysis will help identify systematic error in the uncertainty of measured savings.

Beyond the immediate goal of measuring savings is the also important requirement of quantifying the uncertainty of the savings. One source of uncertainty is due to model extrapolation error, which arises when energy use is predicted at temperatures outside the range of temperatures used to develop the model. An allied source of model error may be

due to seasonal changes in building operation which a short data-set may miss entirely. This chapter attempts to quantify these sources of uncertainty by identifying the general characteristics of how, when and to what extent temperature-dependent models based on short data-sets incorrectly predict annual energy use.

Methodology

Three buildings for which nearly a full year of data were available were chosen for analysis (Table 7.1): the Zachry Engineering Center at Texas A&M University in College Station, the School of Public Health building at the University of Texas Medical Center in Houston and the J.E. Reagan at the Texas state capitol complex in Austin. The climate is generally warm and humid and subsequently more than twice as much energy is used to cool the buildings as is used to heat them (Energy Systems Laboratory, 1993a). The HVAC system in each building is a dual-duct, constant-volume system. Chilled and hot water at the engineering center (EC) and medical center (MC) are generated externally at a physical plant. Cooling and heating energy use at these buildings is determined by measuring the flow rates and temperatures of the chilled and hot water steams as they enter and leave the buildings. Cooling energy at the office building (OB) is measured as the electricity input to the building's chillers.

Cooling and heating energy use at each building appears to be nearly linear with outdoor air temperature (Figure 7.1), thus making the use of change-point models unnecessary. The R^2 statistics for temperature-based simple linear regression models of energy use range from .59 to .88, indicating that between 59% and 88% of the variation in daily energy use is correlated with the variation in the mean daily temperature. The remaining variation may be caused by changing internal loads or operating procedures, or by the variation of other environmental variables in addition to temperature which also influence cooling and heating energy use. The lower cooling density at the office building

is because the cooling energy measured here is electricity to the chillers, and must be multiplied by the coefficient of performance of the chillers before being comparable to the cooling densities at the engineering center and office building.

Table 7.1 Description of buildings. CW is chilled water energy use, HW is hot water energy use and CE is chiller electricity use.

Building	Floor Area (m^2)	Principle Use	Type of Data	Dates of Data Analyzed
Engineering Center	30,149	classrooms, offices, laboratories, computer facilities	CW (GJ/day) HW (GJ/day)	10/1/89 - 9/30/90
Medical Center	21,722	classrooms, offices, laboratories, library	CW (GJ/day) HW (GJ/day)	3/1/91 - 2/29/92
Office Building	7,435	offices	CE (kWh/day)	1/1/91 - 12/31/91

The effect of changing internal loads on cooling and heating energy use can be investigated by including whole building electricity use in the regression model as a predictor variable. Whole building electricity use accounts for all electrically-generated internal loads and is also a good surrogate variable for the sensible and latent loads generated by the building's occupants. At the engineering center, the addition of whole building electricity use as a predictor variable improved the models' R^2 statistic by less than 1%, while it improved the R^2 of the cooling models at the medical center and office building by about 6%. The influence of outdoor air specific humidity and solar radiation on cooling and heating energy use was negligible in all cases except at the medical center (a ten story building) where the inclusion of solar radiation in the heating model improved the model's predictive ability by 10%. Because the inclusion of additional variables did not significantly improve the predictive ability of these models, we chose to consider only

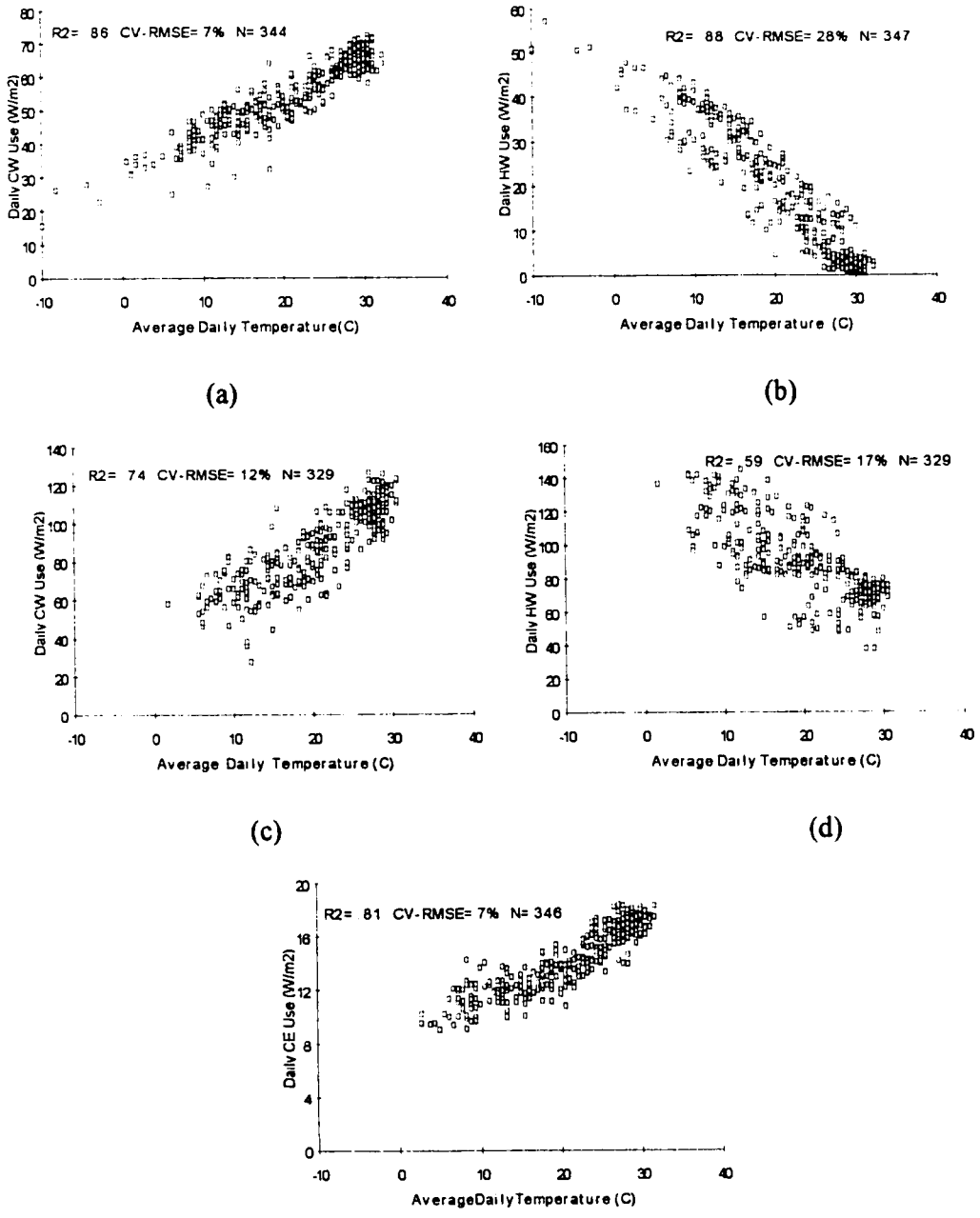

Figure 7.1 Daily energy use for a full year plotted against outside air temperature: a) engineering center chilled water energy use, b) engineering center hot water energy use, c) medical center chilled water use, d) medical center hot water use and e) office building chiller electricity use.

temperature-dependent models and implicitly assume that the other sources of variation are either negligible or that they occur randomly throughout the year. If these assumptions are met, then the focus of this study is on how the *temperature-dependency* of comfort energy use changes during a calendar year.

To determine the accuracy of temperature-dependent models based on short data-sets, the values of annual energy use predicted by models from short data-sets were compared to the annual energy use predicted by a model identified from an entire year of data. The annual energy use identified from an entire year of data was calculated by first identifying a regression model of daily energy use from the set of available data and then driving that model with the annual average daily temperature. This procedure gives the annual average daily energy use which was then multiplied by 365 days/year to determine the annual energy use. We chose to calculate annual energy use in this way, rather than simply summing the values of daily measured energy use because a few values of daily energy use are missing due to metering problems and simply summing the available values of daily energy use would slightly under-predict the true annual energy use.

The values of annual energy use predicted by short data-set models were calculated in the same way as models based on short data-sets of one, three, and five month sliding windows of data. To create twelve sliding windows of lengths three and five months, the data was wrapped around itself. For example, to create twelve five-month data-sets, the last two months of yearly data were attached to the beginning of the yearly data-set and the first two months of yearly data were appended to the end of the yearly data-set.

The ratio of the annual energy use predicted by a model based on the short data-set to the annual energy use predicted by the full year model is called the Normalized Annual Energy Use (NAEU):

$$\mathrm{NAEU} = \frac{E_w}{E_y} \tag{7.1}$$

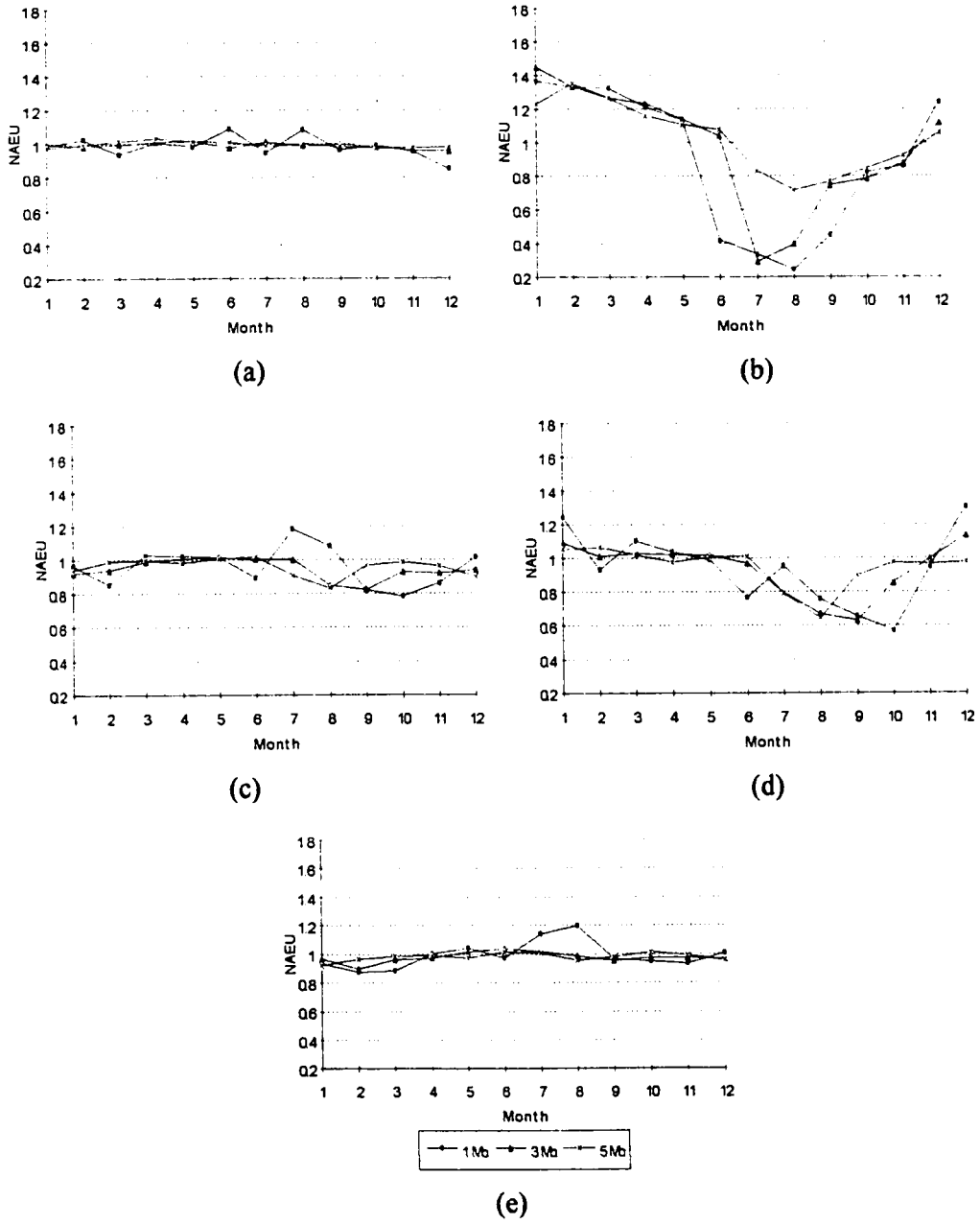

Figure 7.2 Normalized annual energy use (NAEU) for one, three and five month sliding windows: a) engineering center chilled water energy use, b) engineering center hot water energy use, c) medical center chilled water use, d) medical center hot water use and e) office building chiller electricity use.

where E_w is the annual energy use predicted by the model identified from a sliding window of data and E_y is the annual energy use predicted by the model identified from a full year of data. For a given short data-set model, a NAEU close to 1.0 indicates that the short data-set model predicted nearly the same total annual energy use as the model based on a full year of data. A NAEU greater than (or less than) one indicates that the short data-set models over-predicted (or under-predicted) annual energy use.

Time plots of the NAEUs for each type of energy use and for different lengths of sliding windows are displayed in Figure 7.2. From these plots, it is apparent that the cooling energy use predicted by short data-set models ranged from 80% to 120% of the measured annual energy use. The heating energy use predicted by short data-sets at the engineering center, on the other hand, was as little as 20% of the measured annual energy use. Thus, in this climate of central Texas, the prediction accuracy of heating models appears to be much more sensitive to short data-set error than models of cooling energy use.

Several observations about the effects of a short data-set on a model's ability to accurately predict annual energy use follow from Figures 7.1 and 7.2. These observations are discussed in the following sections.

The Effect of Data Set Length on Annual Prediction Accuracy

Intuitively, one would expect the prediction accuracy of annual energy use to improve as the length of the data-set increases. This behavior is evident in Figure 7.2 where the outer bands (representing large prediction error) are composed mostly of one month models and the inner bands (representing small prediction error) are composed mostly of the five month models.

We can compare the prediction accuracy of one, three and five month data sets by calculating an index called the average annual prediction error for each of the one, three

and five month long data sets. The average annual prediction error is the average of the absolute values of the differences between the monthly values of NAEU and unity:

$$\text{Average annual prediction error} = \frac{\sum_{i=1}^{12} |NAEU_i - 1|}{12} \tag{7.2}$$

where $NAEU_i$ is the NAEU (Equation 7.1) for the month on which the short data set is centered. Values of the average annual prediction error for data sets of one, three and five months in length are displayed in Table 7.2. The average annual prediction error declines in every case as the length of the data-set increases. For all of the cooling models combined, the average annual prediction error decreased from 7.3% for one month data-sets, to 3.7% for three month data-sets, to 3.0% for five month data-sets. The magnitude of average prediction error for heating models is four to five times larger than for cooling models, but declines in a similar manner as the length of the data-set increases.

Table 7.2 The average annual prediction error of models based on one, three and five month sliding windows. The averages of the cooling and heating models for all of the buildings are also shown.

Window Length	EC-C	EC-H	MC-C	MC-H	OB-C	All-C	All-H
1 Month	0.049	0.373	0.097	0.177	0.072	0.073	0.275
3 Month	0.017	0.290	0.060	0.116	0.034	0.037	0.203
5 Month	0.017	0.180	0.047	0.078	0.026	0.030	0.129

The Effect of the Season of the Data Set on Annual Prediction Accuracy

One may expect that temperature dependent models identified from data from one season of the year would predict a different annual energy use than models identified from data from a different season. In the following sub-sections we attempt to characterize this

behavior and determine the extent to which the annual energy use predicted by short data-set models is seasonally dependent.

Annual Variation of NAEU and Temperature. From Figure 7.2, it is apparent that the variation of monthly values of cooling NAEU follows the same sinusoidal pattern as the variation of monthly average temperatures. To illustrate this more clearly, we have taken a year of temperature data and divided each month's average temperature by the annual average temperature to produce an index of the variation of temperature, which we call the normalized monthly temperature:

$$\text{Normalized monthly temperature} = \frac{\bar{T}_{month}}{\bar{T}_{year}} \tag{7.3}$$

Normalized monthly temperature values of greater than one indicate months which are warmer than the annual average and vice versa.

Next, the NAEUs from the one, three and five month data-sets are averaged to produce an average NAEU for each month:

$$\overline{NAEU} = \frac{NAEU_{1Month} + NAEU_{3Month} + NAEU_{5Month}}{3} \tag{7.4}$$

Averaging the one, three, and five month NAEUs acts as a filter and provides a more stable indicator of the monthly variation in predictive ability of a model than does using an individual NAEU.

The similar pattern followed by the normalized monthly temperature and the average cooling NAEU of the office building is apparent in Figure 7.3. Although it is not the case for every month (particularly for months in the spring and fall), a general pattern emerges; cooling models derived from data-sets from hot months tend to over-predict annual cooling energy use and models derived from data-sets from cold months tend to under-predict annual cooling energy use.

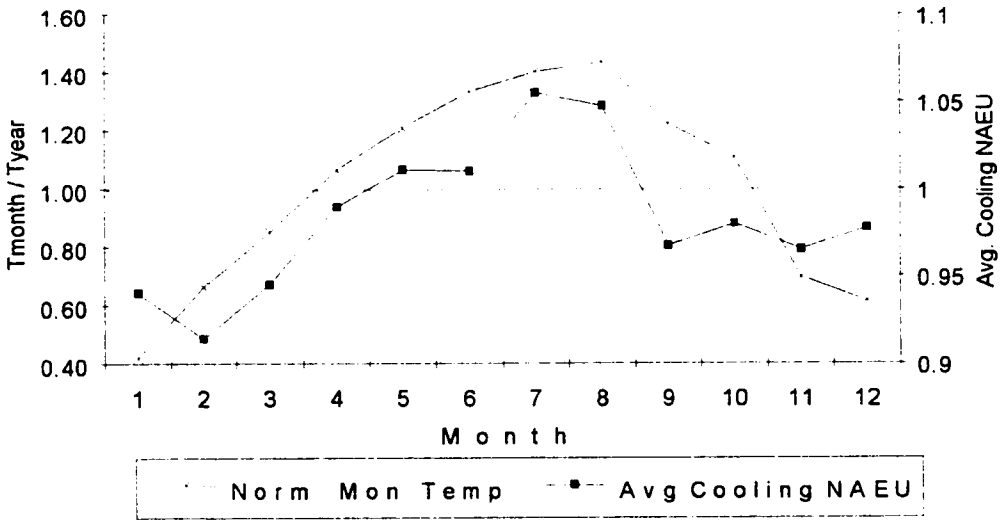

Figure 7.3 Normalized monthly temperatures and average cooling NAEUs for the office building.

From Figure 7.2 it is also apparent that heating NAEUs have the opposite relationship with the annual temperature variation. This inverse relationship is shown in Figure 7.4 where the average heating NAEU and the inverse of the normalized monthly temperature at the engineering center are plotted together. In this case too, a pattern emerges; heating models derived from warmer than average months tend to under-predict annual heating energy use and heating models derived from cooler than average months tend to over-predict annual heating energy use.

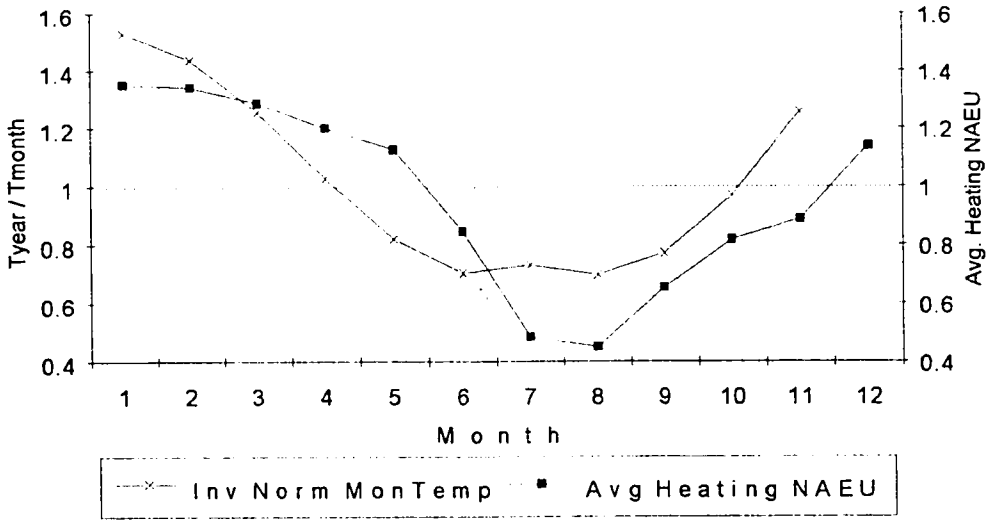

Figure 7.4 Inverse of the normalized monthly temperatures and average heating NAEUs at the engineering center.

Identifying the Best Season for Predicting Annual Energy Use. In practice, constraints other than the ability to most accurately predict annual heating and cooling energy use are likely to dictate the choice of the pre-retrofit data period. However, knowledge of which seasons tend to produce more accurate models is useful for assessing the likely accuracy of a short data-set model.

Building on the work of the previous section, models derived from data-sets that have average temperatures similar to the annual average temperature appear to be good predictors of annual energy use (Figures 7.3 and 7.4). To further investigate this hypothesis, the average monthly prediction error for each data-set is calculated as the absolute value of the deviation of the average NAEU (as defined in Equation 7.4) from unity:

$$\text{Average monthly prediction error} = \left|\overline{\text{NAEU}} - 1\right| \tag{7.5}$$

Figure 7.5 shows that average monthly prediction errors are lowest during the spring months for cooling and during both the spring and fall months for heating. In this climate,

the spring and fall months (which provide the best prediction of annual energy use for the office building) have both a wide range of temperatures and have mean temperatures very similar to the annual mean temperature (Figure 7.6). Thus, it is not clear whether the improved predictive ability of models from the spring and fall months results from implicitly incorporating into the model a wider range of temperatures or whether the improved predictive ability results from having mean temperatures close to the annual mean daily temperature. It is observed, however, that although October has a large range of daily temperatures, several other months (most notably November and December) also have large ranges of daily temperatures. Consequently, it appears that the deciding criteria of which months are the best predictor months seems to be based on the average daily temperature value rather than the range of daily temperatures. This observation was arrived at based on a small sample of buildings at only three locations in Central Texas. Future studies should evaluate the validity of this criteria using data from other buildings and from different geographical locations.

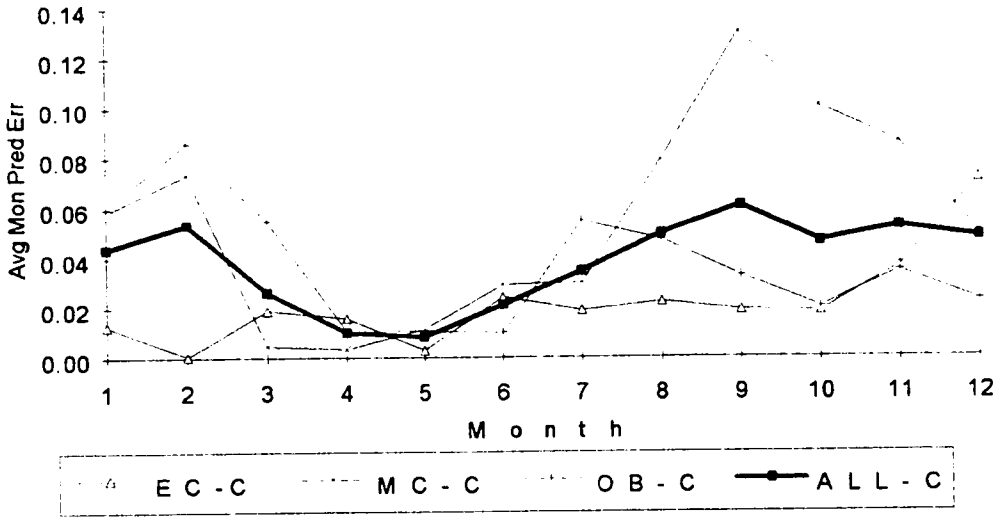

(a)

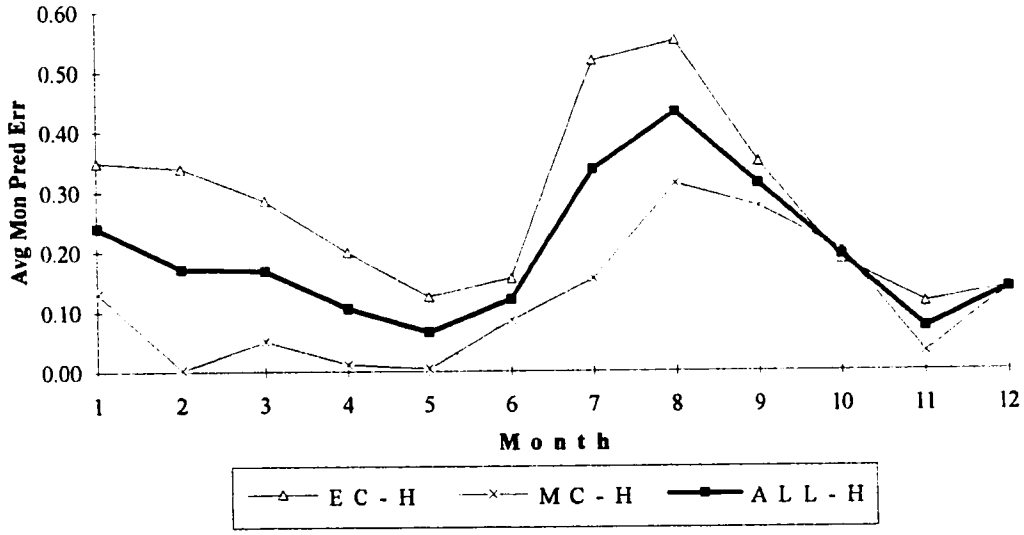

(b)

Figure 7.5 Average monthly prediction error for a) the cooling data sets and b) the heating data sets.

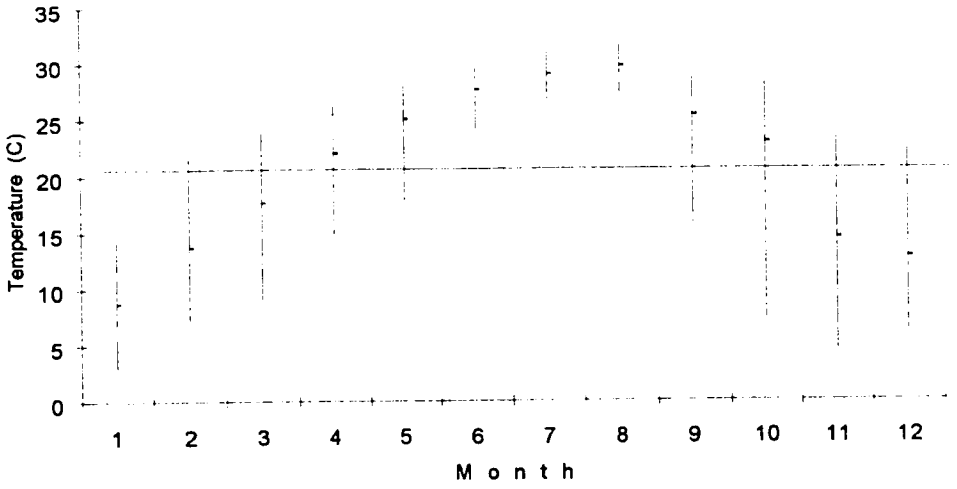

Figure 7.6 Monthly minimum, maximum and mean average daily temperatures for Austin, Texas during 1991. The horizontal bar indicates the annual mean temperature.

We have also explored the use of weighted regression (Draper and Smith, 1981) in order to improve the prediction accuracy of models based on limited data-sets. This approach involved grouping the temperature data into 2 °C bins and weighting the corresponding data points in each bin by the frequency of occurrence during the annual time period. Consequently, the temperature distribution for a particular limited data set would thereby be transformed into one similar to the yearly temperature distribution. Unfortunately, this approach did not improve the prediction accuracy of short data sets and in some cases worsened it. We speculate that this is caused by seasonal changes in certain building operating characteristics. Until a satisfactory methodology is available to account for this effect, we see little promise in pursuing the weighted regression technique any further.

The Effect of the Model Slope on NAEU. The pattern of over prediction by cooling models identified from the summer months and under prediction by cooling models

identified from the winter months (and the reverse for heating models) is determined by the variation of the model coefficients during the year.

Figure 7.7 shows the slopes of cooling models based on one month of data for the office building (the other buildings have similar patterns). Note that the slopes are similar to the annual slope in the spring and fall months and are very low for models identified from July and August data. These low summer slopes are responsible for the over prediction of annual energy use by cooling models based on summer data. Although the exact cause of the reduced temperature dependence of cooling energy during the summer months is unclear, we speculate that it may be caused by cooling systems that are operating at or near their design capacity and hence the dependency of thermal energy use and outside air temperature is reduced. The slopes of models from the spring and fall (which are the best predictors of annual energy use) are similar to the slope of the model based on the full year of data, which is consistent with the results of the previous sections.

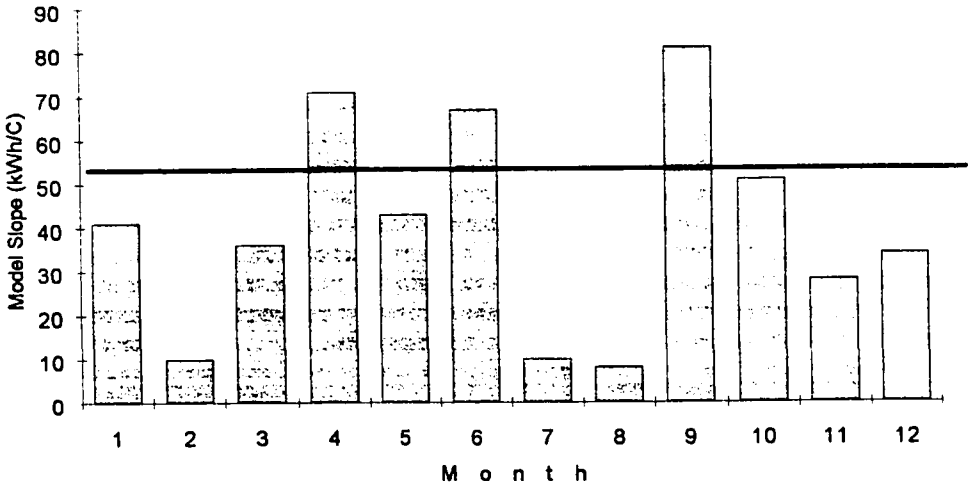

Figure 7.7 Monthly slopes of cooling regression models for the office building. The slope of the model based on a full year of data is depicted by the horizontal line.

The Effect of Model Linearity on Annual Prediction Accuracy

The degree with which a building's heating or cooling energy use is linearly related to temperature influences the accuracy with which short data-set models can predict annual energy use. In the buildings considered here, this relationship is nearly linear and prediction errors due to non-linearity are minimal. However, in many commercial buildings the relationship between heating or cooling energy use and temperature is non-linear. Consequently, models constructed using primarily the low or high temperature regions can seriously err in the prediction of annual energy use.

Figure 7.8 displays an example of non-linear heating energy use common in commercial buildings. The slope of the data at temperatures below 12 °C is steeper than that above 12 °C. Predicting annual energy use from temperature data exclusively from either the high or the low temperature region would seriously misrepresent the building's energy requirements during the other portion of the year.

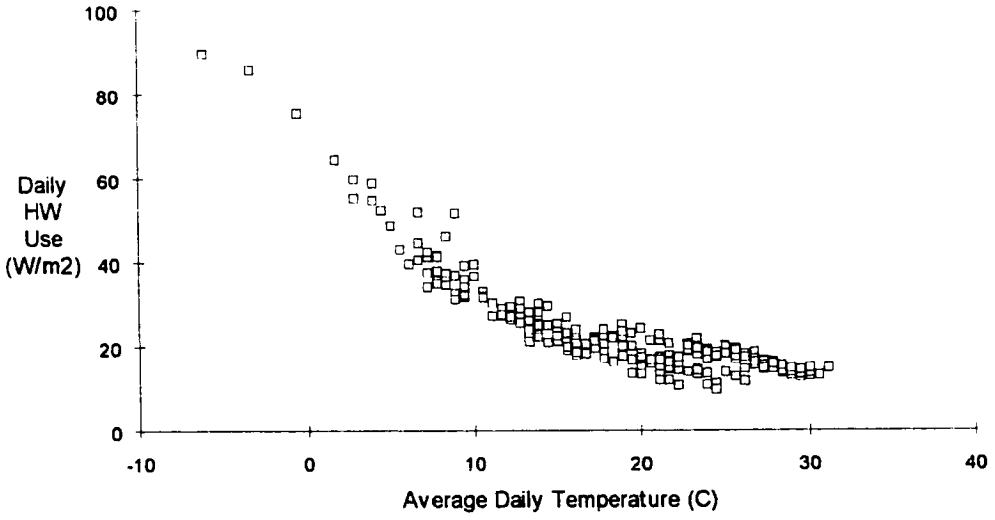

Figure 7.8 An example of heating energy use that is non-linear with outdoor air temperature.

The NAEUs for this building were computed but are not shown, since less than a full year of data was available. The NAEUs did, however, vary from unity by much more than the NAEUs shown in Figure 7.2, thus supporting the arguments made above. In our experience, which is mainly with commercial and institutional buildings in Texas, non-linear relationships between cooling and heating energy and temperature are common. Consequently, one should expect a large annual prediction error if energy use from a short data set is non-linear with temperature.

Chapter Summary

This chapter investigated the accuracy with which models based on short data-sets could predict annual energy use and whether certain general characteristics of the short data-sets could be identified which would be useful in ascertaining annual energy prediction accuracy. We found that annual heating energy use can be more than 400% greater than the annual energy use predicted by a short data-set model. In addition, in this climate of central Texas, models of heating energy use based on short data-sets have prediction errors four to five times as large as cooling energy models. Although this result is almost certainly climate dependent, we conclude that models based on short data-sets may seriously misrepresent annual energy use.

Two characteristics of data-sets were identified which influence their ability to predict annual energy use. As expected, longer data-sets provide a better estimate of annual energy use than shorter data-sets. In this sample of buildings, the average annual cooling prediction error of short data-sets decreased from 7.3% to 3.0% and the average annual heating prediction error decreased from 27.5% to 12.9% as the length of the data-set increased from one month to five months. More important than the length of the data-set, however, was the season during which it occurred. Cooling models from months with

above-average temperatures tend to over predict annual energy and cooling models from months with below-average temperatures tend to under predict annual energy use. The reverse relationship is true for heating models. The best predictors of both cooling and heating annual energy use are models from data-sets with mean temperatures close to the annual mean temperature. The range of variation of daily temperature values in the data-set seems to be less influential. We note that in Figure 7.2, one month data-sets from the spring and fall, when average temperature of the data-set is close to the mean annual temperature, are frequently better predictors of annual energy use than five month data-sets from the winter and summer.

A building's *energy use signature* also influences the ability of short data-sets to accurately predict annual energy use. If the relationship between daily energy use and mean daily temperature is non-linear over an entire year, then a linear model identified from only a portion of that data will almost certainly misrepresent annual energy use.

For a modeler faced with the task of determining annual energy use from a short data-set, the length and mean temperature of the data-set can give an indication of how well the short data-set model is likely to predict annual energy use. In addition, the degree of non-linearity between energy use and temperature may be anticipated by combining knowledge about the HVAC system with the simulation results presented in Chapter III. Unfortunately, the modeler has no way of knowing if the level of occupancy or if HVAC system variables changed during the year. Also, because only a portion of the yearly data is available, the modeler may be unable to actually verify if the relationship between energy use and outside air temperature is linear over the full year. Thus, the annual predictive ability of the short data-set model will necessarily remain somewhat uncertain.

CHAPTER VIII

ENERGY DELIVERY EFFICIENCY

An important characteristic of energy use in dual-duct HVAC systems is the simultaneous heating and cooling, and subsequent mixing of separate air streams in order to maintain building comfort conditions. Other systems, such as re-heat systems, first cool the supply air and then re-heat it to match the individual zone loads within a building. Because of mixing and re-heating, the total heating and cooling energy used to maintain comfort conditions in commercial buildings is almost always greater than the net heating or cooling load on the building. The excess energy consumed in mixing and re-heating processes can be a significant portion the total building energy use.

In this chapter, a new index is proposed which measures the efficiency with which buildings are heated and cooled relative to the minimum energy required to offset the net building and ventilation loads. This index, the Energy Delivery Efficiency (EDE), is the fraction of the total heating and cooling energy that is applied to the building load; the remaining energy being consumed in mixing and re-heating processes. A procedure to calculate the ideal EDE for the multizone case is also presented which allows the fractions of energy mixed within and between building zones to be determined. The use of the EDE to quantify the reduction in energy mixing caused by a CAV to VAV retrofit is demonstrated. The original work for much of this chapter was first reported by Reddy et al. (1993).

Introduction

A typical commercial building will have several zones with different heating and cooling requirements. If each zone had its own heating and cooling plant, the air supplied to the zone could be heated or cooled to just the right temperature to offset the heating or

cooling load on the zone. However, the capital costs of installing such a system in a large, multizone building are prohibitive. The traditional solution has been to build a single heating and a single cooling plant for a group of zones and then mix or re-heat the air supplied to each zone in order to meet the individual zone loads. This process is similar to the way in which the temperature of shower water is controlled in a locker room with multiple showers. Cold water at a fixed temperature and warm water at another fixed temperature are supplied to each shower. The cold and warm water are then mixed to provide water at the proper temperature for each showers.

In addition to the requirement of providing heating and cooling to multiple zones with different heating and cooling requirements, the requirement that a minimum amount of ventilation air be supplied to each zone can also cause supply air to be mixed or re-heated. For example, when there is no heating or cooling load on a zone the cool and warm air streams must be mixed in order to avoid over-cooling or over-heating the room while still satisfying the minimum ventilation requirement..

Two types of control strategies have been developed to minimize energy wasted in mixing processes. The first is to control the temperatures of the air streams so that the cool air stream is just cold enough to meet the cooling requirement of the warmest zone and the warm air stream is just hot enough to meet the heating requirement of the coldest zone. The hot deck reset schedule described in Chapter III is one such method. VAV systems employ a different strategy which is to modulate the flow rates of the warm and cool air streams so that they meet the zone loads with a minimum of mixing. Some control algorithms use a combination of the two methods.

In the following sections we propose an index, called the energy delivery efficiency (EDE), to measure the mixing and re-heating of air streams. The index can be used to compare the effectiveness of heating and cooling systems on an absolute scale and finds particular application in the assessment of retrofits designed to minimize mixing. An ideal

EDE for multizone buildings is also developed which lends insight into the nature of the mixing process. The concept of EDE is demonstrated with simulated data for CAV and VAV systems.

Energy Delivery Efficiency

The EDE can be developed from an energy balance on the entire building. Major energy flows into and out of a typical commercial building can be characterized as in Figure 8.1. Q_{ua} is the conduction heat transfer across the building envelope. Q_{sol} is the solar load. Q_i is the internal load generated by people, fans, electrical equipment, etc. inside the building. Q_v is the ventilation load and equals the product of the flow rate of outside air into the building and the enthalpy difference between the outside and inside air. E_h and E_c are the heating and cooling energy added to and removed from the building respectively.

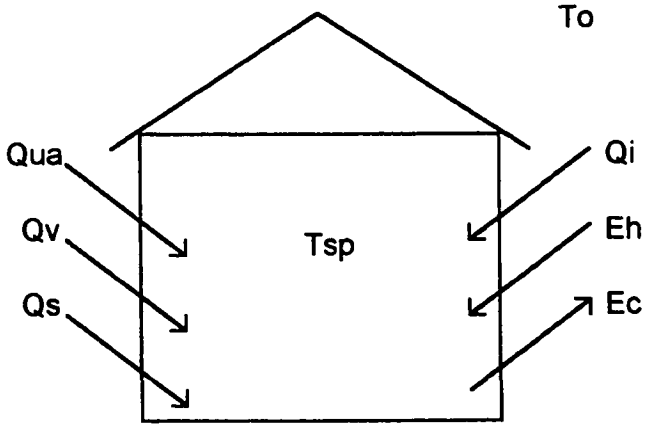

Figure 8.1 Major energy flows into and out of a typical commercial building.

An energy balance on the building gives:

$$E_c - E_h = Q_{ua} + Q_v + Q_s + Q_i \qquad (8.1)$$

The difference between the heating and cooling coil loads, called the net cooling load E_{nc}, equals the sum of the heat loads to the building. This sum is the minimum energy required to heat or cool the building. The actual energy consumed to heat and cool the building is the sum of the heating and cooling coil loads. We define the ratio of the actual to minimum energy required to heat and cool the building to be the energy delivery efficiency (EDE).

$$\text{EDE} = \frac{\text{Minimum Energy Use}}{\text{Actual Energy Use}} \tag{8.2}$$

or

$$\text{EDE} = \frac{E_c - E_h}{E_c + E_h} \tag{8.3}$$

During cold weather, the net cooling, E_c - E_h, may be negative, indicating a net heating load on the building. In order to refine the definition, we take the absolute value of the numerator so that EDE varies between the limits of zero and unity and define the absolute EDE to be:

$$\text{EDE} = \frac{|E_c - E_h|}{E_c + E_h} \tag{8.4}$$

EDE determines the efficiency of a building's energy delivery system using easily measured parameters, E_c and E_h. And because EDE depends only on energy flows into and out of the building, it is independent of a building's HVAC system and control features. Thus, the efficiency of heating and cooling systems before and after retrofits can be easily compared. In addition, EDE rates each system on an absolute scale between zero and unity, and hence indicates the overall potential for reducing mixing and re-heating. It should be remembered, however, that EDE is limited to the air-side system performance only and does not indicate the energy efficiencies of the building envelope or primary equipment.

Ideal Multizone Energy Delivery Efficiency

A principle cause of mixing and re-heating supply air in commercial buildings is the differing zone heating and cooling requirements in a multizone building. Under certain conditions, for example, exterior zones in a building may require heating while interior zones require cooling. We call this phenomenon *inter-zone mixing*. Most current HVAC systems do little to minimize inter-zone mixing. Mixing of warm and cool air streams may also occur within a single zone. This is called *intra-zone mixing*. VAV systems and hot-deck reset schedules attempt to minimize intra-zone mixing. EDE, as developed above, makes no distinction between the two types of mixing.

The usefulness of the EDE concept can be extended, however, by developing a procedure to calculate the energy delivery efficiency when the only simultaneous heating and cooling that occurs is because some zones require cooling while other zones require heating. This ideal situation represents the minimum amount of simultaneous heating and cooling that most current systems are capable of achieving; and hence we name the EDE in this situation the ideal multizone EDE (EDE_i). EDE_i is a standard with which the measured EDE can be compared to in order to judge the effectiveness of control strategies designed to minimize intra-zone mixing. EDE_i can also be interpreted to differentiate between intra-zone and inter-zone mixing and thus lend considerable insight into the nature of energy mixing in commercial buildings.

To understand EDE_i more clearly, consider an alternate formulation of the EDE where E_t is the total thermal energy use, $E_{m,inter}$ is the energy mixed between zones and $E_{m,intra}$ in the energy mixed within the zones:

$$EDE = 1 - \frac{E_{m,inter} + E_{m,intra}}{E_t} \tag{8.5}$$

The EDE_i occurs when there is no inter-zone mixing and hence $E_{m,inter}$ is zero:

$$EDE_i = 1 - \frac{E_{m,intra}}{E_t} \tag{8.6}$$

The fractions of energy wasted in inter-zone mixing, $E_{m,inter}/E_t$ and intra-zone mixing $E_{m,intra}/E_t$ can be easily determined from Equations 8.5 and 8.6 if EDE and EDE_i are known.

The ability to differentiate between inter-zone and intra-zone mixing aids in the evaluation of the effectiveness of energy delivery systems. For example, VAV systems attempt to reduce intra-zone mixing, but can do little to reduce inter-zone mixing. Thus, the effectiveness of a VAV retrofit at reducing mixing is most appropriately determined by measuring the fraction of energy wasted in intra-zone mixing. Advanced HVAC systems capable of transferring low temperature heat from zone to zone are capable of reducing inter-zone mixing, and their effectiveness can be accessed by measuring the fraction of energy wasted in inter-zone mixing.

To develop a mathematical expression for EDE_i, multizone behavior is approximated by dividing a building into an interior and exterior zones as in Chapter III. For simplicity, we consider only sensible cooling loads. The balance point temperature for a zone is defined as the outside air temperature for which no heating or cooling is required to maintain the interior set-point temperature (Mitchell, 1983). It can be determined from an energy balance on the zone. Following Equation 8.1, and noting that the only loads to the interior zone are the internal and ventilation loads, an energy balance on the interior zone is:

$$E_{nc,int} = f_{int} \times Q_i + f_o \times V_{r,int} \times \rho c_p \times (T_o - T_r) \tag{8.7}$$

where $E_{nc,int}$ is the net cooling energy use in the interior zone and the other nomenclature is consistent with that used in Chapter III. The balance point temperature of the interior

zone $T_{b,int}$ can be determined setting the $E_{nc,int}$ equal to zero in Equation 8.2 and solving for T_o:

$$T_{b,int} = T_r - \frac{f_{int} \times Q_i}{f_o \times V_{r,int} \times \rho c_p}. \quad (8.8)$$

The balance point temperature of the exterior zone follows from an energy balance on the exterior zone involving conduction, ventilation, solar and internal loads.

$$E_{nc,ext} = UA_s^*(T_o - T_r) + f_o \times V_{r,ext} \times \rho c_p \times (T_o - T_r) + (s_1 + s_2 \times T_o) + (1-f_{int}) \times Q_i \quad (8.9)$$

where $E_{nc,ext}$ is the net cooling energy use in the exterior zone. We assume here, as in Chapter III that the solar load can be approximated as a linear function of outside air temperature (Vadon et al., 1991). Setting $E_{nc,ext}$ equal to zero gives the balance point temperature of the exterior zone $T_{b,ext}$:

$$T_{b,ext} = \frac{T_r \times (UA_S + f_o \times V_{r,ext} \times \rho c_p) - s_1 - (1 - f_{int}) \times Q_i}{UA_S + s_2 + f_o \times V_{r,ext} \times \rho c_p}. \quad (8.10)$$

Because the interior zone is insulated from conductive heat losses through the building envelope by the exterior zone, the outside air temperature at which the interior zone requires heating is much lower than that at which the exterior zone requires heating. Thus, the balance point temperature of the interior zone is always lower than the balance point temperature of the exterior zone for comparable internal loads. When the outside air temperature is lower than the balance point temperature of the interior zone, both zones require heating. Similarly, when the outside air temperature is greater than the balance point temperature of the exterior zone, both zones require cooling. In these conditions, inter-zone mixing is absent, and EDE_i is unity.

When the outside air temperature is between the balance point temperatures of the interior and exterior zones, the interior zone requires cooling and the exterior zone requires heating. In the ideal case, there is no intra-zone mixing and hence the cold deck

energy use E_c equals the net cooling energy use on the interior zone $E_{nc,int}$. Similarly, the hot deck energy use E_h equals the negative of the net cooling load on the exterior zone $-E_{nc,ext}$. The negative sign occurs because of the sign convention. Substituting $E_{nc,int}$ for E_c and $-E_{nc,ext}$ for E_h in Equation 8.3 gives the ideal multizone energy delivery efficiency (EDE_i):

$$EDE_i = \frac{E_{nc,int} + E_{nc,ext}}{E_{nc,int} - E_{nc,ext}} \quad (T_{b,int} < T_o < T_{b,ext})$$

$$EDE_i = 1 \qquad \text{(otherwise)} \qquad (8.11)$$

As before, we define the absolute EDE_i to be the absolute value of EDE_i.

Knowledge of the value of ideal multizone EDE can yield powerful insight into the mixing problem. Its use is demonstrated in the following section.

EDE in CAV and VAV Systems

Figure 8.2 shows simulated values of the absolute EDE and the ideal multizone EDE for a CAV system at the engineering center. The values of the parameters used to simulate EDE and EDE_i are the same as those listed in Table 3.1. In this simulation, the internal loads and latent loads are held constant in order to demonstrate the variation of the EDE with outside air temperature. It is apparent that in this simulation, the EDE which is the fraction of total energy use applied to the building load, never rises above 35%. Thus, even when the CAV system is operating most efficiently, 65% of the total heating and cooling energy use is wasted in mixing processes. At an outside air temperature of 3 °C, the EDE is zero, indicating that equal quantities of heating and cooling energy were consumed by the building even though there was no net heating or cooling load on the building. Values of EDE appear linearly related to outside air

temperature because values of cooling and heating energy use were also nearly linear with outside air temperature (see Chapter III).

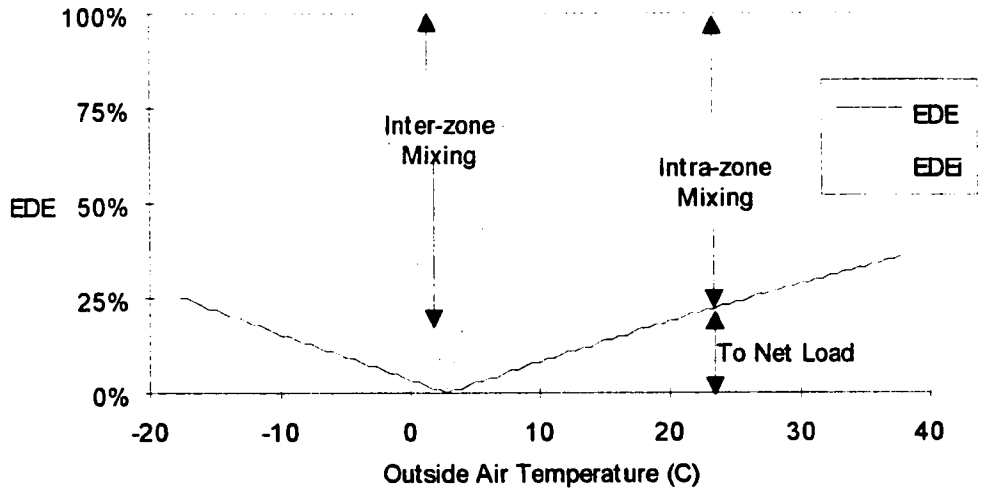

Figure 8.2 Simulated values of absolute EDE and ideal multizone EDE for a CAV system. Internal and latent loads are assumed to be constant.

Further insight into the mixing processes is gained by examining the ideal multizone EDE in Figure 8.2. The interior and exterior zone balance point temperatures are -4 °C and 9 °C respectively. When the outside air temperature is below the interior balance point temperature, both zones require heating and there is no inter-zone mixing. Similarly, when the outside air temperature is greater than the exterior balance point temperature both zones require cooling and again there is no inter-zone mixing. Between the balance point temperatures, the interior zone requires cooling and the exterior zone requires heating. In this temperature region, the inter-zone mixing increases to a maximum of unity at 3 °C where the two zones require equal quantities of heating and cooling. Thus, for any outside air temperature we can determine the fraction of energy applied to the building

load (EDE), the fraction of energy wasted in inter-zone mixing (1 - EDE_i), and the fraction of energy wasted in intra-zone mixing (EDE_i - EDE).

Note that 3 °C is the a balance point temperature only in the sense that an ideal HVAC system would require no thermal energy input at this temperature. For most current HVAC systems, 3 °C is merely the outside air temperature at which the interior zone requires the same amount of cooling energy as the exterior zone requires heating energy. Thus, both heating and cooling are being consumed at this temperature. As is made evident by the differing internal and external zone balance point temperatures, there is no single outside air temperature where no heating and cooling is required.

Figure 8.3 shows simulated values of the EDE and the ideal multizone EDE for a VAV system at the engineering center. Values of the EDE from the VAV system are generally much higher than those from the CAV system because of the improved control of air flow to the zones. Using EDE, the effectiveness of the energy delivery systems can be quantified and compared. For example, at an outside air temperature of 10 °C, the CAV system is effectively utilizing only 10 % of heating and cooling energy while the VAV system effectively uses over 85 % of that energy.

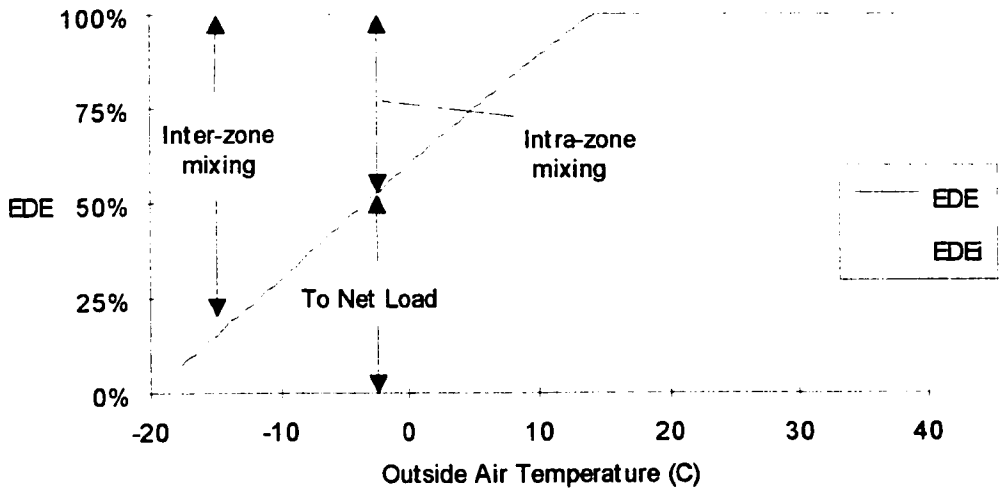

Figure 8.3 Simulated values of absolute EDE and ideal multizone EDE for a VAV system. Internal and latent loads are assumed to be constant.

The value of EDE in the VAV system is unity at outside air temperatures above 15 °C where the VAV system has eliminated the need for heating (Figure 8.3). Comparison of the EDE with the ideal multizone EDE reveals that for outside air temperatures between about -7 °C and 15 °C, significant intra-zone mixing still occurs as a result of the minimum air flow requirement. At outside air temperatures below -7 °C, the balance point temperature of the exterior zone, the exterior zone requires heating while the interior zone requires cooling. Thus, EDE_i decreases significantly to account for this inter-zone mixing. In this temperature range, a comparison of EDE and EDE_i clearly shows that the VAV has eliminated almost all intra-zone mixing, but that inter-zone mixing is still significant. The reduced air flow to the interior zone has caused the balance point temperature of the interior zone to be less than -20 °C and thus it is not shown in Figure 8.3.

Chapter Summary

The EDE determines the efficiency of a building's energy delivery system. Its calculation requires only two easily measured parameters, E_c and E_h and can be calculated using any time interval of data.

The value of EDE is the fraction of energy used to meet the net load on the building. It allows the efficiency of energy delivery systems to be rated on an absolute scale of zero to unity so that their potential for improvement can be identified. EDE also allows the effectiveness of energy delivery system retrofits to be quantified by comparing pre and post-retrofit values of EDE. A further advantage of EDE is that the effectiveness of retrofits to the energy delivery system can be determined even if retrofits to the building's shell or other energy using systems were also performed.

The ideal multizone EDE adds further insight into the mixing process by quantifying the fractions of inter-zone and intra-zone mixing. Calculation of the EDE_i requires substantially more information than calculation of the simple EDE, including knowledge of the overall building load coefficient, the solar load, and the flow rates of air to the interior and exterior zones. In addition, EDE_i should be compared to only daily (or longer) data because energy storage effects can cause the coil loads, E_{cc} and E_{hc}, to lag one or more hours behind the building loads Q_{ua}, Q_s and Q_i when using hourly (or shorter) data. However, if these parameters can be accurately estimated, much can be learned from comparison of EDE and ideal multizone EDE. For example, the low values of EDE for outside air temperatures of below -7 °C in Figure 8.3 appear to be caused almost entirely by inter-zone mixing. Future commercial building energy delivery systems may be able to transfer excess heat from the interior zones to the exterior zones and thereby reduce inter-zone mixing. The potential for such efficiency improvements is clearly quantified by the use of the ideal multizone EDE.

CHAPTER IX

ARTIFICIAL NEURAL NETWORKS AND THEIR APPLICABILITY FOR MEASURING SAVINGS

This chapter serves as an introduction to artificial neural networks (ANNs) and their applicability for modeling commercial building energy use for the purpose of determining savings. It begins by describing the neurobiological roots of ANNs and then proceeds to outline the back-propagation algorithm and investigate the effects of model parameters and network architectures on the rate of convergence and prediction accuracy of ANN models. The chapter concludes by modeling a set of measured energy use data with both ANN and least square regression models in order to compare the attributes of the two data fitting methods.

The Neurobiological Model and ANNs

The human brain is a highly complex organ comprised of some 10^{11} basic units called neurons. Each neuron is connected to about 10^4 other neurons. Because of this highly interconnected nature, the architecture of the brain is referred to as being massively parallel or massively interconnected.

Each neuron consists of a soma, dendrites, axons and synapses (Figure 9.1). The soma is the body of the neuron. Dendrites and axons extend from the soma and branch out like roots. If a neuron receives enough active inputs along its dendrites, it "fires" and sends a voltage spike down the axons. Axons are connected to other dendrites and somas at synapses. When a neuron fires, chemicals called neurotransmitters are diffused across the synapses. Learning is thought to occur at the synapses where the neurotransmitters and neuroreceivers vary to reinforce "good" connections and discourage "bad" connections (Beale and Jackson, 1990).

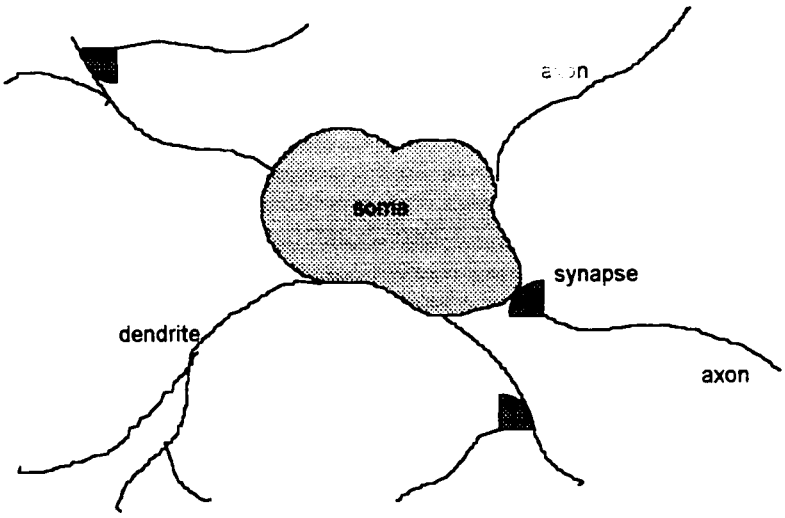

Figure 9.1 Schematic representation of a neuron

ANNs attempt to mimic parts of the architecture and functionality of the brain. Neurons are simulated in ANNs as connected nodes. The parallel processing structure of the brain is simulated by arranging the nodes in layers such that each node is connected to all of the nodes in the adjacent layers. In a manner analogous to the response of a neuron, each node sums the inputs it receives and transmits an output signal to the other nodes to which it is connected. The output signal of each ANN node is multiplied by a weight which is varied during the learning process, just as synaptic neurotransmitters and receivers are varied in the human learning process.

Although ANNs simulate important aspects of human neurobiology, it is instructive to consider a fundamental difference. A digital computer is a serial device in which a single central processing unit (CPU) processes a sequential set of instructions. Today's CPUs can process millions of instructions per second, which is far faster than the processing speed of a human neuron (about 10 responses per second). This raw speed enables digital computers to accomplish serial tasks, such as addition of a long series of numbers, far faster than the human brain.

The tasks that the human brain evolved to accomplish, however, such as vision, speech recognition and learning are not serial tasks. These tasks are characterized by multiple, simultaneous inputs and the search for relationships among the inputs. These "parallel" tasks are performed much more effectively by the parallel processing structure of the human brain. In stark contrast to the single processor in a serial computer, processing in the brain is distributed among many millions of neurons. This parallel distributed architecture enables several processes and comparisons to be made simultaneously, enhancing pattern recognition and learning tasks.

ANN algorithms *simulate* parallel distributed processing in software, and hence attempt to reproduce some of the learning and pattern recognition characteristics of parallel processing in the serial environment. However, they make no attempt to duplicate the sophisticated and complex massively interconnected morphology of the human brain. In addition, very little is known about how high level information is processed and stored in the human brain. Therefore, although ANNs model some primary neurobiological processes, analogies between ANNs and high level human intelligence are tenuous.

The Generalized Delta, Back-Propagation Algorithm

Many different types of ANNs have been devised to accomplish a wide variety of tasks including recognition of handwritten English words, speech recognition and image compression (Wasserman, 1989). The ANNs examined here employ a fully-connected, feed-forward architecture (Figure 9.2). Fully-connected means that each node is connected to all of the nodes in the adjacent layers (or columns of nodes). Feed-forward indicates that information is passed in a single direction from the input to the output nodes.

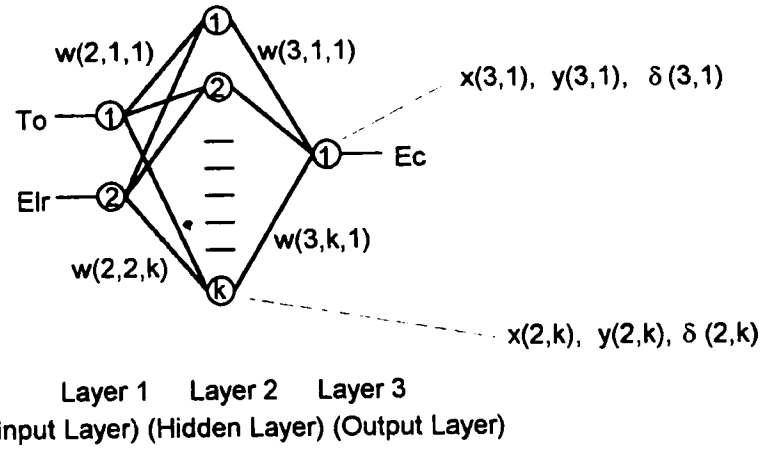

Figure 9.2 Notation used in the description of the ANN computational algorithm. Input variables are outside air temperature T_O and lighting and receptacle electricity use E_{lr}. The output variable is cooling energy use E_C. An activation level x, an output y and an error δ are associated with each node. Each connection, shown as a line between nodes, has a weight w associated with it.

A learning algorithm *trains* an ANN to recognize patterns between the input and output variables. The algorithm employed here is the back-propagation, generalized delta method (Wasserman, 1989). It was chosen because of its applicability to multi-layer, feed-forward architectures and because it has been used in several other HVAC applications (see for example: Miller and Seem, 1991; Kreider and Wang, 1991; and Nelson, 1993). In this algorithm, the value of the output of the ANN is compared to a target value (which in our case is the measured cooling energy use) to determine an error or *delta*. The weights associated with the connections between nodes are then adjusted in a *backward* direction from the output layer to the input layer in order to minimize this error.

The feed forward, back propagation ANN algorithm is computationally quite simple. The entire process is described in the following eight steps using the notation in Figure 9.2.

Step 1. The values of the input and output variables are scaled to vary between 0.1 and 0.9 according to the following equation:

$$d_{normal} = (d - d_{min}) / (d_{max} - d_{min}) \times 0.8 + 0.1 \quad (9.1)$$

where d_{min} and d_{max} are the minimum and maximum values of variable d.

Step 2. A weight is associated with each connection between nodes. The weights associated with the connections between layers L-1 and L are denoted as w(L, j, k), where j is the number of the node in layer L-1 and k is the number of the node in the layer L. The initial value of each weight in the network is set to be a random number between 0.5 and -0.5.

Step 3. The output of node k from the first layer of nodes y(1, k) is equal to the value of the normalized input variable.

Step 4. An activation level x(layer number, node number) and an output y(layer number, node number) are associated with each node in the subsequent layers. The activation level of a node is the sum of the products of the outputs and weights from previous nodes. The activation for node k in layer L is:

$$x(L,k) = \sum_{j=1}^{n(L-1)} w(L,j,k) \times y(L-1,j) \quad (9.2)$$

where n(L-1) is the number of nodes in layer L-1.

The output of each node can be determined using a linear function, a threshold function, a hyperbolic tangent function or a sigmoid function. The sigmoid function is widely used because it simulates the non-linear transfer characteristics of biological neurons. In addition, the sigmoid function aptly handles both small and large activation levels by limiting the value of the output function to values between zero and one regardless of the input activation level (Wasserman, 1989). Using a sigmoid function, the output from node k in layer L is:

$$y(L,k) = \frac{1}{1 + \exp[-\text{gain} \times (x(L,k) + \text{bias})]} \quad (9.3)$$

The gain and bias in Equation 9.3 are parameters which modify the shape and position of the sigmoid function. Their influence on the speed and accuracy of network convergence is investigated in the next section. The activation level and output of each node are calculated in a layer by layer fashion moving from the input layer to the output layer.

Step 5. This step begins the training process where the weights associated with each connection are adjusted. An error δ(layer number, node number) is associated with each node. The error of the output node k in layer L is:

$$\delta(L, k) = y(L, k) \times (1 - y(L, k)) \times (d - y(L, 1)) \tag{9.4}$$

where d is the target value that the network is attempting to model. The quantity $y(L, k) \times (1 - y(L, k))$ is simply the derivative of the sigmoid function with respect to the activation level.

The weights of the connections from node j in layer L-1 to the output node k in layer L are adjusted as follows:

$$w(L, j, k)_{n+1} = w(L, j, k)_n + Lrate \times y(L-1, j) \times \delta(L, k) \tag{9.5}$$

where the subscripts n and n+1 refer to the previous and newly adjusted weights and Lrate is the learning rate. The learning rate varies how much each weight is adjusted. The influence of the learning rate on the speed and accuracy of convergence is also discussed in the following section.

Step 6. All remaining weights are adjusted in the backward direction from the output layer to the input layer using Equation 9.5. However, the procedure to calculate the error δ of the nodes in the hidden layers is different than in Equation 9.4 because no target value is available for these nodes. The error of node j in hidden layer L is:

$$\delta(L, j) = y(L, j) \times (1 - y(L, j)) \times \sum_{i=1}^{n(L+1)} d(L+1, i) \times w(L+1, j, i) \tag{9.6}$$

Step 7. After each of the weights have been adjusted, another set of input values is entered in step 3 and steps 3 through 6 are repeated until the entire data set has been passed through the network.

Step 9. Each pass through the data set is called an epoch, and ANNs typically require several epochs (sometimes as many as several thousand) before convergence. Convergence criteria can be defined in several ways. One way is to stop processing when the accuracy of prediction improves by only a small amount after each epoch. To use this method, calculate the total of the absolute deviations between the output of the network and the target values during each epoch. When the difference between the total deviations of subsequent epochs is less than some tolerance value, processing is stopped.

A complete program listing for a four layer network is included in Appendix C. A detailed treatment of the theory and mathematics of ANNs is provided by McClelland and Rumelhart (1989).

The Effects of Bias, Gain and Learning Rate on the Rate of Convergence and Prediction Accuracy of ANNs

The back-propagation learning method uses a gradient descent search procedure, moving in the direction of the steepest slope downward. Unfortunately, the error surface may not be smooth and may contain several local minimums and maximums. Thus, it is possible for the ANN to become *stuck* in a local minimum and never find the true minimum of the surface. Large step sizes, caused by large values of the gain and learning rate, may also cause the ANN to repeatedly *miss* the true minimum and oscillate back and forth between non-optimal solutions. Although most of these problems can be minimized by using small values of gain and learning rate (Wasserman, 1989), this can dramatically increase the time required for convergence. In this section, we examine the effects of

varying the values of the gain, bias and learning rate on the rate of convergence and on the prediction accuracy of an ANN model.

To examine the effects of these parameters, a small, non-linear, sample data set was synthesized according to the relation:

$$E_C = 1 + .04 \times T_O + (E_{lr} / 600)^8 \tag{9.7}$$

where E_C is cooling energy, T_O is outside air temperature and E_{lr} is lighting and receptacle electricity use Ten values from this three dimensional data space (Figure 9.3) where used as the synthetic data set. The data were submitted to an ANN with three layers and five nodes in the hidden layer. The speed of convergence was measured as the number of training epochs required for the ANN to meet an arbitrarily chosen convergence criteria. Because the initial values of the weights are random, the average number of training epochs of five runs was used as the measure of the speed of convergence.

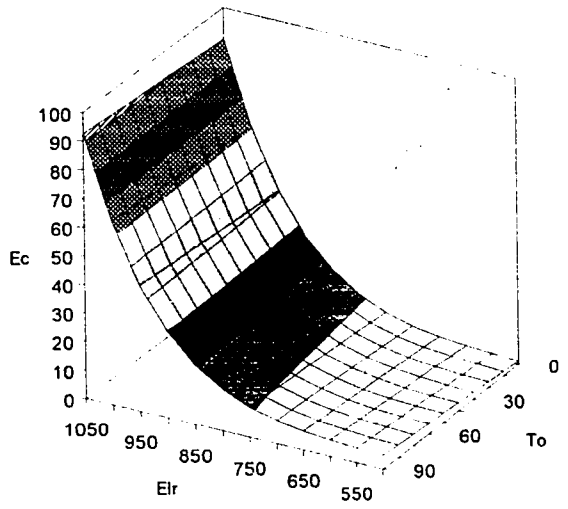

Figure 9.3 Synthetic data space used to test variations of the gain, bias and learning rate.

Bias. Adding a non-zero bias in Equation 9.3 has the effect of shifting the sigmoid function to the right or left and may accelerate the learning process. Two types of biases may be added: constant and variable. A variable bias is created by adding a node to the input and each hidden layer with a fixed activation level of 1.0. Miller and Seem (1991) found that the addition of a variable bias did not significantly improve their results. In this study, we chose to examine only the effects of constant biases.

To test the effect of a non-zero bias on the speed of convergence, a base case was selected in which the gain was set to 0.5 and the learning rate was set to 0.25 while the bias was varied from -1.0 to 1.0. Table 9.1 shows that the average number of training epochs required to meet the convergence criteria increases slightly as the bias deviates from zero. These results suggest that a small non-zero bias may be optimum, however, the improvement in speed of convergence appears to be small and hence the bias was set to zero in all future runs.

Table 9.1 Average number of training epochs required for convergence as the bias varies from -1.0 to 1.0

bias	Average Number of Epochs
-1.0	1168
-0.5	879
0.0	868
0.5	931
1.0	1066

Gain and Learning Rate. Figure 9.4 shows the sigmoid function (Equation 9.3) for three values of the gain: 0.1, 0.5, and 0.9. Increasing the gain increases the slope of the output function y(x) at small values of the activation level x. This makes y(x) more sensitive to changes in x and tends to accelerate the learning process. However, the

relatively large change in y(x) for small changes in x may cause the network to skip over the true minimum and converge on a less than optimal solution.

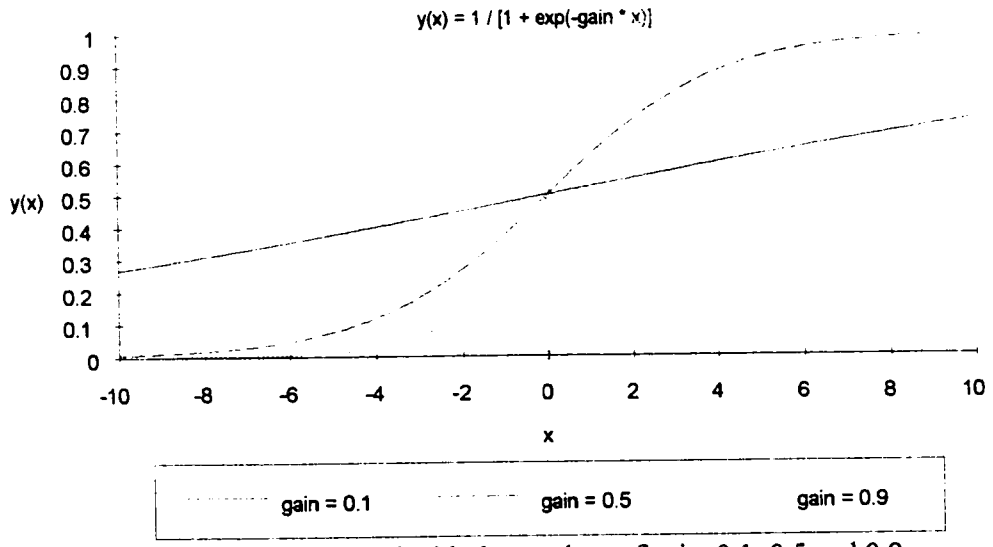

Figure 9.4 Sigmoid function plotted with three values of gain: 0.1, 0.5 and 0.9.

The learning rate scales the adjustments made to each weight during the training process (see Equation 9.5). The effect of increasing the learning rate on the speed and accuracy of convergence is similar to the effect of increasing the gain; it accelerates convergence by making larger incremental changes in the weights, but may hinder the network's ability to locate the minimum error.

Because of the confounding effects of varying the gain and learning rate, a matrix test structure was selected in which the learning rate and the gain were each varied independently. Table 9.2 shows that the speed of convergence increased by over two orders of magnitude as the gain and learning rate were increased.

Table 9.2 Average number of training epochs required for convergence as the learning rate and gain are varied. NC indicates no convergence after 5000 training epochs.

learning rate \ gain	0.1	0.5	0.9
0.25	5000 NC	868	597
1.0	5000 NC	254	124
3.0	2318	70	56
5.0	1856	50	26
7.0	529	37	23

Unfortunately, rapid convergence may decrease the final prediction accuracy of the ANN and may cause the ANN to oscillate between non-optimal solutions as it hunts for the minimum error. The effect of varying the values of the gain and learning rate on the prediction accuracy was tested by recording the average prediction error after 5000 training epochs or after the prediction error had begun to oscillate. The destabilizing effect of large learning rates is clearly evident in Table 9.3; in all cases, high learning rates decrease the prediction accuracy. Learning rates of 1.0 or greater also caused the network to oscillate rather than converge. Thus, only the lowest value of learning rate (0.25) appears to be appropriate for this data set.

Table 9.3 Average prediction error upon convergence as the learning rate and gain are varied. O indicates that the solution had begun to oscillate.

learning rate \ gain	0.1	0.5	0.9
0.25	12.26	7.21	6.81
1.0	12.29	7.40 - O	7.48 - O
3.0	12.31 - O	8.93 - O	8.57 - O

Low values of the gain seem to have slowed the learning process such that even after 5000 training epochs the prediction error was still large. High values of gain accelerated the learning process such that a low prediction error could be achieved after a reasonable amount of training time. However, it is not clear whether the final prediction accuracy for small values of gain would eventually be as low or lower than for high values of gain if the

ANNs were allowed to run indefinitely. In addition, high values of gain appear to have a far less destabilizing influence on the prediction error than high values of the learning rate. Thus, increasing the gain appears to be a more robust way to decrease training time than increasing the learning rate. For this data set and network, the optimal combination seems to be a low value of the learning rate (0.25) and high value of the gain (0.9), although it is possible that even smaller values of the learning rate may improve the accuracy of prediction even further.

The Effect of Network Architectures on the Accuracy of Prediction

In this section, we investigate how three different architectures (Figure 9.5) affect the accuracy of prediction. The first network ANN1 has three layers: an input layer, an output layer and one hidden (or middle) layer. This network was used in the previous section to test how varying the values of the bias, gain and learning rate affected the rate of convergence and accuracy of prediction. The second network ANN2 also has three layers, however, the number of nodes in the hidden layer has been increased from five to ten. The third network ANN3 has two hidden layers of five nodes each. In each network outside air temperature and lighting and receptacle electricity use were used as inputs in order to model cooling energy use.

Results from the previous section suggest that small step sizes created by setting the gain equal to 0.5 and the learning rate equal to 0.25 provide a suitable combination of speed and accuracy. In the discussion that follows, the gain was set to 0.5, the learning rate set to 0.25 and the bias set to zero unless otherwise indicated.

The cooling energy use predicted by typical runs from ANN1, ANN2 and ANN3 are plotted with the target values of cooling energy use from the synthetic data set in Figure 9.6. ANN1 and ANN2 simulate some of the non-linear behavior of the target data set at

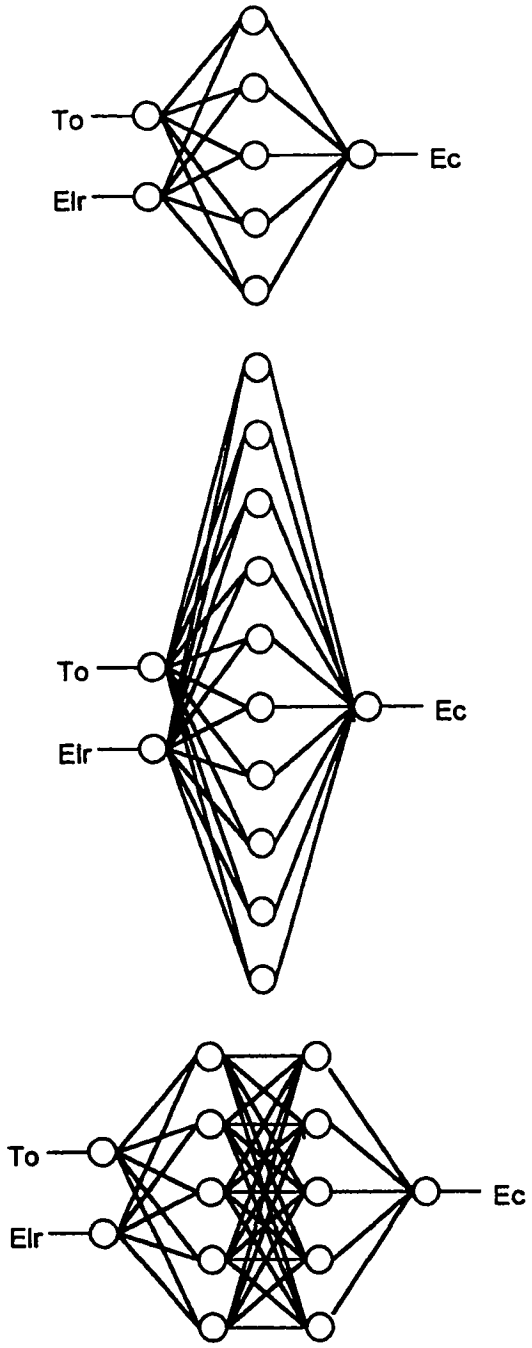

Figure 9.5 Fully-connected, feed-forward ANNs with outside air temperature T_o and lighting and receptacle electricity use E_{lr} as input variables and cooling energy use E_c as the output variable: a) ANN1, three layer architecture with five nodes in the hidden (middle) layer, b) ANN2, three layer architecture with 10 nodes in the hidden layer and c) ANN3, four layer architecture with five nodes in the hidden layers.

low temperatures but appear essentially linear as the temperature increases. The additional nodes in the hidden layer of ANN2 do not appear to improve it's ability to model non-linear behavior. In fact, the average prediction accuracy of runs from ANN2 (as measured by the CV-RMSE) is within one standard deviation of the prediction accuracy of runs from ANN1 indicating nearly identical prediction accuracies.

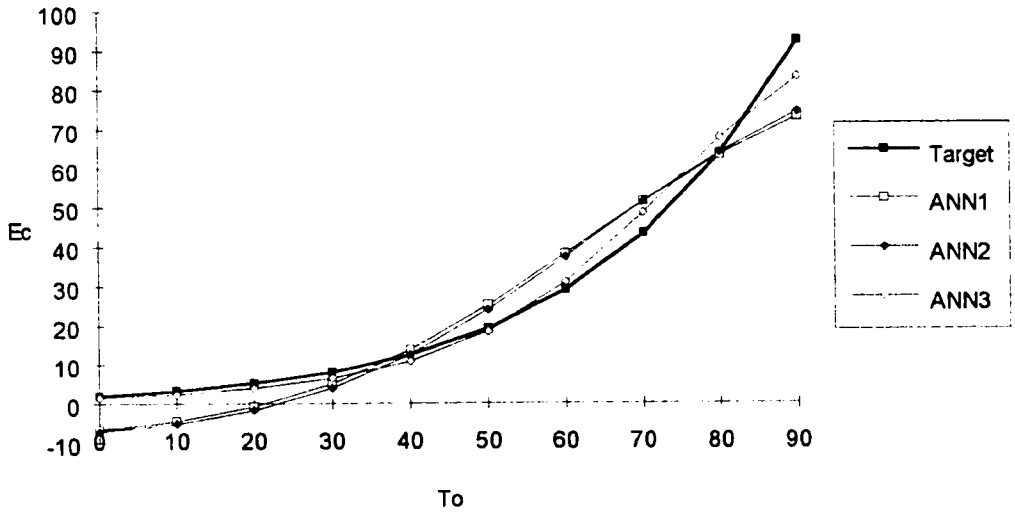

Figure 9.6 Target and predicted values of cooling energy use E_C plotted against outside air temperature T_O from the synthetic data set. ANN3 most accurately simulates the non-linear behavior of the target data set.

The non-linear behavior evident in the target data set was much more accurately modeled by ANN3 (Figure 9.6). Thus, it appears that non-linear relationships may be better modeled by ANNs with multiple hidden layers. ANN3's improved fit to the data is also evident in Table 9.4. Note that only in the case of ANN3 did the smaller step size created by setting the gain equal to 0.5 significantly improve the prediction accuracy of the model.

Table 9.4 Average prediction error measured as CV-RMSE (%) for three ANN architectures and two values of gain. ANN3 provides the best fit.

	gain = 0.5	gain = 0.9
ANN1	32.8	32.4
ANN2	31.9	32.2
ANN3	0.3	4.4

Comparison of ANN and Least Square Regression Models

A sample data set of measured average daily outside air temperature, daily lighting and receptacle electricity use, and daily cooling energy use from the Winship building on the University of Texas at Austin campus was used to compare the prediction accuracy of ANN and ordinary least square (OLS) regression models. The 162 daily observations were collected between October 16, 1990 and July 1, 1991 and are shown plotted in Figure 9.7. The non-linear behavior between cooling energy use and outside air temperature is fit with a four-parameter, change-point regression model. The CV-RMSE of the model is 10.0%. When electricity use is added as another independent variable, the CV-RMSE decreases to 9.0%.

In this data set, the prediction accuracy of the ANN models and regression models were very similar (Table 9.5). Thus, from an ease of use perspective, the major differences between the two modeling approaches are convergence time and the number of coefficients required in order to specify the model. Using EModel, the time required for the regression models to converge is more than two orders of magnitude less than the time required for the ANN models to converge. In addition, specification of an ANN model requires that the values of each weight in the network be recorded. Thus, specification of ANN models typically require many more parameters than for regression models. These comparisons favor the OLS regression approach. A further benefit of OLS regression is the well defined methodology to estimate the uncertainty of prediction of these models.

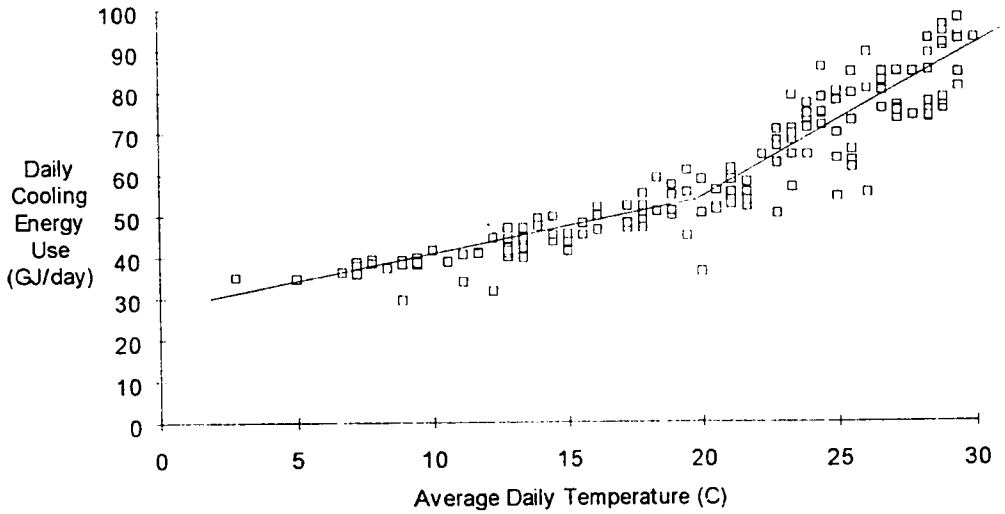

Figure 9.7 Scatter plot of measured cooling energy use versus average daily temperature. A four parameter, change-point model is fit to the data.

Table 9.5 Average CV-RMSE (%), convergence time, and the number of regression parameters needed to specify the model for three ANN and two regression models of measured cooling energy use.

	CV-RMSE (%)	Convergence Time (minutes)	Regression Parameters
ANN1	9.5	27.2	15
ANN2	9.4	62.8	30
ANN3	9.0	64.7	40
4P-CP	10.0	0.13	4
4P-CP + E	9.0	0.13	5

Chapter Summary

This chapter's treatment of the ANN concept was highly simplified in order to provide an introduction to the subject. Advanced ANNs combining Bayesian statistics, improved learning algorithms and advanced architectures and have been shown to accurately model highly complex relationships. The winner of a 1993 ASHRAE competition to model

hourly building energy use, for example, employed such advanced techniques (McKay, 1993).

The greatest asset of ANN models of commercial building energy use may be their inherent non-linearity. Several aspects of energy use in commercial buildings are essentially non-linear. These include control influenced coil loads (Chapter III) and solar and infiltration loads. OLS regression models attempt to fit each of these patterns with linear models and as such compromise the overall model fit. Multi-layer ANN models may prove to be extremely useful in characterizing complex non-linear relationships which OLS regression can only approximate.

Thus the potential for ANN models of commercial building energy use appears to be promising even though the simple ANN models investigated here did not appear to exhibit any significant advantages over regression models. In particular, advanced ANN techniques may improve the accuracy and reduce the training time of ANN models so as to be competitive or superior to regression models.

CHAPTER X

MEASURING SAVINGS IN THE LOANSTAR PROGRAM: CASE STUDY EXAMPLES

In this chapter, the methodology developed in the previous chapters is used to determine retrofit savings in nine buildings participating in the Texas LoanSTAR program. The methodology is demonstrated in detail at the Texas A&M University Zachry Engineering Center. Modeling and savings results are presented for the other buildings.

The Texas LoanSTAR Program

The Texas LoanSTAR (Loans to Save Taxes and Resources) program is a $98.6 million dollar revolving loan program to provide energy conservation retrofits to state, county, and local government buildings (Turner, 1990; Claridge et al., 1991). The program was established in 1988 from oil overcharge dollars. An important mission of the program is to verify the effectiveness of the energy conservation retrofits from monitored energy use data. Monitored energy use data are also used to identify operational and maintenance problems (Athar et al., 1992), guide the selection of future retrofits and initiate a data base of commercial and institutional building energy use (Lopez and Haberl, 1992).

The LoanSTAR Monitoring and Analysis Program (MAP) has technical responsibility for metering the buildings, analyzing the data and determining the savings. As of May, 1993, the LoanSTAR MAP is collecting hourly data from over 200 buildings and 50 national weather service stations throughout Texas. This amounts to over 1600 channels of end-use data. The size of the LoanSTAR data-base is increasing by over three megabytes per week (Haberl, 1993).

The LoanSTAR MAP provides a six page, monthly report (Claridge et al., 1992a) to program participants which summarizes energy consumption and savings information. The report identifies unusual energy consumption patterns and provides comments on the past month's energy use and savings performance. This information is used by participants to ensure that savings are accruing long before loan payments are due and to identify opportunities for additional energy savings.

The procedure for installing metering equipment at a new site begins as soon as a loan for an energy conservation retrofit is approved. The procedure is described in detail by O'Neal et al. (1990) and includes determination of metering requirements, sub-contractor selection, data acquisition system selection and installation and maintenance of the systems. Although sufficient data must be collected to verify savings, the metering expense must not undermine the cost-effectiveness of the retrofits. Thus, four levels of metering have been defined ranging from Level 0 metering, which relies on previously existing meters and data such as utility billing data, to Level 3 metering where more than 20 channels of hourly, sub-metered data are collected. Level 3 metering is cost-justified only for buildings where the cost of the retrofit exceeds $500,000.

In addition to other channels, metering Levels 1, 2 and 3 collect whole building electricity, cooling energy and heating energy use data. The savings methodology developed in this dissertation can be appropriately applied to these data channels. In some cases, however, savings can be more accurately measured by sub-metering the system directly affected by the retrofit. Savings determined from sub-metered data eliminate the noise and variability from end uses which are not affected by the retrofit. A common sub-metered channel for HVAC retrofits in the LoanSTAR program is motor control center electricity use. The motor control center distributes electricity to major HVAC equipment such as pumps and air handler fans. Motor control center electricity use is referred to as the air handler electricity use channel in the remainder of this chapter because the air

handlers are almost always the largest power draw. The case-study examples in this chapter use the sub-metered air handler electricity use data to determine HVAC related electricity savings whenever this channel is available. In three buildings, air handler electricity use was not sub-metered and electricity savings are determined from whole building electricity measurements.

Weather data are collected from a LoanSTAR weather station in the same city as the building and from a nearby National Weather Service (NWS) station. LoanSTAR weather data typically include ambient dry-bulb temperature, ambient humidity (as either relative humidity or dew-point temperature), horizontal solar radiation and wind speed.

Depending on the number of channels being monitored, ensuring the quality of the data can be a formidable task. Meters must be correctly calibrated when installed and periodically re-calibrated to avoid "drift" in the signal (Robinson et al., 1993). To help assure data quality, a National Institute of Standards and Technology traceable calibration laboratory has been established at Texas A&M University as part of the MAP. The objectives of the calibration laboratory are to test sensors to verify their compatibility with selected monitoring systems, trouble-shoot faulty field sensors, verify portable field instrumentation used for field testing, pre-qualify hardware systems prior to field installation and develop field calibration and error analysis techniques (O'Neal et al., 1990). Several papers describe the calibration and testing effort (Sparks et al., 1992; Robinson et al., 1992; Turner et al., 1992; and O'Neal et al., 1993).

In addition to the calibration laboratory, data quality assurance procedures in the LoanSTAR program include range checks on all incoming data, cross-checks with NWS and utility billing data, and weekly inspection of time series and relational plots (Lopez and Haberl, 1992). Machine learning algorithms for recognizing unusual values of data (Sparks and Haberl, 1993) and an interactive graphical interface for reviewing the data (Willis and Haberl, 1992) are also being explored.

Measuring Savings at the Zachry Engineering Center

The Texas A&M University Zachry Engineering Center (ZEC) is a 30,000 m^2 (23,000 m^2 of conditioned space) classroom, office, computer and laboratory facility comprised of four stories and an underground parking garage. It was constructed in the early 1970s. The building is a high mass structure with 0.15 m (6 inch) concrete floors and exterior walls made of pre-cast concrete and porcelain-plated steel. About 12% of the exterior wall area is covered with single pane, bronze-tinted glazing. The windows are recessed about 0.6 m from the exterior walls, providing some shading. Approximately 288 m^2 of northeast facing clearstory windows admit daylight into the core of the building (Bronson, 1992).

The building is served by 12 dual-duct air handling units located in the parking garage underneath the building. Chilled and hot water for the cooling and heating coils are supplied to the building by the campus physical plant. Two multizone units and a dedicated centrifugal chiller serve a super-computer facility located within the building. Outside air dampers are set to supply about 10% to 20% outdoor air (Katipamula and Claridge, 1992) and do not operate on an economizer schedule.

The flow of chilled water to the cooling coils is modulated to maintain the air leaving the cooling coils at a temperature of 12.8 °C. In the pre-retrofit period, the temperature of air leaving the hot decks was nominally controlled by an outdoor air, hot-deck reset schedule. However, measurements showed that controls were not functioning properly and the air leaving the hot-decks varied only slightly (Katipamula and Claridge, 1992).

The primary retrofit at the ZEC was the replacement of the existing CAV air distribution system with a VAV air distribution system. This entailed installing variable frequency drives on the fan motors, replacing the CAV mixing boxes with VAV mixing boxes, and upgrading the energy management and control system (Texas Energy Cost Containment Program, 1986).

The ZEC was instrumented in May, 1989 and was the first Texas LoanSTAR building to have metering equipment installed. Over 40 channels of hourly data, including weather data from a station located on the roof, are monitored and collected. The most important channels for measuring retrofit savings are air handler electricity use, cooling energy use and heating energy use. Air handler electricity use is measured by metering the motor control panel which distributes energy to all of the air handlers and pumps. Cooling and heating energy use are determined by measuring the flow rate and temperature of the cool and hot water streams as they enter and leave the building. Energy use is computed as the product of the mass flow rate, the specific heat of the fluid (water) and the temperature difference between the entering and exiting streams.

Identification of the Pre-Retrofit and Post-Retrofit Periods. The first step in the process of measuring savings is identifying the pre-retrofit, construction and post-retrofit periods. This can be accomplished by examining the EModel time-series plot of ZEC air handler electricity before, during and after the CAV to VAV retrofit (Figure 10.1). Air handler electricity use changes from a nearly constant signal during the pre-retrofit period to a signal with small irregularites during construction and then to a variable signal during the post-retrofit period when the variable-air-volume system becomes operational. The dates defining the pre-retrofit, construction and post-retrofit periods can thus be unambiguously identified by using EModel's zoom and data point identification functions with this plot.

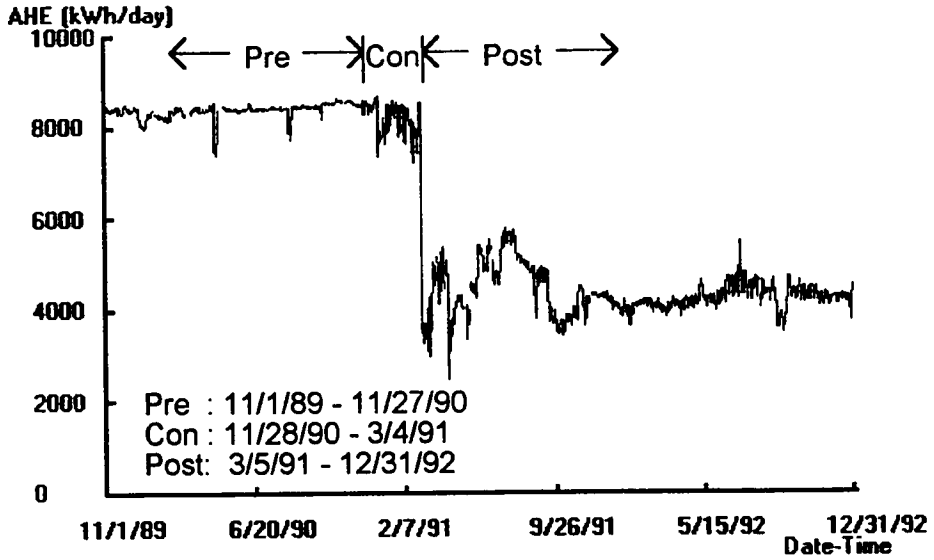

Figure 10.1 Time series plot of daily air-handler electricity use showing pre-retrofit, construction and post-retrofit periods during a constant-air-volume to variable-air-volume retrofit at the ZEC.

Measuring Air Handler Electricity Savings. Because CAV air handler electricity use is nearly constant in the pre-retrofit period, it can be modeled with a one-parameter model. Figure 10.2 shows one-parameter mean models of pre- and post-retrofit (excluding the construction period) electricity use. Baseline pre-retrofit energy use is 8,411 kWh/day. The post-retrofit model does not capture the appreciable variation in post-retrofit electricity use and is shown only for comparison and is not used in the savings calculation.

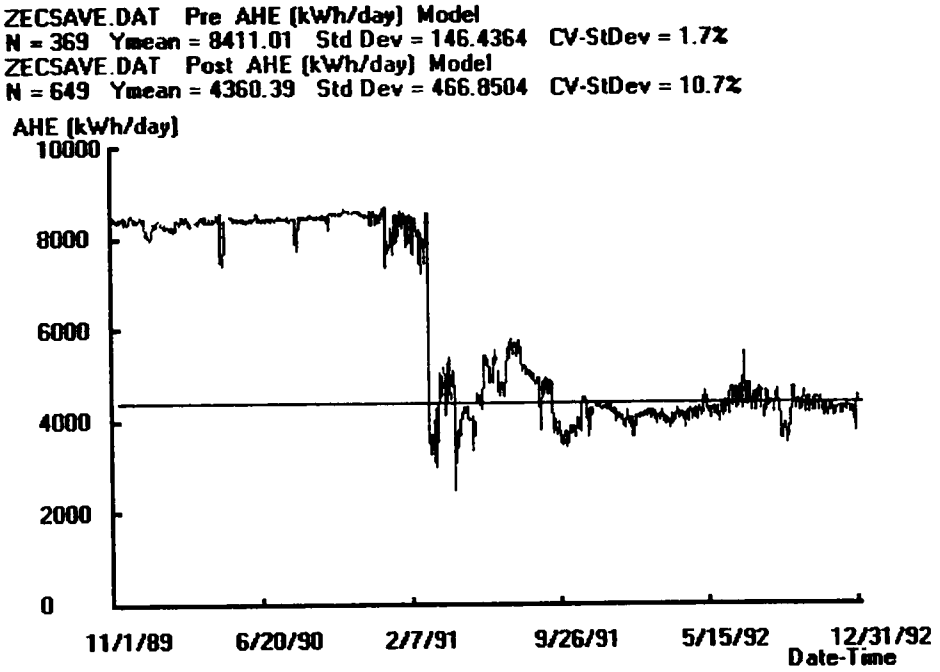

Figure 10.2 EModel value and graph windows showing pre and post-retrofit models of air handler electricity use at the ZEC.

Retrofit savings are determined by subtracting measured energy use in the post-retrofit period from the baseline energy use predicted by the pre-retrofit model as described by Equation 4.4. EModel calculates the total savings for the 649 days in the post-retrofit period to be 2,633,467 kWh or an average of 4,051 kWh/day.

The uncertainty of savings is determined by the program PredErr using the hybrid OLS-AR methodology developed in Chapter VI. PredErr will be integrated into future versions of EModel. For mean models, the X and X_* matrices (Equation 5.14) are simply column vectors of ones. The autocorrelation coefficient of the pre-retrofit residuals is 0.86, clearly indicating the need for the hybrid OLS-AR approach. PredErr calculates the 95% prediction uncertainty of the mean model to be 44,294 kWh. Assuming a $\pm$ 2% electrical power measurement uncertainty (Katipamula and Claridge, 1993), the average daily savings are 4051 $\pm$ 111 kWh/day with an uncertainty of $\pm$ 2.7%.

Measuring Cooling and Heating Energy Savings. When choosing a two, three or four parameter cooling or heating use model, we attempt to maximize the goodness-of-fit using the simplest possible model. At the ZEC, all-days, two-parameter models of pre-retrofit heating and cooling energy use were selected because the improvement in fit from three and four parameter models and from weekday/weekend models was modest (Table 10.1). The pre and post-retrofit daily cooling energy use data points and models are shown in Figure 10.3. The linear relationship between cooling energy use and outside air temperature in the pre-retrofit period is consistent with simulation results in Figure 3.7 for CAV systems without economizer cycles or hot-deck reset schedules. Likewise, the segmented linear shape of post-retrofit cooling energy use is consistent with the VAV simulation results in Figures 3.17 and 3.18.

Table 10.1 R^2 and CV-RMSE statistics for base-line regression models of cooling and heating energy use at the ZEC. The improvement in fit by the more complex models over the all-days, two parameter models is modest.

R^2/CV-RMSE (%)	Cooling Energy		Heating Energy	
	2-Parameter	4-Parameter	2-Parameter	4-Parameter
All-days	0.85 / 8.0	0.86 / 7.7	0.88 / 26.1	0.90 / 24.4
Weekday/weekend	0.85 / 7.8	0.87 / 7.5	0.89 / 25.8	0.90 / 24.0

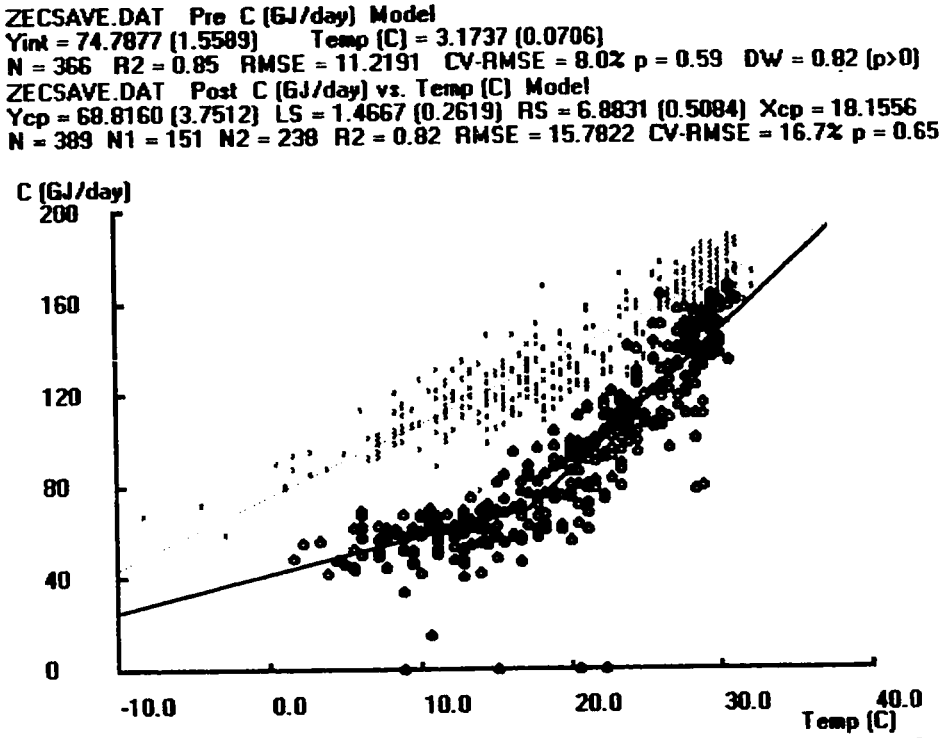

Figure 10.3 EModel value and graph windows showing pre- and post-retrofit cooling energy use and models at the ZEC.

EModel calculates the cooling energy savings during the 389 days of available post-retrofit data to be 17,130 GJ. Note that even with the relatively good fit of the pre-retrofit model (Figure 10.3) (R^2= .80, CV-RMSE = 8.0%), the auto-correlation of the residuals cannot be overlooked (p = 0.59) and the residuals fail the Durbin-Watson test (p > 0). Thus, the hybrid OLS-AR approach developed in Chapter VI is clearly needed. At the 95% confidence level, PredErr calculates the baseline model uncertainty to be $\pm$ 1,240 GJ. Assuming $\pm$ 5% chilled water measurement error (Robinson et al., 1993), the post-retrofit measurement uncertainty is $\pm$ 1,835 GJ. The total uncertainty of savings is calculated by Equation 5.21 to be $\pm$ 2,214 GJ. The average daily savings are therefore 44.0 $\pm$ 5.7 GJ/day with an uncertainty of $\pm$ 12.9%.

Pre and post-retrofit heating energy use data points and models are shown in Figure 10.4. As in the case of cooling energy use, the pre- and post retrofit energy use patterns are similar to those predicted by simulation for the respective CAV and VAV systems in Chapter III.

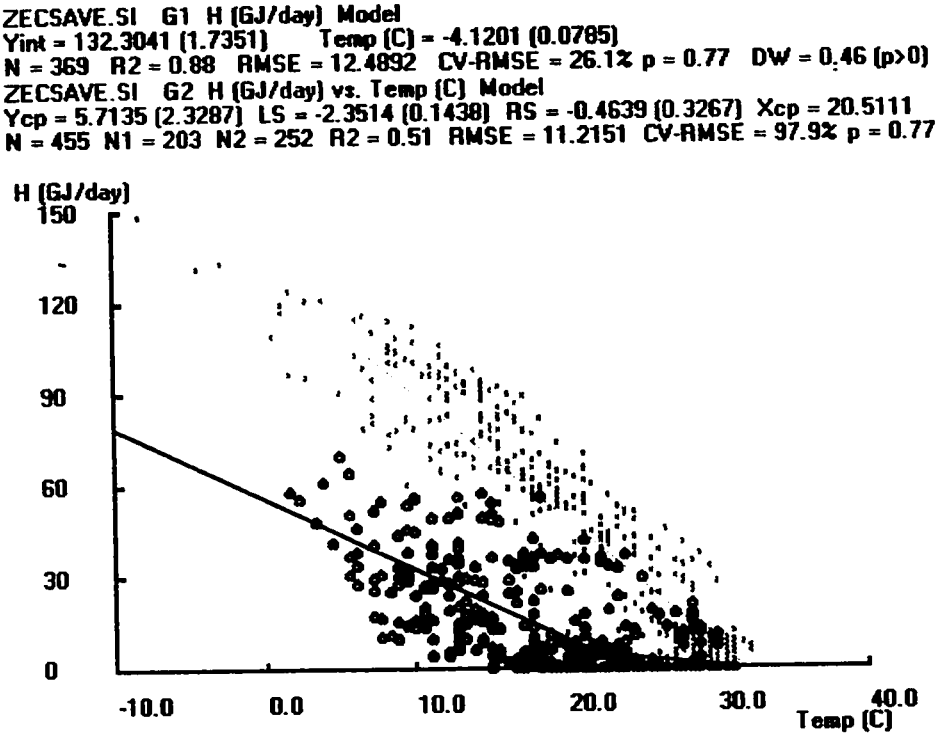

Figure 10.4 EModel value and graph windows showing pre and post-retrofit heating energy use and models at the ZEC.

Heating energy use savings are calculated by EModel to be 16,928 GJ over the 455 days of available data in the post-retrofit period. Once again, the autocorrelation coefficient is high (0.77) and the OLS-AR hybrid approach for determining model uncertainty is warranted. At the 95% confidence level, PredErr calculates the uncertainty of the baseline model to be $\pm$ 2,186 GJ. Once again assuming a $\pm$ 5% hot water

measurement error, the average daily heating energy savings are 37.2 $\pm$ 4.8 GJ/day with an uncertainty of $\pm$ 13.0%.

Accounting for Missing Post-Retrofit Data. Occasionally, energy consumption data from the post-retrofit period are unavailable due to equipment failure or normal maintenance of the metering equipment. In this example, nearly a year of post-retrofit heating and cooling energy use data were lost due to metering difficulties. In cases like these, the post-retrofit models shown in Figures 10.3 and 10.4 can be used to estimate the energy use for those days when the measured data is missing. Savings can then be calculated as before using Equation 4.4; however, the uncertainty of the measured savings must now include the uncertainties of both the baseline and post-retrofit models.

Energy Delivery Efficiency. Daily values of the pre- and post-retrofit EDE are shown in Figure 10.5. The significant improvement in post-retrofit EDE at all temperatures is clearly evident. At temperatures above approximately 18 °C the EDE is in most cases 100%, indicating that no mixing or re-heating is occurring and that the retrofit is performing ideally.

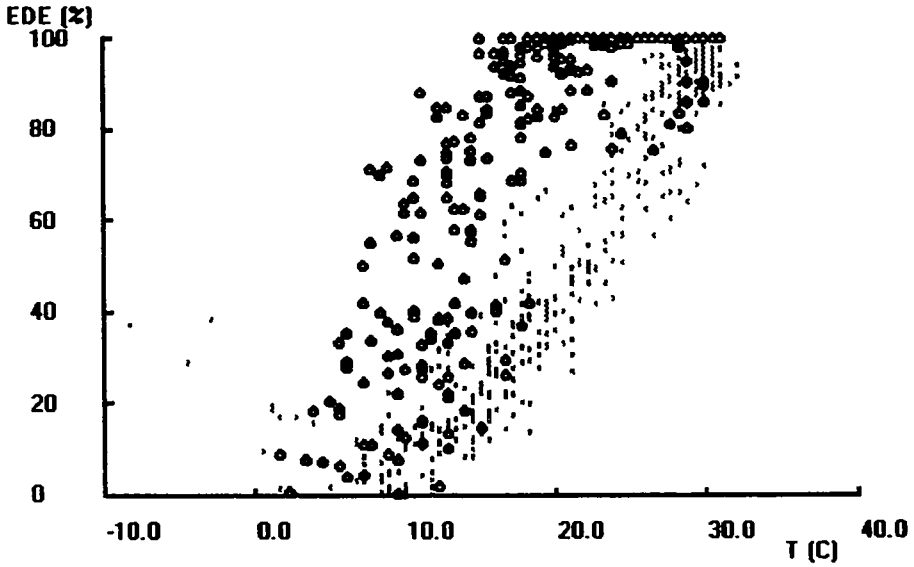

Figure 10.5 Pre and post-retrofit plot of the energy delivery efficiency at the ZEC.

Retrofit Savings at Eight Other LoanSTAR Sites

As of May, 1993, savings are currently being measured at 29 sites in the LoanSTAR program (ESL, 1993b). The methodology used to measure the savings depends on the type of retrofit, the amount of pre-retrofit data and the level of metering installed. At sites at which pre-retrofit data is unavailable, two methods are used to determine savings. In the first method, pre-retrofit energy use is estimated by a simplified systems model which has been calibrated to the post-retrofit data. The model is then adjusted to match the pre-retrofit HVAC system (Katipamula and Claridge, 1993). This method is currently being implemented at two sites. In the second method, utility billing data is used as the basis of pre-retrofit energy use (Liu, 1993). This method is also being implemented at two sites. When the principle cost savings are derived from reducing the peak electrical demand, such as in thermal storage projects, a procedure which uses hourly or 15 minute data is used to measure the savings. This method is being implemented at one site. At the 24 remaining sites, energy savings are determined using the methodology developed in this dissertation.

Information about the building size, use and type of retrofit for eight of these sites is listed in Table 10.2. The pre-retrofit periods range in length from 3 to 13 months. In every case except at the Garrison and Hogg buildings, the pre-retrofit period is either greater than one year in length or spans the Spring months when average temperatures are close to the annual average temperature. Thus, for these buildings, we anticipate little error in the baseline energy use models due to short data sets (Chapter VII). At Garrison and Hogg, the pre-retrofit period was limited to the winter months, and thus we suspect that the baseline model of cooling energy use may underestimate annual cooling energy use and the baseline model of heating energy use may overestimate annual heating energy use (Chapter VII).

Table 10.2 Description of case-study buildings.

Building Name (Abbreviation)	Use	Conditioned Floor Area (m^2)	Primary Retrofit	Pre-Retrofit Period
Zachry (ZEC)	offices, labs, classrooms	23,000	CAV to VAV	11/1/89 - 11/27/90
Education (EDB)	offices, classrooms	23,300	CAV to VAV	10/24/90 - 4/29/91
Garrison (GAR)	offices, classrooms, auditorium	5,000	CAV to VAV	10/21/90 - 2/28/91
Waggener (WAG)	offices, labs, classrooms	5,400	CAV to VAV	10/16/90 - 5/22/91
Burdine (BUR)	offices, labs, classrooms	9,600	CAV to VAV	10/16/90 - 5/14/91
Winship (WIN)	offices, theater classrooms	10,100	CAV to VAV	10/16/90 - 7/1/91
Painter (PAI)	offices, labs, classrooms	11,900	CAV to VAV	10/16/90 - 5/31/91
Hogg (WCH)	offices, classrooms, auditorium	4,500	CAV to VAV	10/16/90 - 1/31/91
Texas Dept. Health (TDH)	offices, labs, computers	22,800	Added EMCS	7/15/91 - 8/15/92

Graphical representations of retrofit savings at eight of these sites are plotted in Figure 10.6. Each row of four graphs shows normalized, pre- and post-retrofit energy use at a different site. These sites were selected in order to demonstrate the diverse patterns of commercial building energy use and savings encountered in a retrofit program. The first graph in each row is a time-series plot of daily electricity use with pre- and post-retrofit models. The first four sites show sub-metered air handler electricity use, while at the other sites, air handler electricity use was not sub-metered and whole building electricity use is shown. At all of the sites except the Painter Building, the pre- and post-retrofit periods can be easily determined by inspecting the time-series plots. At the Painter building, additional information about the retrofit construction dates was required to differentiate between the pre- and post-retrofit periods. At the Education and Burdine Buildings, the air handlers were regularly shut-down on weekends and separate pre-retrofit models for weekdays and weekends were required. Separate weekday and weekend models were also required for sites where electricity savings were derived from whole building electricity use. At the Texas Department of Health, Saturday and Sunday electricity use were different enough that separate weekday, Saturday and Sunday models were needed.

The second graph in each row shows daily cooling energy use plotted against outside air temperature. At the Education and Burdine Buildings, the weekday/weekend variation in pre-retrofit air handler scheduling necessitated separate weekday and weekend models. In each case except the Painter Building, the graphs show substantial cooling energy savings at all temperatures. At the Painter building, post-retrofit cooling energy use is actually greater than pre-retrofit energy use at low temperatures, indicating that the retrofit is not performing as planned and that further investigation is warranted. At the Garrison Building, cooling and heating energy use are nearly zero on Sundays when the air-handlers are turned off.

Daily heating energy use is shown in the third graph of each row. Once again, the significant reduction in heating energy use after the VAV retrofits is readily apparent. The best retrofits, however, lower heating energy use to nearly zero at about 22 °C and above. At these warm temperatures, there is no heating load on the building because the outside air temperature is equal to or warmer than the interior set-point temperature. Thus, any space heating energy use is merely a "control load", i.e. the heating is used merely to balance cooling in order to control zone comfort conditions, and is being consumed in mixing processes. The VAV systems at the ZEC, Garrison and Wagner buildings have succeeded in eliminating the control load and the associated energy mixing. At the other buildings there appears to be a potential for further energy savings during warm weather. At the Winship Building, heating energy use is essentially unrelated to the outdoor air temperature, strengthening the notion that the current heating energy use is largely used for "control" purposes and could be significantly reduced by fine-tuning the VAV system. The building operators have been notified and are investigating the causes of this behavior and looking for ways to reduce the unnecessary heating.

The fourth graph in each row is a plot of daily values of pre- and post-retrofit EDE. The most significant improvements in the EDE occur at buildings where the heating energy use is nearly zero during warm weather, such as the ZEC, Garrison and Waggener Buildings. At these buildings, the EDE is often 100% at high temperatures and remains much higher than pre-retrofit values of EDE as outside air temperature decreases. At the other buildings, daily values of the EDE improved slightly; however, the large number of daily values below 80% indicates that the VAV systems in these buildings are still not fully optimized to reduce thermal mixing. The simulation in Chapter VIII shows that the EDE in VAV systems should approach 100% during warm weather when the system is operating properly.

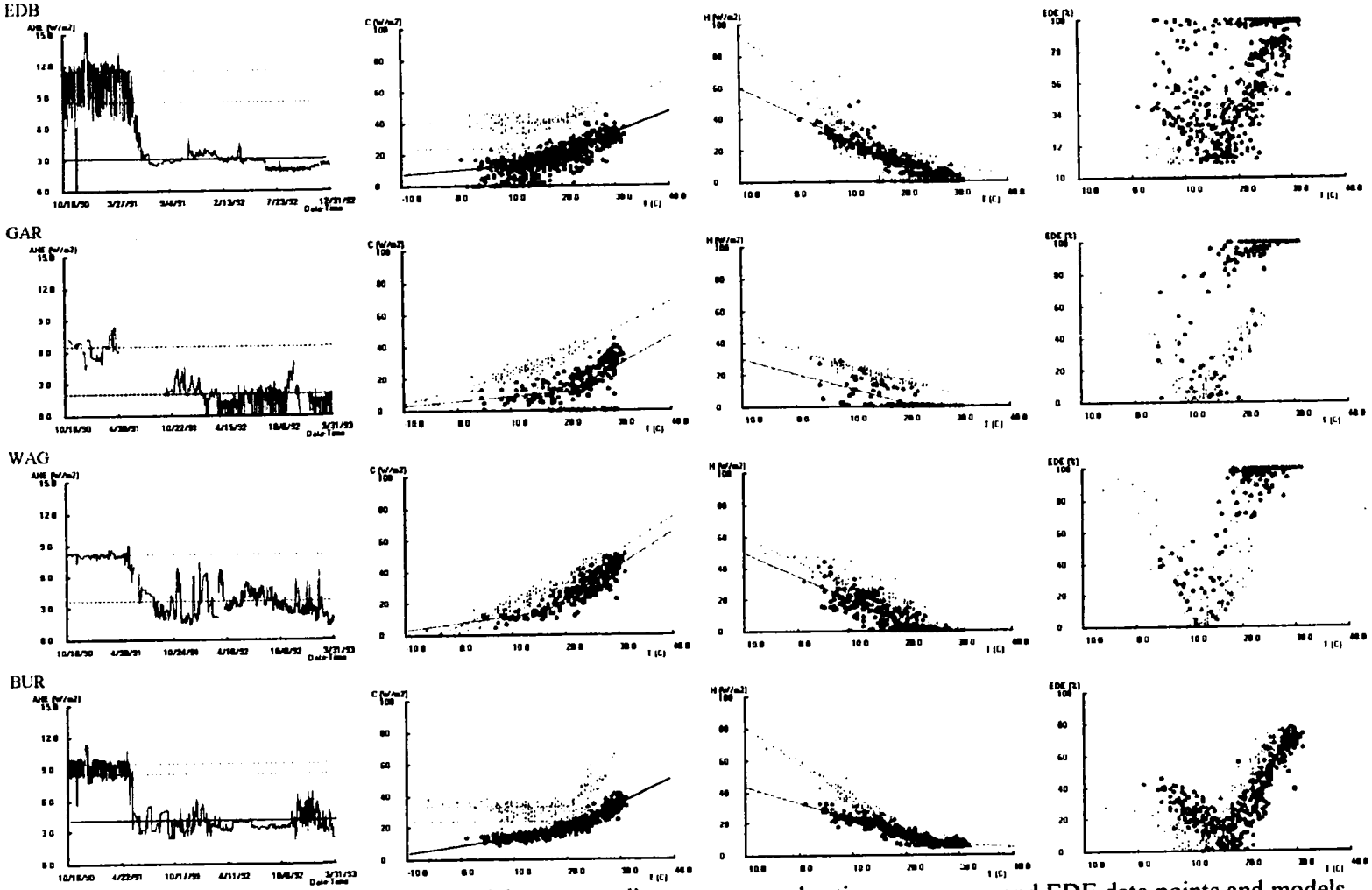

Figure 10.6. Daily pre and post-retrofit electricity use, cooling energy use, heating energy use and EDE data points and models.

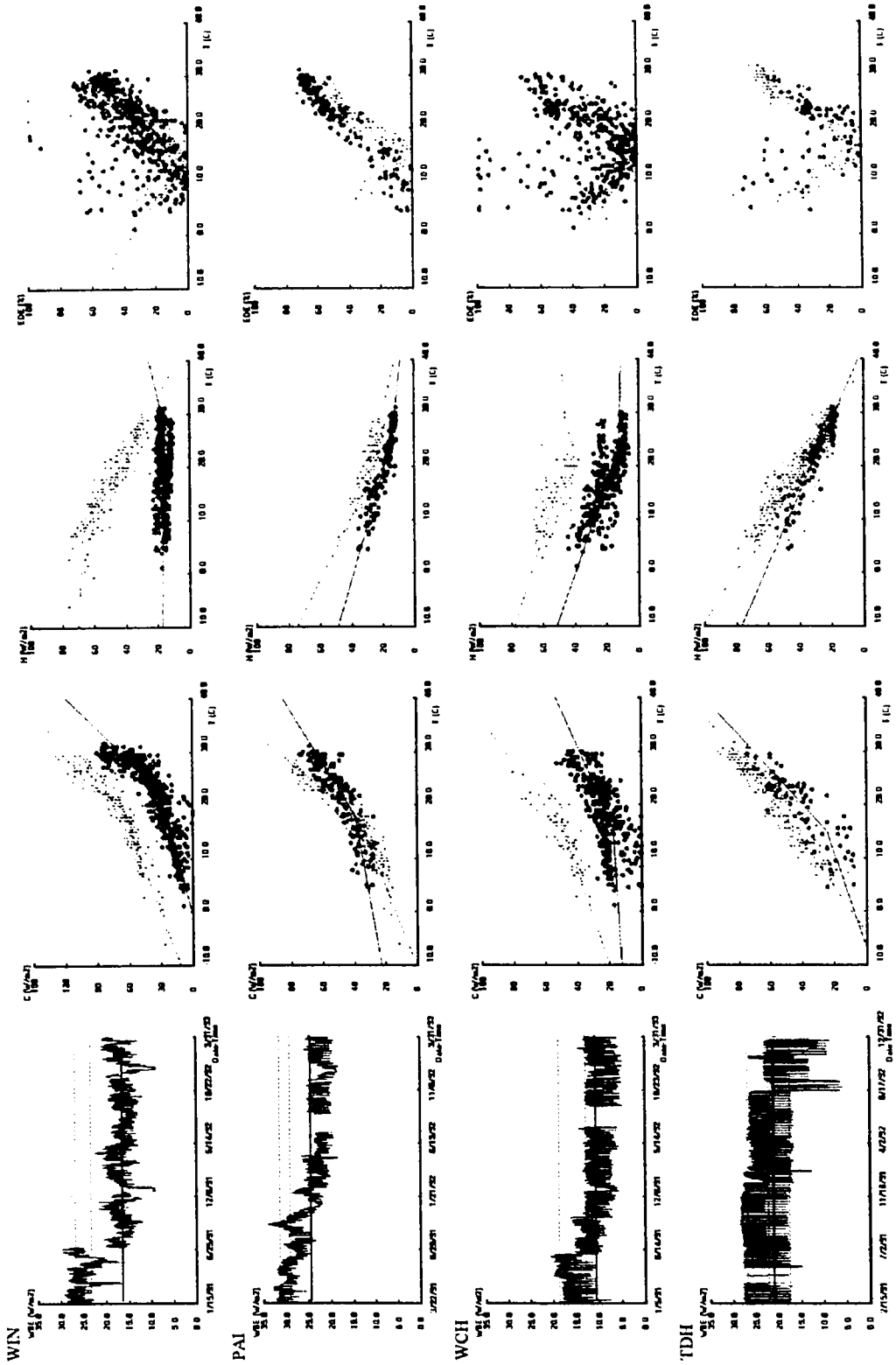

Figure 10.6 Continued.

Summary statistics from the pre-retrofit models are listed in Table 10.3. When weekday and weekend models were used, the weighted average of their inferential statistics is given. The one parameter models of electricity use were generally very accurate with a mean CV-SD of only 3.3%. The uncertainty of electricity savings will be similarly low. The accuracy of the cooling and heating energy use models, as measured by CV-RMSE, averaged 11.4% and 14.1% respectively. The magnitude of error could be reduced somewhat by inclusion of other predictor variables in the models, but at the cost of increasing the complexity of the models and the data requirements. Note that the low average R^2 value for the cooling energy use models at EDB does not reflect on the model's predictive ability. The CV-RMSE of cooling models at EDB are among the lowest in this sample.

Table 10.3 Summary of model statistics for case study buildings. Weighted averages of weekday and weekend statistics are presented. The last row shows the mean and standard deviation of each column.

	Electricity		Cooling			Heating		
	Model Type	CV-SD (%)	Model Type	R^2	CV-RMSE (%)	Model Type	R^2	CV-RMSE (%)
ZEC	1	1.7	2	.85	8.0	2	.88	26.1
EDB	1	5.1	3	.39	8.9	4	.88	13.1
GAR	1	3.0	4	.82	11.6	2	.90	8.2
WAG	1	2.2	4	.87	14.7	2	.73	23.3
BUR	1	3.2	3	.67	12.2	4	.95	11.9
WIN	1	3.5	4	.90	10.1	4	.86	10.0
PAI	1	2.5	4	.89	13.1	4	.76	10.0
WCH	1	4.9	4	.60	14.3	4	.42	11.9
TDH	1	3.9	2	.90	9.6	4	.92	12.7
Mean		3.3 (1.2)		.77 (.18)	11.4 (2.4)		.81 (.16)	14.1 (6.3)

The savings are summarized in Table 10.4. The mean percent reduction in overall energy costs was 38.8%. The lowest overall savings were at the Texas Department of Health where an EMCS were added; the primary retrofits at the other buildings were CAV to VAV conversions and savings were higher.

Table 10.4 Summary of 1992 savings for case-study buildings (ESL, 1993a). Electricity savings at the Education Building (EDB) include a lighting retrofit. Savings at TDH are from September through December. The last row shows the mean and standard deviation for each column.

	Electricity		Cooling Energy		Heating Energy		Total
	Average Daily Savings (W/m^2)	Percent Reduction in Energy Use	Average Daily Savings (W/m^2)	Percent Reduction in Energy Use	Average Daily Savings (W/m^2)	Percent Reduction in Energy Use	Percent Reduction in Energy Costs
ZEC	7.5	15.4	22.1	31.1	19.7	82.9	30.6
EDB	13.8	59.8	19.3	46.8	4.8	28.6	49.7
GAR	6.6	48.9	21.1	56.6	8.4	74.0	56.3
WAG	4.4	16.1	9.6	26.5	5.6	47.9	23.4
BUR	7.2	39.3	20.1	46.8	2.7	17.3	39.6
WIN	10.1	37.4	44.2	56.6	25.4	58.6	51.4
PAI	7.3	23.9	12.5	21.9	10.0	34.6	25.0
WCH	7.5	41.1	36.2	57.6	30.4	66.4	56.1
TDH	3.7	10.8	26.8	27.3	2.7	9.1	17.0
Mean	7.6 (3.0)	32.5 (16.8)	23.5 (10.9)	41.2 (14.5)	12.2 (10.4)	46.6 (25.8)	38.8 (15.2)

Chapter Summary

The savings methodology developed in this dissertation was applied to nine buildings participating in the LoanSTAR program. The methodology was implemented in the programs EModel and PredErr using daily energy use and outside air temperature data. The pre-retrofit period at each site was identified by inspecting the time-series plot of air handler or whole building electricity use. Models of pre-retrofit energy use which minimized model error while maintaining simplicity were selected. Where appropriate, separate models for the different operational periods were identified. Savings were

determined by subtracting measured daily energy use from the baseline energy use predicted by the pre-retrofit model. PredErr was used to determine the uncertainty of the savings. The use of EDE to identify opportunities for further improvement of the VAV systems was demonstrated.

For the sample of buildings considered here, the CV-RMSE of the one-parameter electricity models averaged 3.3%, the cooling energy use models 11.4% and the heating energy use models 14.1%. In 1992, the average reduction in energy costs due to the retrofits was 38.8%.

Measured savings information such as discussed above provides a tool to judge the effectiveness of energy conservation retrofits. In the case of the Texas LoanSTAR program, these results help justify the program to taxpayers who want to know that their tax money is being effectively spent. Because of the long life span of LoanSTAR buildings and the short payback period of the retrofits (averaging under four years), the long term savings generated by the LoanSTAR program are enormous. The $49 million invested so far is projected to save over $250 million over the next 20 years, and if the program is fully implemented the projected 20 year savings are over $850 million (TEES, 1993).

CHAPTER XI

SUMMARY AND FUTURE DIRECTIONS

World population, which is currently about 5.3 billion, is growing at a rate of 1.7% per year (Postel, 1992). At this rate world population will double in about 40 years. Barring catastrophe, few experts believe world population can be stabilized at less than nine billion people and many believe it may balloon to over 14 billion people before it stabilizes (Holdren, 1990). Over 96% of this growth is occurring in the less developed countries (Postel, 1992) in which per-capita energy consumption is as much as 20 times less than in developed countries (Davis, 1990). If the living conditions in the less developed countries are to substantially improve, then per-capita energy use will have to rise dramatically, and with it the prospect of vast increases in world energy demand.

The worldwide demand for and use of current levels of energy (about 350 quadrillion Btu per year, (Energy Information Agency, 1991) has already strained economic, environmental and political conditions. The quadrupling of the real price of oil in the 1970s left a legacy of inflation, spiraling debt, world wide recession and undue hardship on oil poor countries in the Southern Hemisphere. Carbon dioxide emissions are projected to nearly double by the year 2010 if the current mix of fuels and level of energy efficiency persist. And although the link between atmospheric carbon dioxide and global warming is still uncertain, the Inter-governmental Panel on Climate Change concludes that world mean temperatures could rise 0.3 °C per decade under these conditions (Davis, 1990). Finally, the uneven distribution of global energy resources creates tensions that can easily become armed conflicts, such as the 1990 Gulf War. A significant increase in the worldwide demand for energy can only aggravate these problems.

Although there is no single solution to any of these problems, energy conservation is a partial solution to all of them. Improvements in energy efficiency can offset population

and economic growth, and thereby stabilize and even reduce energy consumption (Kissock, 1989). Simply put, energy conservation buys time -- time to develop renewable energy resources and sustainable economies. Virtually every scenario of a sustainable future, a future "of development instead of decline", calls for massive improvements in energy efficiency (see for example: Stobauch and Yergin, 1983; Ruckelshaus, 1989; or Flavin, 1992).

The potential for cost-effective energy efficiency improvements in the building sector is well documented. Realization of this potential is often hampered by lack of will, capital, and technical expertise, areas where measuring retrofit savings can help. Measured retrofit savings can be used to evaluate the effectiveness of energy conservation retrofits and thus demonstrate the potential for and cost-effectiveness of savings to others who are considering retrofits. Measuring retrofit savings can help secure capital for a retrofit when used to guide loan payments or as part of a shared-savings contract. Measured savings can also guide the selection of future retrofits and enhance the ability of planners to accurately predict energy savings. This dissertation attempts to contribute to the science and practice of measuring savings with the hope that it will help encourage energy conservation and speed the transition to a sustainable future.

Chapter II discussed the selection of appropriate data time intervals for energy use models. Estimates of space cooling load time lags in typical commercial buildings ranged from three quarters of an hour to five hours. Thus, for multiple regression models of hourly cooling energy consumption, the use of lagged lighting and solar energy variables should be investigated. In addition, it was found that steady state models are appropriate when used with data having a time interval of a day or longer. The procedure used to identify the time lag from measured data, if extended, could be used to verify numerical, transfer function and thermal network approximations of space cooling time lags.

In Chapter III, simulation results suggested that temperature dependent, one, two, three and four parameter regression models could adequately describe many of the thermal energy use signatures exhibited by CAV and VAV air side systems. Some energy signatures, however, would be better modeled by multiple change-point models, a point that should be addressed in future work. In addition, the models developed here were only for the air side HVAC equipment and future work could extend these models to include primary systems. In this methodology, operational and occupancy changes were modeled using separate models for each period. The development of multi-variable, change-point models could eliminate the need for separate models in some cases. Finally, the use of simplified systems simulations could be extended to help identify operational and maintenance problems by comparing simulation results to measured data.

Chapter IV presented an overview of the methodology. The usefulness of the methodology could be extended by the inclusion of normalized savings error statistics so that predicted and measured savings could be unambiguously compared. Also, because electrical demand savings are often a substantial part of retrofit savings, the inclusion of a procedure to identify electrical demand savings would broaden the applicability of the methodology.

The use of these models to measure savings was demonstrated using the EModel software in Chapter V. EModel makes a significant contribution to the field of building energy analysis by providing an integrated, user-friendly environment for the exploration and modeling of energy use data. A significant addition to EModel would be the integration of the PredErr program so that the uncertainty of savings can be determined in the EModel environment. In addition, the uncertainty of the regression coefficients for change-point models, which are only estimated in the present version of EModel, needs to be made more accurate. The capability to automatically consider more than two model types would enhance modeling flexibility. Finally, a recorder of all the keystrokes used

when determining savings, would permit the entire savings calculation process to be recorded for future reference. This option, and the standardization of the methodology to measure savings, may be useful to parties negotiating shared savings contracts.

In Chapter VI, the methodology to determine the uncertainty of savings measured using regression models was developed. This methodology makes a major contribution to the effort to measure savings by providing an explicit treatment of the effect of autocorrelation on the uncertainty of savings, something other methods may ignore. This methodology needs to be extended to include change-point models.

Chapter VII presented a study of the effects of short data periods on the annual prediction accuracy of temperature dependent models. This study quantified the potential magnitude of the problem and identified characteristics of data sets which influence their predictive ability. Future studies should attempt to identify numerical adjustments to regression models from short data periods that improve their annual predictive accuracy. Future work should also attempt to identify the causes of slope variations throughout the year.

In Chapter VIII a new index called the energy delivery efficiency was introduced and its use demonstrated with simulated data from CAV and VAV systems. The use of EDE gives the analyst powerful insight into the problem of simultaneous heating and cooling and can be used to gauge the effectiveness of air side retrofits at reducing mixing. Additional attributes of EDE include its simplicity and requirement of only two types of easily measured data: heating and cooling energy use. The ideal multizone EDE provides more detailed diagnostics by disaggregating mixing into inter-zone and intra-zone components. Future work should focus on identifying the parameters required to compute the ideal multizone EDE from energy use data. This will greatly improve the accuracy and utility of the EDE concept.

An introduction to the concept and use of artificial neural networks was provided in Chapter IX. Future work should be devoted to developing advanced ANN models and learning algorithms and applying them to energy use data. The selection of appropriate network architectures and parameter values could be made much more efficient if it were better informed by theory. Thus, a more comprehensive examination of the ANN literature is warranted. In addition, the response of ANN models to input values outside of the range of input values used to train the ANN and the methods for quantifying the overall uncertainty of ANN models need to be investigated.

In Chapter X a case study demonstration of the savings methodology was presented. Nine buildings were examined, with pre-retrofit periods ranging from 3 to 13 months. The average CV-RMSE of electricity use models was 3.3%, of cooling energy use models was 11.4%, and of heating energy use models was 14.1%. The acceptability of this level of accuracy is a subjective decision. Increased accuracy can almost certainly be obtained by more detailed modeling and finer sub-metered data, but at the cost of additional modeling time and metering expense. Using the methodology developed in this dissertation and the EModel software, baseline models can be developed and savings measured in a few minutes. In addition, the graphical analysis capabilities of EModel greatly enhance the ability of the analyst to quickly identify opportunities for further savings. Thus, the tools and techniques developed here reduce the time required for retrofit savings analysis and increase the potential for further savings, thus enhancing the overall cost effectiveness of energy conservation retrofits.

This methodology could be extended to determine the savings that would have occurred during a period of "normal" weather, such as is done in the PRISM method. This would entail using "average" temperature data as inputs to both pre- and post-retrofit models. The uncertainty of normalized savings would increase due to the additional uncertainty introduced by the post-retrofit model.

REFERENCES

American Society of Heating, Refrigerating and Air-Conditioning Engineers, 1981, *ASHRAE Handbook: Fundamentals*, Atlanta, GA.

Analytical Sciences Corporation, 1991, "Lodestar Utility Load Research Software", Reading, MA.

Anderlind, G., Bengtsson, L., Karlsson, H., Rondberg, P., Hoglung, L., Rolen, C., Hjalmarsson, C., Norlen, U., Jonsson, J., Nordlander, J. and Johansson, H., 1986, "Effect of Energy Conservation Measures: Results From A Swedish Before-After Study", *Proceedings of the ACEEE Summer Study on Energy Efficiency in Buildings*, Pacific Grove, CA, August, pp. 9.7 - 9.10.

Anderson, D., 1990, "Electrical Usage Predictors Based on the Singular Value Decomposition Algorithm", M.S. Thesis, Civil, Environmental and Architectural Engineering Department, University of Colorado at Boulder.

Anderson, D., Graves, L, Reinert, W., Kreider, J., Dow, J. and Wubbena, H., 1989, "A Quasi-Real-Time Expert System for Commercial Building HVAC Diagnostics", *ASHRAE Transactions*, Vol. 95, Pt. 2, pp. 954 - 960.

Athar, A., Abbas, M., Challa, V., Haberl, J. and Claridge, D., 1992, "Improving the Performance of Retrofits by Providing Operator Feedback from Measured Data", *Proceedings of the Eighth Symposium on Improving Building Systems in Hot and Humid Climates*, Mechanical Engineering Department, Texas A&M University, Dallas, TX, May, pp. 188 - 196.

Beale, R. and Jackson, T., 1990, *Neural Computing: An Introduction*, Adam Hilger, New York, NY.

Bevington, R. and Rosenfeld, A., 1990, "Energy for Buildings and Homes", *Scientific American*, September, pp. 76 - 86.

Box, G., Hunter, W. and Hunter, J., 1978, *Statistics For Experimenters*, John Wiley and Sons, New York, NY.

Braun, J., Mitchell, J., Klein, S. and Beckman, W., 1987, "Performance and Control Characteristics of a Large Cooling System", *ASHRAE Transactions*, Vol. 93, Pt. 1, pp. 1830 - 1852.

Bronson, D., 1992, "Calibrating DOE-2 to Weather and Non-Weather-Dependent Loads for a Commercial Building", M.S. Thesis, Mechanical Engineering Department, Texas A&M University.

Building Energy Predictor Shootout, 1993, ASHRAE Symposium, Denver, CO, June.

Claridge, D., Haberl, J., Turner, W., O'Neal, D., Heffington,W., Tombari, C., Roberts, M. and Jaeger, S., 1991, "Improving Energy Conservation Retrofits With Measured Savings", *ASHRAE Journal*, October, pp. 14 - 22.

Claridge, D., Haberl, J., Sparks, R., Lopez, R. and Kissock, K., 1992a, "Monitored Commercial Building Energy Data: Reporting the Results", *ASHRAE Transactions*, Vol. 98, Pt. 1, pp. 881 - 889.

Claridge, D., Haberl, J., Sparks, R., Poyner, R., Belur, R., Bryan, J., 1992b. "Use of Energy Management and Control Systems for Performance Monitoring of Retrofit Projects", ESL-TR-91/09-02, Energy Systems Laboratory, Mechanical Engineering Department, Texas A&M University, College Station, TX.

Claridge, D., Norford, L. and Balasubramanya, R., 1992c. "A Thermal Mass Treatment for the TC 4.7 Simplified Energy Analysis Procedure", *ASHRAE Transactions*, Vol. 98, Pt. 1, pp. 320 - 377.

Cox, R., 1993, "Analysis of Grocery Store Energy Use", M.S. Thesis, Mechanical Engineering Department, Texas A&M University.

Davis, G., 1990, "Energy for Planet Earth", *Scientific American*, September, pp. 54 - 62.

Draper N. and Smith H., 1981, *Applied Regression Analysis*, John Wiley and Sons, New York, NY.

Energy Information Administration, 1986, *Energy Facts 1986*, DOE/EIA-0469(86), Washington, DC.

Energy Information Administration, 1991, *Energy Facts 1991*, DOE/EIA-0469(91), Washington, DC.

The Energy Policy Act of 1992, Public Law 102-486-October 24, Washington, DC.

Energy Systems Laboratory, 1993a, "LoanSTAR Monitoring and Analysis Program: Annual Energy Consumption Report, 1992", Mechanical Engineering Department, Texas A&M University, College Station, TX, May.

Energy Systems Laboratory, 1993b. "LoanSTAR Monitoring and Analysis Program: Monthly Energy Consumption Report, May 1993", Mechanical Engineering Department, Texas A&M University, College Station, TX.

Eto, J., 1988, "On Using Degree-days to Account for the Effects of Weather on Annual Energy Use in Office Buildings", *Energy and Buildings*, Vol. 12, No. 2, pp. 113 - 127.

Fels, M., 1986, "Special Issue Devoted To Measuring Energy Savings: The Scorekeeping Approach", *Energy and Buildings*, Vol. 9, Nos.1 and 2.

Fels, M. and Reynolds, C., 1991, "Toward Standardizing The Measurement of Whole-Building Energy Savings in DSM Programs", *Proceedings of the Energy Program Evaluation Conference*, Chicago, IL, August, pp. 75 - 85.

Fireovid, J. and Fryer, L., 1991, *ASEAM 3.0: A Simplified Energy Analysis Method*, U.S Department of Energy, Office of Federal Energy Management Programs, Washington, DC.

Flavin, C., 1992, "Building a Bridge to Sustainable Energy", *State of the World: 1992*, W. W. Norton Company, Inc., New York, NY, pp. 27 - 45.

Forrester, J. and Wepfer, W., 1984, "Formulation of a Load Prediction Algorithm for a Large Commercial Building", *ASHRAE Transactions*, Vol. 90, Pt 1, pp. 536 - 551.

Greely, K., Harris, J., and Hatcher, A., 1990, "Measured Savings and Cost-Effectiveness of Conservation Retrofits in Commercial Buildings", Lawrence Berkeley Laboratory Report - 27586, Berkeley, CA.

Haberl, J. and Vajda, E., 1988. "Use of Metered Data Analysis To Improve Building Operation and Maintenance: Early Results From Two Federal Complexes", *Proceedings of the ACEEE 1988 Summer Study on Energy Efficient Buildings*, Pacific Grove, CA, August, pp. 3.98 - 3.111.

Haberl, J., Belur, R., Kissock, J., Sparks, R. and Cambell, S. 1993, "Exploring New Data Displays For Facility Energy Data", *Proceedings of the Fifteenth National Industrial Energy Technology Conference*, Mechanical Engineering Department, Texas A&M University, Houston, TX, pp. 257 - 265.

Haberl, J., 1993, personal communication, College Station, TX, May 31.

Hirst, E. and Goeltz, R., 1984, "Comparison of Actual and Predicted Energy Savings in Minnesota Gas-Heated Single-Family Homes, ORNL/CON-147, Oak Ridge National Laboratory, Oak Ridge, TN.

Hirst, E., Clinton, J., Geller, H. and Kroner, W., 1986, *Energy Efficiency in Buildings: Progress and Promise*, American Council for an Energy Efficient Economy, Washington, D.C.

Holdren, J., 1990, "Energy in Transition", *Scientific American*, September, pp. 157 - 163.

Holman, J., 1978, *Experimental Methods for Engineers*, McGraw-Hill, Inc., New York, NY.

Incropera, F., and DeWitt, D., 1985. *Fundamentals of Heat and Mass Transfer*, Second Edition, John Wiley and Sons, Inc., New York, NY.

Jamieson, D. and Qualmann, R., 1990, "Computer Simulation Energy Use Metering or Can We Count On Energy Savings Estimates In Designing Demand Side Programs", *Proceedings of the ACEEE Summer Study on Energy Efficiency in Buildings*, Pacific Grove, CA, August, pp. 10.105 - 10.114.

Katipamula, S. and Claridge, D., 1992, "Monitored Air Handler Performance and Comparison with a Simplifed System Model, *ASHRAE Transactions*, Vol. 98, Pt. 2, pp. 341 - 351.

Katipamula, S. and Claridge, D., 1993, "Use of Simplified System Models to Measure Retrofit Savings", *ASME Journal of Solar Energy Engineering*, Vol. 115, pp. 57 - 68.

Kissock, K., 1989, "The Effect of Population, Economy and Energy Use on Sulfur Emissions in the United States since 1900", M.S. Research Project, Washington University, St. Louis, MO.

Kissock, K., Claridge, D., Haberl, J., and Reddy, A., 1992, "Measuring Retrofit Savings for the Texas LoanSTAR Program: Preliminary Methodology and Results", *Solar Engineering 1992: Proceedings of the ASME/JSES/KSES International Solar Energy Conference*, Hawaii, March, pp. 299 - 308.

Kissock, K., 1993. *EModel User's Guide*, Texas Engineering Experiment Station, Texas A&M University, College Station, TX.

Kissock, K., Reddy, A., Fletcher, D., and Claridge, D., 1993a, "The Effect of Short Data Periods on the Annual Prediction Accuracy of Temperature Dependent Regression Models of Commercial Building Energy Use", *Solar Engineering, 1993: Proceedings of the ASME-SED Conference*, Washington, DC, April, pp. 455 - 463.

Kissock, K., Reddy, A., Haberl, J., and Claridge, D., 1993b, "EModel: A New Tool for Analyzing Building Energy Use Data", *Proceedings of the Fifteenth National Industrial Energy Technology Conference*, Mechanical Engineering Department, Texas A&M University, Houston, TX, pp. 237 - 243.

Knebel, D., 1983, *Simplified Energy Analysis Using the Modified Bin Method*, American Society of Heating, Refrigerating, and Air-Conditioning Engineers Inc., Atlanta, GA.

Kreider, J. and Wang, X., 1991, "Artificial Neural Networks Demonstrated For Automated Generation of Energy Use Predictors For Commercial Buildings", *ASHRAE Transactions*, Vol. 97, Pt. 1, pp. 775 - 779.

Krieg, B. and Baker, M., 1992, "ACT^2 Project: Measuring Energy Savings", *The Eighth Symposium on Improving Building Systems In Hot and Humid Climates*, Mechanical Engineering Department, Texas A&M University, Dallas, TX, May, pp. 141 - 148.

Lantern Corporation, 1990. *Voyager Data Exploration Software*, Clayton MO.

Lawrence Berkeley Laboratory, 1980, "DOE-2 User Guide, Version 2.1", LBL Report No. LBL-8689 Rev. 2, Berkeley, CA.

Lee, E., 1992, "Electric Eye", Supersymetry, Inc., Singapore, Thailand, personal communication, 9/2/92.

Liu, Yue, 1993, "Determining Weather and/or Schedule Dependent Retrofit Savings For Buildings with Limited Monitored Data", M.S. Thesis in preparation, Texas A&M University.

Lopez, R. and Haberl, J., 1992, "Data Processing Routines for Monitored Building Energy Use Data", *Solar Engineering 1992: Proceedings of the ASME-JSES-KSES International Solar Energy Conference*, Maui, HI, March, pp. 329 - 336.

MacDonald, J. and Wasserman, D.,1989, "Investigation of Metered Data Analysis Methods for Commercial and Related Buildings", ORNL/CON-279, Oak Ridge National Laboratory, Oak Ridge, TN.

MacKay, D. 1993, "Bayesian Non-linear Modeling for the Energy Predictor Competition", Draft paper submitted at the Building Energy Predictor Shootout ASHRAE Symposium, Denver, CO, June.

McClelland, J. and Rumelhart, D., 1989, *Explorations in Parallel Distributed Processing*, Massachusetts Institute of Technology, Boston, MA.

Meier, A. and Nordman, B., 1988, "The Incremental Value of Monitored Building Energy Data", *Proceedings of the ACEEE Summer Study on Energy Efficiency in Buildings*, Pacific Grove, CA, August, pp. 10.169 - 10.172.

Microsoft®, 1990-1992. "Windows™ Operating System Software", Windows™ is a trademark of the Microsoft Corporation. Redmond, WA.

Miller, B. and Hittle, D., 1993, "Optimum Designs of the CSU Low Energy Building", *Solar Engineering 1993: Proceedings of the ASME International Solar Energy Conference*, Washington, DC, April, pp. 107 - 116.

Miller, R. and Seem, J., 1991, "Comparison of Artificial Neural Networks With Traditional Methods of Predicting Return Time From Night Setback", *ASHRAE Transactions*, Vol. 97, Pt. 2, pp. 500 - 508.

Mitalas, G. and Stephenson, D., 1967, "Cooling Load Calculation by Thermal Response Factor Method", *ASHRAE Transactions*, Vol. 73, Pt. 2, p. 111.2.1.

Mitchell, J., 1983, *Energy Engineering*, John Wiley & Sons, New York, NY

Nelson, 1993, "Delay Time Determination Using An Artificial Neural Network", Draft paper submitted to *Building Simulation '93: Proceedings of the International Building Performance Simulation Association Conference*, Australia.

Neter, J., Wasserman, W. and Kutner, M., 1989, *Applied Linear Regression Models*, Richard D. Irwin, Inc., Boston, MA.

Norford, L., 1984, "An Analysis of Energy Use in Office Buildings: The Case of ENERPLEX", Ph.D. Dissertation, Mechanical and Aerospace Engineering, Princeton University, Princeton, NJ.

O'Neal, D., Bryant, J., Turner, W. and Glass, M., 1990, "Metering and Calibration in LoanSTAR Buildings", *The Seventh Symposium on Improving Building Systems In Hot and Humid Climates*, Mechanical Engineering Department, Texas A&M University, Ft. Worth, TX, October, pp. 41 - 46

O'Neal, D., Bryant, J., Boecker, C and Bohmer, C., 1993, "Instrumenting Buildings to Determine Retrofit Savings: Murphy's Law Revisited", *Proceedings of the Fifteenth National Industrial Energy Technology Conference*, Mechanical Engineering Department, Texas A&M University, Houston, TX, March, pp. 244 - 252.

Pacific Gas and Electric, 1990, *Facts on ACT*^{2}, Issue 1, October, San Ramon, CA.

Postel, S., 1992, "Denial in the Decisive Decade", *State of the World: 1992*, W. W. Norton Company, Inc., New York, NY, pp. 3 - 8.

Quantum Consulting Inc., 1992, "LoadView 2.0 Pro Software", Berkeley, CA.

Rabl, A., 1988, "Parameter Estimation in Buildings: Methods for Dynamic Analysis of Measured Energy Use", *ASME Journal of Solar Energy Engineering*, Vol. 110, pp. 52 - 62.

Reddy, A., 1989, "Identification of Building Parameters Using Dynamic Inverse Models: Analysis of Three Occupied Residences Monitored Non-Intrusively", Princeton University, Center for Energy and Environmental Studies Report No. 236, Princeton, NJ.

Reddy, A. and Claridge, D., 1993, "Using Synthetic Data To Evaluate Multiple Regression and Principal Component Analysis for Statistical Modeling of Daily Building Energy Consumption", Draft Energy Systems Laboratory Report, Mechanical Engineering Department, Texas A&M University.

Reddy, A., Kissock, K., Katipamila, S. and Claridge, D., 1993, "An Energy Delivery Efficiency Index to Evaluate Simultaneous Heating and Cooling Effects in Large Commercial Buildings", Submitted to the *ASME Journal to Solar Energy Engineering*.

Robinson, J., Bryant, J., Turner, W. and Haberl, J.S., 1992. "Calibration of Tangential Paddlewheel Insertion Flow Meters", *Proceedings of the Eighth Symposium on Improving Building Systems in Hot and Humid Climates*, Mechanical Engineering Department, Texas A&M University, Dallas, TX, May, 222 - 228.

Robinson, J., Bryant, J. and Turner, W., 1993 "Insertion Paddlewheel Flow Meters: An Evaluation After Two Years of Use", *Proceedings of the Fifteenth National Industrial Energy Technology Conference*, Mechanical Engineering Department, Texas A&M University, Houston, TX, March, pp. 253 - 256.

Ruch D. 1992. "Hybrid Energy Models", Energy Systems Laboratory Technical Report, Mechanical Engineering Department, Texas A&M University, August, 1992.

Ruch, D. and Claridge, D., 1992a, "A Four Parameter Change-Point Model for Predicting Energy Consumption in Commercial Buildings", *Journal of Solar Energy Engineering*, Vol. 114, pp. 77 - 83.

Ruch, D. and Claridge, D., 1992b, "NAC for Linear and Change-Point Energy Models," *Proceedings of the 1992 ACEEE Summer Study on Energy Efficiency in Buildings*, Pacific Grove, CA, August, pp. 3.263 - 3.273.

Ruch, D., Chen, L., Haberl, J. and Claridge, D., 1993a, "A Change-Point Principle-Component Analysis (CP/PCA) Method for Predicting Energy Usage in Commercial Buildings: The PCA Model", *Journal of Solar Energy Engineering*, Vol. 115. pp. 77 - 84.

Ruch, D., Kissock, K. and Reddy, T., 1993b, "Model Identification and Prediction Uncertainty of Linear Building Energy Use Models with Autocorrelated Residuals", *Solar Engineering, 1993: Proceedings of the ASME-SED Conference*, Washington, DC, April, pp. 465 - 473.

Ruckelshaus, W., 1989, "Toward a Sustainable World", *Scientific American*, September, 166 - 174.

SAS, 1984, *SAS/ETS User's Guide*, Version 5 , SAS Institute, Inc., Cary, NC.

SAS, 1989, *SAS/STAT User's Guide*, Version 6, Fourth Edition, Volume 2, SAS Institute, Inc., Cary, NC.

SAS, 1992. PC-SAS 6.04, SAS Institute Inc., Cary, NC.

Schrock, D. and Claridge, D., 1989, "Predicting Energy Usage in a Supermarket", *Proceedings of the Sixth Symposium on Improving Building Systems in Hot and Humid Climates*, Mechanical Engineering Department, Texas A&M University, Dallas, TX, October, pp. 45 - 54.

Seem, J. and Braun, J., 1991, "Adaptive Methods for Real Time Forecasting of Building Electrical Demand", *ASHRAE Transactions*, Vol: 97, Pt. 1, pp. 710 - 721.

Sondregger, R., 1978, "Dynamic Models of House Heating Based on Equivalent Thermal Parameters", Ph.D. Dissertation, Princeton University, Princeton NJ

Sparks, F., Haberl, J., Bhattacharrya, S., Rayaprolu, M. and Wang, J., 1992, "Testing Data Acquisition Systems for Use in Monitoring Building Energy Conservation Systems", *The Eighth Symposium on Improving Building Systems In Hot and Humid Climates*, Mechanical Engineering Department, Texas A&M University, Dallas, TX, May, pp. 197 - 204.

Sparks, R. and Haberl, J., 1993, "Applying Machine Learning Techniques To Assure Data Quality Control in Monitoring Projects", Draft Energy Systems Laboratory Report, Mechanical Engineering Department, Texas A&M University.

Stobaugh, R. and Yergin, D., 1983, *Energy Future*, Vintage Books, New York, NY.

Taylor, R., 1986, *Value-Added Processes in Information Systems*, Ablex Publishing Corporation, Norwood, NJ.

Taylor, T. and Pratt, R., 1988, "The Effects of Model Simplifications on Equivalent Thermal Parameters Calculated from Hourly Building Performance Data", *Proceedings of the 1988 ACEEE Summer Study on Energy Efficiency in Buildings*, Pacific Grove, CA, August, pp. 10.269 - 10.285.

Texas Energy Cost Containment Program, 1986, "Energy Cost Reduction Analysis of Texas A&M University".

Texas Engineering Experiment Station, 1993, "LoanSTAR Program Saves Texas Taxpayers Millions in Energy Bills", TEES News Release, Texas A&M University, April.

Theil, H., 1971, *Principles of Econometrics*, John Wiley and Sons, New York, NY.

Treado, J. and Bean, J., 1990, "Experimental Evaluation of Lighting / HVAC Interaction", *ASHRAE Transactions*, Vol. 96, Pt. 2, pp. 773 - 779.

Tukey, J., 1988, *The Collected Works of John W. Tukey: Volume V: Graphics: 1965-1985*, Edited by W. Cleveland, Wadsworth and Brooks/Cole Advanced Books & Software, Pacific Groves, CA.

Turner, W., 1990, "Overview of the Texas LoanSTAR Monitoring Program", *The Seventh Symposium on Improving Building Systems In Hot and Humid Climates*, Mechanical Engineering Department, Texas A&M University, Ft. Worth, TX, October, pp. 28 - 34.

Turner, W., Haberl, J., Bryant, J., Finstad, C. and Robinson, J., 1992, "Calibration Facility for the LoanSTAR Program", *Solar Engineering 1992: Proceedings of the ASME-JSES-KSES International Solar Energy Conference*, Maui, HI, March, pp. 329 - 336.

Vadon, M., Kreider, J. and Norford, L., 1991, "Improvement of the Solar Calculation in the Modified Bin Method", *ASHRAE Transactions*, Vol. 97, Pt. 2, pp. 204 - 211.

Wasserman, P., 1989, *Neural Computing: Theory and Practice*, Van Nostrand Reinhold, New York, NY.

Willis, D. and Haberl, J., 1992, "A Collaborative Support System for the Review of Building Energy Data in the LoanSTAR Monitoring and Analysis Program", *The Eighth Symposium on Improving Building Systems In Hot and Humid Climates*, Mechanical Engineering Department, Texas A&M University, Dallas, TX, May, pp. 213 - 221.

Zaheer-uddin, M., 1990, "Combined Energy Balance and Recursive Least Squares Method For the Identification of System Parameters", *ASHRAE Transactions*, Vol. 96, Pt. 2, pp. 239 - 243.

Zuboff, S. 1988. *In the Age of the Smart Machine: The Future of Work and Power*, Basic Books, Inc., New York, NY.

APPENDIX A

ENERGY USE CALCULATIONS FOR SIMULATION

Input Parameters

The following parameter values were used:

$T_{sp} = 72$	'(°F) set-point temperature
$T_c = 55$	'(°F) cold-deck temperature
$T_h = 120$	'(°F) hot-deck temperature
$f_{int} = .65$	'fratio interior to total floor area
$f_o = .1$	'ratio of outside to total ventilation air
$UA_s = 20000$	'(Btu/hr°F) total building load coefficient
$V_r = 1.666666 * 300000 * 60$	'(ft3/hr) = cfm/ft2 * ft2 * 60(min/hr) for CV 'total air volume flow rate
$V_{min,int} = .33 * 300000 * 60 * f_{int}$	'(ft3/hr) = cfm/ft2 * ft2 * 60(min/hr) for VAV 'minimum air flow requirement to interior zone
$V_{min,ext} = .33 * 300000 * 60 * (1 - f_{int})$	'(ft3/hr) = cfm/ft2 * ft2 * 60(min/hr) for VAV 'minimum air flow requirement to exterior zone
$pcp = .018$	'(Btu/ft3°F) air density * specific heat at constant pr.
$phfg = 80$	'(Btu/ft3) air density * latent heat of vaporization
$s_1 = 10000$	'(Btu/hr) solar load constant
$s_2 = 400$	'(Btu/hr°F) solar load slope

Sensible Cooling Loads to Interior and Exterior Zones

The number of building occupants is estimated as a linear function of the whole building electricity use.

$$numoccs = -1071 + 3.571 * E_{wb} \qquad (AA.1)$$

The total internal loads are the sum of whole building electricity use and the sensible heat given off by the building occupants.

$$Q_i = (E_{wb} * 3412) + (numoccs * 255) \qquad (AA.2)$$

3412 Btu/kWh is a conversion constant and 255 Btu/hr·person is an average value for sensible heat gain given off by a person doing light work (Mitchell, 1983). The sensible cooling load to the interior zone is the internal load multiplied by the fraction of floor area taken by the internal zone.

$$Q_{int} = f_{int} * Q_i \quad \text{(AA.3)}$$

The sensible cooling load to the exterior zone is the sum of the internal load to the exterior zone, the shell conduction load and the solar load.

$$Q_{ext} = (1 - f_{int}) * Q_i + UA_S * (T_O - T_{sp}) + (s_1 + s_2 * T_O) \quad \text{(AA.4)}$$

The solar load is estimated as a linear function of the outside air temperature.

Hot-Deck Reset Schedule

If the outside air temperature is less than 50 °F then the hot deck temperature is 120 ° F. If the outside air temperature is greater than 80 °F then the hot deck temperature is 80 °F. If the outside air temperature is between 50 °F and 80 °F then the hot deck temperature varies linearly between 120 °F and 80 °F according to the outside air temperature.

Economizer Cycle

If the outside air temperature is less than the cold deck temperature, then the fraction of outside air f_O varies to maintain the return air at the cold deck temperature.

$$f_O = (T_C - T_{sp}) / (T_O - T_{sp}) \quad \text{(AA.5)}$$

If the outside air temperature is between the cold deck temperature and the zone set-point temperature then 100% outside air is used. If the outside air temperature is greater than the zone set-point temperature then the fraction of outside air is set to 10%.

Latent Loads

The latent ventilation load is the product of the total volume flow rate, the fraction of outside air, the density of air, the latent heat of vaporization of water and the positive difference between the specific humidity of the outside air and the specific humidity of air leaving the cooling coil.

$$Q_{lat,v} = V_r * f_o * phfg * (W_o - .0092) \quad (AA.6)$$

The latent load due to the building occupants is calculated from the average latent load given off by people doing light work, 255 Btu/hr·person (Mitchell, 1983).

$$Q_{lat,p} = numoccs * 255 \quad (AA.7)$$

The total latent load is the sum of the latent ventilation load and the latent load due to the building occupants.

$$Q_{lat} = Q_{lat,v} + Q_{lat,p} \quad (AA.8)$$

Cold and Hot-Deck Volume Flow Rates for Constant-Air-Volume Systems

The air volume flow rates through the interior and exterior zones are functions of the floor areas of the interior and exterior zones.

$$V_{r,int} = f_{int} * V_r \quad (AA.9)$$

$$V_{r,ext} = (1 - f_{int}) * V_r \quad (AA.10)$$

Energy balances on the interior and exterior zones give the volume flow rates of air through the cooling coil for the interior and exterior zones.

$$V_{c,int} = (V_{r,int} * pcp * (T_{sp} - T_h) - Q_{int}) / (pcp * (T_c - T_h)) \quad (AA.11)$$

$$V_{c,ext} = (V_{r,ext} * pcp * (T_{sp} - T_h) - Q_{ext}) / (pcp * (T_c - T_h)) \quad (AA.12)$$

The total volume flow rate through the cooling coil is the sum of the cool air flowing to the interior and exterior zones.

$$V_c = V_{c,int} + V_{c,ext} \quad (AA.13)$$

The total volume flow rate through the heating coil is the difference between the total (or return air) volume flow rate and the flow rate of air through the cooling coil.

$$V_h = V_r - V_c \quad (AA.14)$$

Cold and Hot-Deck Volume Flow Rates for Variable-Air-Volume Systems

When the total cooling load to the interior zone Q_{li} is positive, no warm air is used and the volume flow rate of cooling air to the interior zone is modulated to exactly meet the cooling load.

$$V_{h,int} = 0 \tag{AA.15}$$

$$V_{c,int} = Q_{int} / (pcp * (T_{sp} - T_c)) \tag{AA.16}$$

If the volume flow rate of cooling air $V_{c,int}$ calculated above is less than the minimum required flow rate $V_{min,int}$, then the volume flow rate of cooling air to the interior zone can be calculated from an energy balance on the zone where the flow rate of air exhausted from the zone is $V_{min,int}$.

$$V_{c,int} = (V_{min,int} * pcp * (T_{sp} - T_h) - Q_{int}) / (pcp * (T_c - T_h)) \tag{AA.17}$$

The volume flow rate of heating air to the interior zone can be found from a mass balance on the zone.

$$V_{h,int} = V_{min,int} - V_{c,int} \tag{AA.18}$$

When the total cooling load to the interior zone Q_{int} is negative, no cooling is required and the volume flow rate of heating air is modulated to exactly meet the heating load.

$$V_{c,int} = 0 \tag{AA.19}$$

$$V_{h,int} = Q_{int} / (pcp * (T_{sp} - T_h)) \tag{AA.20}$$

If the volume flow rate of heating air $V_{h,int}$ is less than the minimum required flow rate $V_{min,int}$, then the volume flow rates of the cooling and heating air are calculated as before using Equations AA.17 and AA.18.

The calculation of volume flow rates to the exterior zone is analogous to the calculation of volume flow rates to the interior zone.

Mixed Air Temperature

The mixed air temperature is given by an energy balance on the mixing box.

$$T_{ma} = f_o * T_o + T_{sp} * (1 - f_o) \quad \text{(AA.21)}$$

Cold and Hot-Deck Energy Use

The total sensible cooling energy use is calculated from an energy balance on the cold-deck.

$$E_{c,sen} = (V_c * pcp * (T_{ma} - T_c)) \quad \text{(AA.22)}$$

Total cooling energy use is the sum of the sensible and latent cooling requirements.

$$E_c = E_{c,sen} + Q_{lat} \quad \text{(AA.23)}$$

The total heating energy use is given by an energy balance on the hot-deck.

$$E_h = V_h * pcp * (T_h - T_{ma}) \quad \text{(AA.24)}$$

APPENDIX B

EMODEL ACCURACY COMPARISONS

The model parameters and inferential statistics computed by EModel were compared to other benchmark statistical software packages in order to test the precision of EModel's statistical algorithms. The results of these comparisons are presented here.

In nearly every comparison between EModel and SAS (SAS, 1992), model parameters and inferential statistics agreed to at least four significant figures or to the precision reported by EModel. Parameters identified by EModel's three and four parameter change-point models showed good agreement with those from PRISM and FourP (Ruch and Claridge, 1992a); however, it should be noted that the computational algorithms used by EModel, PRISM and FourP are not identical, and so precise agreement should not be expected.

EModel Mean Model Comparison with SAS

EModel Data Set: winsave.sht
SAS Data Set: winsave.sht (emtest1.lst)
Dependent Variable: whole building chilled water energy

Table AB.1 EModel mean model comparison with SAS.

	EModel	SAS
N	245	245
Mean	51.41	51.4102041
Standard Deviation	16.6914	16.6914212

EModel Simple Linear Regression Model Comparison with SAS

EModel Data Set: winsave.sht
SAS Data Set: winsave.sht (emtest1.lst)
Dependent Variable: whole building steam energy
Independent Variable: outdoor air dry bulb temperature

Table AB.2 EModel simple linear regression model comparison with SAS.

	EModel	SAS
N	245	245
ao (Standard Error ao)	87.9089 (1.28886)	87.908923 (1.28864863)
a1 (Standard Error a1)	-0.7481 (0.0195)	-0.748104 (0.01952847)
R-Square	0.86	0.8579
Root Mean Square Error	3.9692	3.96921
CV-RMSE (%)	10.0	10.04657
Autocorrelation Coefficient	0.75	0.752
Durbin Watson	0.49	0.491

EModel Simple Linear Regression Model Comparison with SAS Using 3971 Observations

EModel Data Set: aallcln.dat
SAS Data Set: aallcln.dat (emtest2.lst)
Dependent Variable: whole building chilled water energy
Independent Variable: outdoor air dry bulb temperature

Table AB.3 EModel simple linear regression model comparison with SAS using 3971 observations.

	EModel	SAS
N	3971	3971
ao (Standard Error ao)	1.5908 (0.0322)	1.590847 (0.03224871)
a1 (Standard Error a1)	0.0572 (0.0005)	0.057194 (0.00050501)
R-Square	0.76	0.7637
Root Mean Square Error	0.5011	0.50110
CV-RMSE (%)	9.8	9.76730
Autocorrelation Coefficient	0.93	0.927
Durbin Watson	0.15	0.146

EModel Multiple Linear Regression Model Comparison with SAS

EModel Data Set: aallcln.dat
SAS Data Set: aallcln.dat (emtest2.lst)
Dependent Variable: whole building chilled water energy
Independent Variable: outdoor air dry bulb temperature
Independent Variable: specific humidity
Independent Variable: solar radiation

Table AB.4 EModel multiple linear regression model comparison with SAS.

	EModel	SAS
N	3971	3971
ao (Standard Error ao)	1.9364 (0.0308)	1.936375 (0.03080254)
a1 (Standard Error a1)	0.0433 (0.0006)	0.043271 (0.00063857)
a2 (Standard Error a2)	63.7853 (1.9191)	63.785318 (1.91911454)
a3 (Standard Error a3)	0.0004 (0.0000)	0.000355 (0.00003352)
R-Square	0.82	0.8155
Root Mean Square Error	0.44	0.44287
CV-RMSE (%)	8.6	8.63236
Autocorrelation Coefficient	0.91	0.909
Durbin Watson	0.18	0.182

EModel Three-Parameter, Change-Point Model Comparison with PRISM

EModel Data Set: winsave.sht
PRISM Data Set: met114b.co, temps.aus, (pout114b.co)
Dependent Variable: whole building chilled water energy
Independent Variable: outdoor air dry bulb temperature
Note: EModel and PRISM use different algorithms to calculate model parameters and so precise agreement should not be expected. Standard errors of regression coefficients reported by EModel for change-point models are only estimates. A more sophisticated technique for determining model errors in change-point models will be included in future versions of EModel.

Table AB.5 EModel three-parameter, change-point model comparison with PRISM.

	EModel	PRISM
N	245	245
ycp (Standard Error ycp)	31.1933 (0.6252)	30.5030 (1.1401)
ls (Standard Error ls)	0	0
rs (Standard Error rs)	1.4587 (0.3057)	1.4424 (0.0538)
xcp (Standard Error xcp)	52.2000	51.75 (1.08)
R-Square	0.87	0.8210
Root Mean Square Error	5.9684	-
CV-RMSE (%)	11.6	-
Autocorrelation Coefficient	0.63	-
Durbin Watson	0.74	-

EModel Four-Parameter, Change-Point Model Comparison with FourP

EModel Data Set: winsave.sht
FourP Data Set: cw4ptst.dat (cw4ptst.lst)
Dependent Variable: whole building chilled water energy
Independent Variable: outdoor air dry bulb temperature
Note: EModel and FourP use different algorithms to calculate model parameters and so precise agreement should not be expected. Standard errors of regression coefficients reported by EModel for change-point models are only estimates. A more sophisticated technique for determining model errors in change-point models will be included in future versions of EModel.

Table AB.6 EModel four-parameter, change-point model comparison with FourP.

	EModel	FourP
N	245	245
ycp (Standard Error ycp)	47.6582 (2.5689)	46.690
ls (Standard Error ls)	0.7439 (0.0446)	0.729
rs (Standard Error rs)	1.8880 (0.1056)	1.845
xcp (Standard Error xcp)	66.5000	65.683
R-Square	0.90	0.966
Root Mean Square Error	5.1855	5.038
CV-RMSE (%)	10.1	10.273
Autocorrelation Coefficient	0.60	-
Durbin Watson	0.80	-

EModel Four-Parameter, Change-Point Model Comparison with SAS

EModel Data Set: winsave.sht
FourP Data Set: cw4ptst.dat (cw4ptst.lst)
Dependent Variable: whole building chilled water energy
Independent Variable: outdoor air dry bulb temperature
Note: EModel determines the value of the X change-point by searching for the X change-point value which yields the lowest overall model error. In this comparison, Xcp is identified by EModel and substituted into an indicator model in SAS. This procedure allows SAS to determine a four parameter model. Standard errors of regression coefficients reported by EModel for change-point models are only estimates. A more sophisticated technique for determining model errors in change-point models will be included in future versions of EModel.

Table AB.7 EModel four-parameter, change-point model comparison with SAS.

	EModel	SAS
N	245	245
ycp (Standard Error ycp)	47.6582 (2.5689)	47.65826
ls (Standard Error ls)	0.7439 (0.0446)	0.743903
rs (Standard Error rs)	1.8880 (0.1056)	1.88802
xcp (Standard Error xcp)	65.5000	65.5000 (from EModel)
R-Square	0.90	0.9043
Root Mean Square Error	5.1855	5.18553
CV-RMSE (%)	10.1	10.08658
Autocorrelation Coefficient	0.60	0.591
Durbin Watson	0.80	0.804

APPENDIX C

ANN: ARTIFICIAL NEURAL NETWORK PROGRAM

```
'Program listing of ANN.BAS
'ANN.BAS is an artificial neural network modeling program for
'a 4 layer, two input, one output, 5 middle node architecture

DIM d(200, 3), w12(2, 5), w23(5, 5), w34(5, 1), x(4, 5), y(4, 5), delta(4, 5)

CLS
PRINT "ANN3.BAS Version Beta 1.0 by Kelly Kissock"

'input parameters
gain = .5
bias = 0
lrate = .25
maxerror = .1
maxepoch = 10000
tolerance = .0001
infile$ = "testdat.dat"

'input and output file
OPEN infile$ FOR INPUT AS #1
OPEN "ANN3.log" FOR OUTPUT AS #2
OPEN "ANN3.trd" FOR OUTPUT AS #3


'STEP 1: Input variables and normalize between .1 and .9
n = 0
WHILE NOT EOF(1)
  n = n + 1
  FOR F = 1 TO 3
    INPUT #1, d(n, F)
  NEXT F

  IF n = 1 THEN
    tmin = d(1, 1)
    emin = d(1, 2)
    cmin = d(1, 3)
    tmax = d(1, 1)
    emax = d(1, 2)
    cmax = d(1, 3)
```

```
  END IF

  IF d(n, 1) < tmin THEN tmin = d(n, 1)
  IF d(n, 1) > tmax THEN tmax = d(n, 1)
  IF d(n, 2) < emin THEN emin = d(n, 2)
  IF d(n, 2) > emax THEN emax = d(n, 2)
  IF d(n, 3) < cmin THEN cmin = d(n, 3)
  IF d(n, 3) > cmax THEN cmax = d(n, 3)
  ctotal = ctotal + d(n, 3)
WEND
trange = tmax - tmin
erange = emax - emin
crange = cmax - cmin
cmean = ctotal / n
FOR i = 1 TO n
    d(i, 1) = (d(i, 1) - tmin) / trange * .8 + .1
    d(i, 2) = (d(i, 2) - emin) / erange * .8 + .1
    d(i, 3) = (d(i, 3) - cmin) / crange * .8 + .1
NEXT i


'STEP 2: randomize weights between -.5 and .5
FOR i = 1 TO 2
  FOR j = 1 TO 5
    RANDOMIZE (TIMER)
    r = RND
    IF r < .5 THEN
      w12(i, j) = r
    ELSE
      w12(i, j) = r - 1
    END IF
  NEXT j
NEXT i
FOR i = 1 TO 5
  FOR j = 1 TO 5
    RANDOMIZE (TIMER)
    r = RND
    IF r < .5 THEN
      w23(i, j) = r
    ELSE
      w23(i, j) = r - 1
    END IF
  NEXT j
NEXT i
```

```
FOR j = 1 TO 5
  RANDOMIZE (TIMER)
  r = RND
  IF r < .5 THEN
    w34(j, 1) = r
  ELSE
    w34(j, 1) = r - 1
  END IF
NEXT j


toterror = 0: i = 0   'initialize counting variables
WHILE epoch < maxepoch
  i = i + 1

  'STEP 9: checks if if avgerror < maxerror at end of each epoch
  IF i = n + 1 THEN
    epoch = epoch + 1
    avgerror = toterror / n
    CLS
    PRINT "ANN3.BAS Beta Version 1.0 by Kelly Kissock"
    PRINT "Please do not turn this computer off until it reaches 10,000 epochs."
    PRINT "Epoch = "; epoch
    PRINT "Average Error = "; avgerror
    p% = epoch / 10
    IF (epoch / 10) = p% THEN PRINT #3, epoch; avgerror
    IF avgerror < maxerror THEN
      PRINT "avgerror < maxerror"
      GOTO done:
    ELSEIF ABS(lastaerr - avgerror) < tolerance THEN
      PRINT "tolerance < "; tolerance
      GOTO done:
    END IF
    'GOTO done:
    lastaerr = avgerror
    toterror = 0
    sse = 0
    i = 1
  END IF


  'STEP 3:  Set output of first layer equal to input
  FOR j = 1 TO 2
    y(1, j) = d(i, j)
```

```
NEXT j

'STEP 4: Calc activation (x) and output (y) of second layer
FOR j = 1 TO 5
  x(2, j) = 0
  FOR k = 1 TO 2
    x(2, j) = x(2, j) + y(1, k) * w12(k, j)
  NEXT k
  y(2, j) = 1 / (1 + EXP(-gain * (x(2, j) + bias)))
NEXT j

'STEP 4.5: Calc activation (x) and output (y) of third layer
FOR j = 1 TO 5
  x(3, j) = 0
  FOR k = 1 TO 5
    x(3, j) = x(3, j) + y(2, k) * w23(k, j)
  NEXT k
  y(3, j) = 1 / (1 + EXP(-gain * (x(3, j) + bias)))
NEXT j

'STEP 5: Calc activation (x) and output (y) of output layer
x(4, 1) = 0
FOR j = 1 TO 5
  x(4, 1) = x(4, 1) + y(3, j) * w34(j, 1)
NEXT j
y(4, 1) = 1 / (1 + EXP(-gain * (x(4, 1) + bias)))

'STEP 6: Calc total absolutue error in this epoch
cpred = (y(4, 1) - .1) / .8 * crange + cmin
c = (d(i, 3) - .1) / .8 * crange + cmin
abserror = ABS(c - cpred)
toterror = toterror + abserror
sse = sse + (c - cpred) ^ 2

'STEP 7: Begin training, adjust w34 weights
delta(4, 1) = y(4, 1) * (1 - y(4, 1)) * (d(i, 3) - y(4, 1))
FOR j = 1 TO 5
  w34(j, 1) = w34(j, 1) + lrate * y(3, j) * delta(4, 1)
NEXT j
```

```
 'STEP 7.5: Adjust w23 weights
 FOR j = 1 TO 5
   delta(3, j) = y(3, j) * (1 - y(3, j)) * (delta(4, 1) * w34(j, 1))
 NEXT j
 FOR j = 1 TO 5
   FOR k = 1 TO 5
     w23(j, k) = w23(j, k) + lrate * y(2, j) * delta(3, k)
   NEXT k
 NEXT j


 'STEP 8: Adjust w12 weights
 FOR j = 1 TO 5
   delta(2, j) = 0
   FOR k = 1 TO 5
     delta(2, j) = delta(2, j) + y(2, j) * (1 - y(2, j)) * (delta(3, k) * w23(j, k))
   NEXT k
 NEXT j
 FOR j = 1 TO 2
   FOR k = 1 TO 5
     w12(j, k) = w12(j, k) + lrate * y(1, j) * delta(2, k)
   NEXT k
 NEXT j
WEND

done:  'prints output
PRINT "Done!"
PRINT USING "&####.#"; "CV-RMSE = "; ((sse / (n - 1)) ^ .5) / cmean * 100
PRINT #2, "ANN.BAS Beta Version 1.0 by Kelly Kissock"
PRINT #2,
PRINT #2, "Epochs = "; epoch
PRINT #2, "Average Error = "; avgerror
PRINT #2, "Max Allowable Error = "; maxerror
PRINT #2, "n = "; n
PRINT #2, USING "&#######.###"; "RMSE = "; (sse / (n - 1)) ^ .5
PRINT #2, USING "&#######.###"; "CV-RMSE = "; ((sse / (n - 1)) ^ .5) / cmean * 100
PRINT #2,

PRINT #2, "Weights"
FOR j = 1 TO 2
  'PRINT #2, "w12("; j; ")";
  FOR k = 1 TO 5
```

```
    PRINT #2, USING "####.######"; w12(j, k);
  NEXT k
  PRINT #2,
NEXT j
PRINT #2,

FOR j = 1 TO 5
  'PRINT #2, "w23("; j; ")";
  FOR k = 1 TO 5
    PRINT #2, USING "####.######"; w23(j, k);
  NEXT k
  PRINT #2,
NEXT j
PRINT #2,

FOR k = 1 TO 5
  'PRINT #2, "w34("; k; ")";
  PRINT #2, USING "####.######"; w34(k, 1);
NEXT k
PRINT #2,
PRINT #2,
PRINT #2,

'calculates and prints predicted values
PRINT #2, "  temp    wbe    cw    predcw    residual"
FOR i = 1 TO n
  'STEP 3:  Set output of first layer equal to input
  FOR j = 1 TO 2
    y(1, j) = d(i, j)
  NEXT j

  'STEP 4: Calc activation (x) and output (y) of second layer
  FOR j = 1 TO 5
    x(2, j) = 0
    FOR k = 1 TO 2
      x(2, j) = x(2, j) + y(1, k) * w12(k, j)
    NEXT k
    y(2, j) = 1 / (1 + EXP(-gain * (x(2, j) + bias)))
  NEXT j

  'STEP 4.5: Calc activation (x) and output (y) of third layer
  FOR j = 1 TO 5
    x(3, j) = 0
    FOR k = 1 TO 5
```

```
      x(3, j) = x(3, j) + y(2, k) * w23(k, j)
    NEXT k
    y(3, j) = 1 / (1 + EXP(-gain * (x(3, j) + bias)))
  NEXT j

  'STEP 5: Calc activation (x) and output (y) of output layer
  x(4, 1) = 0
  FOR j = 1 TO 5
    x(4, 1) = x(4, 1) + y(3, j) * w34(j, 1)
  NEXT j
  y(4, 1) = 1 / (1 + EXP(-gain * (x(4, 1) + bias)))

  'print output
  t = (d(i, 1) - .1) / .8 * trange + tmin
  e = (d(i, 2) - .1) / .8 * erange + emin
  c = (d(i, 3) - .1) / .8 * crange + cmin
  cpred = (y(4, 1) - .1) / .8 * crange + cmin
  resid = c - cpred
  PRINT #2, USING "######.#"; t; e; c; cpred; resid
NEXT i
CLOSE
END
```

APPENDIX D

THE T-TEST AND F-TEST FOR MODEL SIMILARITY

If weekday energy use is different from weekend energy use, then the coefficients of weekday and weekend models are likely to be very different. In this case, it is appropriate to consider separate weekday and weekend models. If the weekday and weekend model coefficients are nearly identical, then it is probable that no difference between weekday and weekend energy use actually exists and that the building's energy use can be accurately represented by a single model which includes both weekdays and weekends. The use of separate weekday and weekend models in this case is unnecessary and statistically incorrect. Statistical procedures such as a t-test (for one-parameter models) and an f-test (for multiple parameter models) can determine if separate weekday and weekend models or if a single all-day model of energy use is appropriate.

For one-parameter mean models, the t-test (Box et al., 1978, p. 76) is the appropriate test. The sample standard deviation of weekday energy use is:

$$sd_{wd} = \left[\frac{\sum_{d=1}^{n_{wd}} (E_d - \bar{E}_{wd})^2}{(n_{wd} - 1)} \right]^{\frac{1}{2}} \qquad \text{(AD.1)}$$

where E_d is daily weekday energy use, $\bar{E}_{wd}$ is the mean daily weekday energy use, and n_{wd} is the number of weekdays in the sample. The sample standard deviation of weekend energy use is found by substituting values of weekend energy use and the number of weekend days into Equation AD.1. The combined sample standard deviation of the weekday and weekend energy use is:

$$sd_c = \left[\frac{(n_{wd}-1)(sd_{wd})^2 + (n_{we}-1)(sd_{we})^2}{(n_{wd}+n_{we}-2)} \right]^{\frac{1}{2}} \quad \text{(AD.2)}$$

The t-statistic, t_o, is defined:

$$t_o = \frac{(\bar{E}_{wd} - \bar{E}_{we}) - (M_{wd} - M_{we})}{sd_c \sqrt{\frac{1}{n_{wd}} + \frac{1}{n_{we}}}} \quad \text{(AD.3)}$$

where M_{wd} and M_{we} are the unknown values of the true weekday and weekend population means. If the implicit assumption of random sampling holds true, then t_o is distributed as the t-distribution.

The t-distribution can be used to test any hypothesized difference in population means. We are interested in testing the hypothesis that weekday and weekend energy use are identical. If this hypothesis is true, then separate weekday and weekend models are unnecessary and energy use can be more succinctly described by the use of a single all-day model. The mathematical formulation of this hypothesis is known as the null hypothesis and is $M_{wd} = M_{we}$. To test this hypothesis, we assume that it is true and so $(M_{wd} - M_{we}) = 0$ in Equation AD.3. The degrees of freedom (df) associated with t_o are:

$$df = n_{wd} + n_{we} - 2. \quad \text{(AD.4)}$$

The probability that the null hypothesis is true, i.e., that energy use is actually the same on weekdays and on weekends, is determined by referring t_o to a t-table with df degrees of freedom. T-tables are available in any standard statistical text.

Any confidence level can be chosen as the criteria for separate models. In this example, we choose $\alpha = 0.05$. If the probability that weekday and weekend energy use are equal is less than 0.05, we conclude that separate weekday and weekend models are appropriate. If the probability that weekday and weekend energy use are equal is greater than 0.05, we conclude that the weekday/weekend models may have come from the same population and we reject the weekday/weekend models. This decision criteria rejects

separate weekday and weekend models unless there is strong evidence that weekday and weekend energy use are indeed different.

For two, three and four-parameter models, the f-test (Neter et al., 1989, pp. 87-100, 368) is the appropriate statistical test to determine if separate weekday and weekend models are needed. The use of the f-test to determine if separate weekday and weekend models are needed for the case of simple linear models is described below. The first step is to combine weekday and weekend models into a single regression model using an indicator variable, I. The combined weekday and weekend regression model for daily energy use is:

$$\hat{E}_d = \beta_1 + \beta_2 T_d + \beta_3 I + \beta_4 T_d I \qquad \text{(AD.5)}$$

where $\hat{E}_d$ is daily energy use predicted by the model, T_d is the average daily outdoor air dry-bulb temperature, I is the indicator variable, and $\beta 1$, $\beta 2$, $\beta 3$ and $\beta 4$ are regression coefficients.

The indicator variable I is defined to be 1 for weekdays and 0 for weekends. For weekdays, I=1 and daily energy use is given by:

$$\hat{E}_d = (\beta_1 + \beta_3) + (\beta_2 + \beta_4) T_d . \qquad \text{(AD.6)}$$

For weekends, I=0 and daily energy use is given by:

$$\hat{E}_d = (\beta_1) + (\beta_2) T_d . \qquad \text{(AD.7)}$$

The f-test tests the null hypothesis, Ho: $\beta_3 = \beta_4 = 0$, against the alternative hypothesis, Ha: not both $\beta_3 = \beta_4 = 0$. The null hypothesis is accepted when separate weekday and weekend models are unnecessary.

To test this hypothesis, the sum of squared error for the "full" model, SSE(F), and the sum of squared error for the "reduced" model, SSE(R), must be calculated. The sum of squared error is:

$$SSE = \sum_{d=1}^{n} (E_d - \hat{E}_d)^2 \qquad \text{(AD.8)}$$

where E_d is daily measured energy use, $\hat{E}_d$ is the daily energy use predicted by the model, and n is the number of observations of daily energy use in the sample. To calculate SSE(F) use the full model, Equation AD.6, to calculate $\hat{E}_d$ in Equation AD.8. The "reduced" model is the model that results when the conditions given by the null hypothesis are enforced and is given by Equation AD.7. To calculate SSE(R) use Equation AD.7 to calculate $\hat{E}_d$ in Equation AD.8. The number of degrees of freedom associated with the full model, df_F, and with the reduced model, df_R, are:

$$df_F = n - 4 \qquad \text{(AD.9)}$$

$$df_R = n - 2 \qquad \text{(AD.10)}$$

where n is the number of observations of daily energy use data that are used in the regression models.

The general linear f-Test is:

$$F_o = \frac{SSE(R) - SSE(F)}{df_R - df_F} \div \frac{SSE(F)}{df_F} \qquad \text{(AD.11)}$$

The probability that the null hypothesis is true, i.e. that separate weekday and weekend models are essentially identical, can be found by referring F_O to the F-distribution with $(df_R - df_F)$ numerator degrees of freedom and df_F denominator degrees of freedom. Tables of the F-distribution are found in most statistics text. Our decision criterion is to use separate weekday and weekend models if the probability that the weekday and weekend models are identical (i.e., that Ho is true) is less than 0.05. Like the decision criterion used for the t-test of one parameter models, this decision criteria rejects separate weekday and weekend models unless there is strong evidence that weekday and weekend energy use are different.

VITA

John Kelly Kissock was born in Ft. Collins, Colorado on June 14, 1958. He received a B.S. degree in Mechanical Engineering from the University of Colorado at Boulder in 1982, a M.S. degree in Engineering and Policy from Washington University in St. Louis, Missouri in 1987 and a Ph.D. degree in Mechanical Engineering from Texas A&M University in College Station, Texas in 1993. He has worked in the fields of solar energy engineering, education, air pollution analysis and building energy analysis.

He can be reached through his parents at:

John Kelly Kissock

1920 Pawnee Street

Ft. Collins, Colorado 80525

(303) 482 - 1741.